Optimal Control of Column Flotation Process using Dynamic Fundamental Models

by

Maryam Azhin

A thesis submitted in partial fulfillment of the requirements for the degree of

Doctor of Philosophy

in

Chemical Engineering

Department of Chemical and Materials Engineering
University of Alberta

Abstract

Column flotation, as a selective separation process based on differences in surface properties, is used for a broad range of applications in the mineral processing industry, including metallic, non-metallic, and coal ores, as well as wastewater treatment over the last fifty years. Flotation is a commonly used method for the separation of valuable minerals (metals) from gangue. Application of flotation columns is dominant in Australia, the USA, and China, while in North America the use of flotation column has declined significantly. The reason for this decline is that still many unanswered questions exist regarding flotation column operational performance. Operational performance is related to having control over the system in order to keep the system in the preferable operational region to reach desired product grades and/or recovery and/or performance objectives while ensuring the stability of the hydrodynamic system.

Moreover, available industrial flotation technology is effective over a size range of approximately 15 to 150 microns. The above consideration provides a strong motivation for the development of a hybrid column geometry to extend the refining range from very fine to very coarse particles by adding a mixer to the geometry of the flotation column.

The main goal of this thesis is on-line model-based monitoring and control of the

hybrid flotation column system. In this regard, optimal controller (OC) design, as the ideal solutions for high-quality control, which explicitly accounts for optimality and stability is applied. Although OC has been successfully implemented in many processes, so far the common control approach in flotation plants is knowledge-based (fuzzy logic, supervisory, and PID). This research addresses the question of how the state-of-the-art column flotation control realization is close to successful application of advanced OC. In particular, it is demonstrated that the limits of the application of OC are specific difficulties in having reliable dynamic models, state estimation, controller design and having good measurements.

For the purpose of designing a controller the following goals have been achieved, 1) a three-phase continuous hybrid flotation column that seeks to obtain the benefits of both mechanical cells and flotation columns is modelled as the interconnection of a CSTR representing the well-mixed zone and two plug-flow reactors (PFR) representing pulp and froth zones. The dynamic plant model representation of the novel flotation column accounts for both dynamic variations and micro-scale processes such as bubble-particle collision and attachment, and the appearance and breakage of bubbles. This complex distributed parameter system (DPS) is described by sets of nonlinear coupled conservation counter-current hyperbolic partial differential equations (PDEs) and one set of ordinary differential equations (ODEs). 2) The dynamic conservation law based model for the continuous hybrid flotation column is utilized in an optimal model-based controller design. The stability of the system is ensured (i.e. the controller does not make the system unstable), in addition, this modern state-of-the-art controller synthesis accounts for optimality and performance. The controller design utilizes a linear model obtained by linearization at operating

steady states of interest. A full-state optimal feedback control law is designed and controller performance has been demonstrated through a numerical simulation of physically meaningful and relevant plant operating conditions. The LQR-based optimal controller outperforms PI-based control in terms of a return to steady state after a perturbation in the initial condition, 3) model-based state estimators and observers are explored. This was due to the fact that in practice some essential properties for the monitoring and control purposes cannot be measured directly (for example, the amount of metal extracted from ore at the column exit); instead, they must be estimated from available measurements.

Finally, the proposed model and real-time state estimation is validated using real-time measurements based on experimental data.

Preface

This thesis is an original work by 'Maryam Azhin'. No part of this thesis has been previously published.

The work in this thesis is based on the research carried under the supervision of Dr Vinay Prasad and Dr Qi Liu. It is a paper based thesis, and contribution and details of each chapter/paper are discussed below.

Chapter 2 of this work is submitted as Azhin, M.; Popli, K.; Liu, Q.; Afacan, A.; Prasad, V., 2020 'Mineral Flotation Column Model : A Dynamic Framework for Three Phase Hybrid Flotation Column', Minerals Engineering. I developed and performed the dynamic modelling simulation on a pilot flotation column setup. Dr Vinay Prasad, Dr Qi Liu, Artin Afacan, and Dr Khushaal Popli were engaged in the experimental setup. Dr Vinay Prasad supervised the development of the modelling and simulation effort. Maryam Azhin under the guidance of Dr Vinay Prasad, wrote the initial drafts of the manuscripts, and all authors contributed to the editing of the final manuscript.

Chapter 3 of this work is submitted as Azhin, M.; Popli, K.; Prasad, V., 2020 'modelling and Boundary Optimal Control Design of Hybrid Column Flotation', to the Canadian Journal of Chemical Engineering. I developed and performed the optimal controller design for the hybrid column flotation system. Dr Vinay Prasad supervised

the development of the simulation effort. Maryam Azhin under the guidance of Dr Vinay Prasad, wrote the initial drafts of the manuscripts, and all authors contributed to the editing of the final manuscript.

Chapter 4 of this work was partially presented in Canadian Society of Chemical Engineering, 2017 and 2018. I developed and designed two estimators (Luenberger and EnKF) for a two-phase semi-batch flotation column and an EnKF estimator for a three-phase continuous flotation column. All the model development and computer programming, analysis and manuscript composition as well as the other chapters of the thesis were completed by myself under Prof. Vinay Prasad and Prof. Qi Liu.

Acknowledgements

This journey would not have been possible without the support of my professors, mentors, family and friends.

I would like to express my appreciation to my advisor Dr Vinay Prasad who encouraged and guided me through all stages of my research. I was very fortunate to benefit from Vinay's invaluable advice, which his suggestions were invaluable basis for successfully completion of my research. His guidance provided me with the opportunity to learn how think critically, solve problems effectively and conduct research independently. I would also like to express my gratitude to my co-advisor, Dr Qi Liu, for his support and helpful suggestions which improved the quality of my work.

I would like to thank Dr Biao Huang, Dr Rajender Gupta and Dr Syed Imtiaz who accepted invitations to be members of my thesis committee and kindly reviewed and evaluated this thesis with care and attention. I would also like to thank Artin Afacan for the technical discussions and help he provided to set up a pilot-scaled column flotation to be applied for this project. I also thank Khushaal Popli for introducing me to the flotation separation field of research. I also thank Artin Afacan for accepting the role of the Committee Chair. I am grateful to the professors of the process control group in the Chemical & Material Engineering Department,

University of Alberta, Dr Biao Huang, Dr Zukui Li and Dr Jinfeng Liu from whom I learned a lot in process control during my PhD program.

To my family, thank you for encouraging me in all of my pursuits and inspiring me to follow my dreams. I want to thank to my parents, mother-in-law, and my family for their love, support, and being there for me.

I would like to thank Stevan, my loving husband, for his faith in my capabilities, love, and support from start to finish of this thesis, this project would not have been possible were it not for his love, and Lena and Ava, my beautiful daughters, who were the greatest inspiration and joy during this work.

Lastly, I would like to acknowledge the funding from the Natural Sciences and Engineering Research Council of Canada through a Discovery grant.

Table of Contents

1 Introduction **1**

1.1 An introduction to column flotation process 1

1.2 An introduction to monitoring, estimation, and control of column flotation 7

1.3 Terminology 11

1.4 Problem formulation and framework 15

1.4.1 Objectives and challenges 17

1.4.2 Novelty and key challenges 18

1.4.3 Thesis outline 19

2 A dynamic model for a three phase hybrid column flotation system 21

2.1 Introduction 22

2.1.1 Scope 22

2.1.2 Related work 25

2.2 Mathematical model 30

2.2.1 Hybrid column flotation and volumetric flows 30

2.2.2 Particle models in the CSTR 38

2.2.3 Particle models in the pulp 38

2.2.4 Particle models in the froth 39
2.2.5 Gas holdup model 41
2.2.6 Interface boundary conditions 47
2.3 Grade and Recovery 48
2.4 Matrix representation of the model 49
2.5 Numerical method 51
2.6 Results and Discussion 52
2.6.1 Effect of gas velocity 62
2.6.2 Effect of agitation 65
2.6.3 Industrial relavent case study (Galena/Quartz) 70
2.7 Conclusion 74

3 Modelling and Boundary Optimal Control Design of Hybrid Column Flotation 76

3.1 Introduction 77
3.2 Model development for hybrid column flotation 84
3.2.1 Hybrid column 84
3.2.2 Modelling 86
3.2.3 Linearized model 93
3.2.4 Boundary to in-domain input transformation 97
3.2.5 Boundary to in-domain input transformation 99
3.3 Boundary optimal (LQ) regulator design of a hybrid system of coupled hyperbolic PDEs and ODEs 103
3.4 Results and discussion 109

3.5 Conclusions 116

4 Monitoring and State Estimation of Column Flotation with Fundamental Dynamic Models 117

4.1 Introduction 118

4.1.1 Column flotation process measurement 119

4.1.2 State estimation techniques for nonlinear systems 120

4.2 Monitoring the gas holdup distribution in a two-phase semi-batch column flotation 123

4.2.1 Two-phase column flotation model development 123

4.2.2 Ensemble Kalman filtering (EnKF) for a state space model . . 124

4.2.3 Luenberger observers 137

4.2.4 Experimental Validation 152

4.3 Monitoring the recovery, gas holdup, and concentrations in a three-phase continuous column flotation 159

5 Conclusions and Recommendations 170

5.1 Concluding remarks 170

5.2 Original contributions 170

5.3 Future work 173

Bibliography 175

Appendix A: Simulation example for Chapter 2 185

Appendix B: Detailed expressions for the elements of $\mathscr{F}$ 187

Appendix C: Simulation Parameters for Chapter 3 **188**

List of Figures

1.1 Copper cleaner/recleaner flotation plant [1]. 1

1.2 Schematic of a three-phase column flotation [6]. 3

1.3 Collision, attachment and detachment phenomena. 4

1.4 Conventional flotation data for industrial sulphide flotation circuits. . 7

1.5 General representation of a feedback control system. 15

2.1 Conceptual presentation of the hybrid flotation column. 31

2.2 Experimental presentation of the hybrid flotation column. 32

2.3 Reynolds transport theorem (RTT) schematics. 34

2.4 Schematic of mass transfer phenomena in a three-phase flotation column for a) hydrophobic, b) hydrophilic particles. 37

2.5 Schematic of concentration profile across the interface, x^* is the concentration at the interface 47

2.6 a) The concentration of attached hydrophobic particles through the column, b) the concentration of attached, free hydrophobic and free hydrophilic particles in the well-mixed zone. 54

2.7 a) The concentration of free hydrophobic particles through the column in downflow, b) in upflow. 56

2.8 The concentration of free hydrophilic particles through the column in downflow. 57
2.9 Propagation of gas holdup for three bubble size classes (left(a), left(b), right(a)) and total gas holdup through the column (right(b)) 58
2.10 The steady state propagation of hydrophobic particles concentration through the column with Danckwerts' boundary conditions at the interface 59
2.11 Propagation of recovery and grade of hydrophobic particles in the concentrate in a hybrid flotation column vs a conventional flotation column 60
2.12 The steady state propagation of gas holdup through the column with Danckwerts' boundary condition at the interface; Experimental data for gas holdup obtained through the conductivity measurement by Cruz 1997 is used for model verification (Simulation is conducted for the same conditions: $Q_a = 0.002m^3/min$, initial $\epsilon_c = [0.02, 0.02, 0.2]$, constant froth depth) 61
2.13 Transport rate of attached hydrophobic particles across the interface. 62
2.14 Gas holdup versus gas rate 64
2.15 Grade versus gas rate. 64
2.16 Recovery versus gas rate. 65
2.17 Effect of agitation on the steady state total gas holdup profile through the column. 66
2.18 Effect of agitation on the steady state profile of attached hydrophobic particles concentration through the column. 67

2.19 Effect of agitation on the recovery. 68
2.20 Effect of agitation and particle size on the attachment rate in CSTR. 69
2.21 Effect of agitation and particle size on the detachment rate in CSTR. 69
2.22 Effect of agitation and particle size on the attachment and detachment rate in CSTR. 70
2.23 a) The concentration of attached Galena through the column, b) the concentration of attached, free Galena and free Quartz in the well-mixed zone. 72
2.24 The steady state propagation of Galena concentration through the column with Danckwerts' boundary conditions at the interface. 73
2.25 Propagation of recovery and grade of Galena in the concentrate in a hybrid flotation column 74

3.1 Model presentation 83
3.2 Schematic of a three-phase column flotation system considering the transport of hydrophobic particles 84
3.3 The steady state concentration profiles through the column obtained by the simulation of the full nonlinear model $X_{5ss}([0, L_1])$-$X_{8ss}([L_1, L_2])$: solid line, $X_{4ss}([0, L_1])$-$X_{7ss}([L_1, L_2])$: dashed line, $X_{3ss}([0, L_1])$-$X_{6ss}([L_1, L_2])$: dotted line. 93
3.4 Schematic of the steady state gas hold up profiles through the column. 94
3.5 Spatial characteristics of the gain 107
3.6 Concentration perturbation propagation of hydrophobic particles: free, x_4 and x_7, and attached, x_5 and x_8, in the pulp and froth. 111

3.7 Integral of the squared concentration perturbation of free minerals in the up-flow in the pulp, $\int_{L_1}^{L_2} x_4^2(z,t)dz$. Thick line: LQR, dotted: open-loop, dashed: PI, thin line: LQR with disturbance applied at 4 min. 114

3.8 Integral of the squared concentration perturbation of free minerals in the up-flow in the froth, $\int_{L_1}^{L_2} x_7^2(z,t)dz$. Thick line: LQR, dotted: open-loop, dashed: PI, thin line: LQR with disturbance applied at 4 min. 115

3.9 Integral of the squared concentration perturbation of attached minerals in the froth, $\int_{L_1}^{L_2} x_8^2(z,t)dz$. Thick line: LQR, dotted: open-loop, dashed: PI, thin line: LQR with disturbance applied at 4 min. 115

4.1 Schematic of the EnKF estimation process [119]. 126

4.2 True and predicted values, using EnKF, for the gas holdup of three bubble size classes through a two-phase flotation column. 133

4.3 True and predicted values, using EnKF, for the total gas holdup through a two-phase flotation column. 134

4.4 Relative prediction error, using EnKF, for the gas holdup of three bubble size classes through a two-phase flotation column. 135

4.5 Relative prediction error, using EnKF, for the total gas holdup through a two-phase flotation column. 136

4.6 Schematic of Luenberger Observer design. 140

4.7 The true and estimated state propagation for ϵ_1 through a two-phase flotation column obtained by the Luenberger observer (measurements at the column exit). 143
4.8 The true and estimated state propagation for ϵ_2 through a two-phase flotation column obtained by the Luenberger observer (measurements at the column exit). 144
4.9 The true and estimated state propagation for ϵ_1 through a two-phase flotation column obtained by the Luenberger observer (measurements at the column exit and interface). 145
4.10 Relative estimation error for ϵ_1 through a two-phase flotation column obtained by the Luenberger observer (measurements at the column exit and interface). 146
4.11 The true and estimated propagation for ϵ_2 through a two-phase flotation column by the Luenberger observer (measurements at the column exit and interface). 147
4.12 Relative estimation error for ϵ_2 through a two-phase flotation column by the Luenberger observer (measurements at the column exit and interface). 148
4.13 The true and estimated propagation for ϵ_3 through a two-phase flotation column by the Luenberger observer (measurements at the column exit and interface). 149
4.14 Relative estimation error for ϵ_3 through a two-phase flotation column obtained by the Luenberger observer (measurements at the column exit and interface). 150

4.15 The true and estimated state propagation for ϵ_{total} through a two-phase flotation column obtained by the Luenberger observer (measurements at the column exit and interface). 151
4.16 Experimental setup for a two-phase semi-batch flotation column. . . . 153
4.17 Probable steady state propagation of gas holdup for three different bubble size classes in a semi-batch flotation column based on measurement on top of the pulp zone. 154
4.18 Propagation of gas holdup in size class 3 through a semi-batch flotation column by the Luenberger observer based on empirical data. 155
4.19 Relative prediction error for ϵ_3 through a semi-batch flotation column by the Luenberger observer based on empirical data. 156
4.20 Propagation of total gas holdup through a semi-batch flotation column by the Luenberger observer based on empirical data. 157
4.21 Relative prediction error for ϵ_{total} through a semi-batch flotation column by the Luenberger observer based on empirical data. 158
4.22 True and predicted values, using EnKF, for X_5 (in pulp) and X_8 (in froth) through a three-phase flotation column. 162
4.23 Relative prediction error for X_5 and X_8 through a three-phase flotation column. 163
4.24 True and predicted values, using EnKF, for X_4 (in pulp) and X_7 (in froth) through a three-phase flotation column. 164
4.25 True and predicted values, using EnKF, for X_3 (in pulp) and X_6 (in froth) through a three-phase flotation column. 164

4.26 True and predicted values, using EnKF, for ϵ_1 through a three-phase flotation column. 165
4.27 True and predicted values, using EnKF, for ϵ_2 through a three-phase flotation column. 166
4.28 True and predicted values, using EnKF, for ϵ_3 through a three-phase flotation column. 166
4.29 True and predicted values, using EnKF, for ϵ_{total} through a three-phase flotation column. 167
4.30 Relative prediction error, using EnKF, for ϵ_{total} through a three-phase flotation column. 168
4.31 True and predicted values, using EnKF, for recovery in a three-phase flotation column. 169

List of Symbols

$1 - \alpha_i$ – percentage of the liquid phase in the upflow in zone i, (i=p or f): dimensionless

II – gas control volume in the CSTR

III, III' – liquid control volumes in the pulp for the downflow and upflow

IV – gas control volume in the pulp

L_2 – height of the froth zone. $[m]$

Q_a – air volumetric flow rate. $[m^3.min^{-1}]$

Q_c – concentrate volumetric flow rate $(Q_f + Q_w - Q_t)$

Q_w – wash water volumetric flow rate. $[m^3.min^{-1}]$

$Q_{r,i}$ – downward liquid volumetric flow rate in zone i, (i=p or f). $[m^3.min^{-1}]$

V, V' – liquid control volumes in the froth for the downflow and upflow

VI – gas control volume in the froth

$V_j(z)$ – transport velocity of state j. $[m.min^{-1}]$

V_c – volume of the CSTR zone. $[m^3]$

X_5 and X_8 – concentrations of attached hydrophobic particles in the pulp and froth. $[kg.m^{-3}]$ (Chapter3)

$X_{1,0}$ – Initial concentration of hydrophobic particles in the feed, which denotes the input into the CSTR. $[kg.m^{-3}]$ (Chapter3)

X_1 and X_2 – concentrations of free and attached hydrophobic particles in the CSTR. $[kg.m^{-3}]$ (Chapter3)

X_3 and X_4 – concentrations of free hydrophobic particles in the liquid downflow and upflow in the pulp. $[kg.m^{-3}]$ (Chapter3)

X_6 and X_7 – concentrations of free hydrophobic particles in the liquid downflow and upflow in the froth. $[kg.m^{-3}]$ (Chapter3)

Ψ – the collision success factor

α_i – percentage of the liquid in the downflow in zone i, (i=p or f): dimensionless

δ – a Dirac function

$\epsilon_{i,n}$ – gas holdup of bubbles in size class n in zone i

ϵ_i – total gas holdup in zone i, (i=p or f): dimensionless

η – the wash water input. $[kg/m^3]$

μ – slurry viscosity. $[Pa.s]$

$\rho_{g,i}$ – gas density. $[kg/m^3]$

$\rho_{l,i}$ – slurry/liquid density. $[kg/m^3]$

$\xi_{i,n,j}$ – symmetric matrix of bubbles collision probabilities

h, h_f – mass transfer coefficients of particles from upward to downward liquid flow in the pulp and froth, respectively. $[min^{-1}]$

h_i and h_{i2} – mass transfer coefficients of hydrophobic particles from upward to downward liquid flows in zone i, (i=p or f). $[min^{-1}]$

k_{di} – particle-bubble detachment rate constant in zone i, (i=c, p, or f). $[min^{-1}]$

$l = L_1 + L_2$ – the overall transport length of the pulp and froth zone. $[m]$

t – time. $[min]$

$v_{\epsilon,n,i}$ – bubble velocity of bubble size class n in zone i, (i=p or f). $[m.min^{-1}]$

x – perturbation of concentrations (states) around the steady state. $[kg.m^{-3}]$ (Chapter3)

x_5, x_8 – attached hydrophobics concentration in pulp and froth. $[kg.m^{-3}]$

$x_{1,0}$ – Initial concentration of hydrophobic particles in the feed. $[kg.m^{-3}]$

x_1, x_2 – free and attached hydrophobics concentration in the well-mixed zone. $[kg.m^{-3}]$

x_3, x_4 – free hydrophobics concentration in pulp liquid downflow and upflow. $[kg.m^{-3}]$

$x_{q1,0}$ – Initial concentration of hydrophilic particles in the feed. $[kg.m^{-3}]$

x_{q1} – free hydrophilic particle concentration in the well-mixed zone. $[kg.m^{-3}]$

x_{q2}, x_{q3} – free hydrophilic particle in the pulp upflow and downflow. $[kg.m^{-3}]$

x_{q4}, x_{q5} – free hydrophilic particles in the froth upflow and downflow. $[kg.m^{-3}]$

z – height, axial direction. $[m]$

A, A_c – cross-sectional area of the column. $[m^2]$

Db_n – bubble diameter in size class n. $[m]$

G and m – attachment rate equation constants. dimensionless

I – liquid control volume in the CSTR

K_{47} – interface mass transfer coefficient for free upflow hydrophobics. $[m^{-1}]$

K_{58} – interface mass transfer coefficient for attached hydrophobics. $[m^{-1}]$

K_{63} – interface mass transfer coefficient for free downflow hydrophobics. $[m^{-1}]$

K_{ϵ} – interface mass transfer coefficient for gas bubbles. $[m^{-1}]$

K_{q35} – interface mass transfer coefficient for free downflow hydrophilics. $[m^{-1}]$

L_1 – height of the pulp zone on top of the well-mixed zone. $[m]$

Q_f – feed volumetric flow rate. $[m.min^{-1}]$

Q_t – tailing volumetric flow rate. $[m^3.min^{-1}]$

$Q_{e,i}$ – upward liquid volumetric flow rate in zone i, (i=p or f). $[m^3.min^{-1}]$

c – CSTR or well-mixed zone

d – distributed parameter system (DPS)

d_c – diameter of the column. $[m]$

f – froth zone

h', h'_f – mass transfer coefficients of particles from downward to upward liquid flow in the pulp and froth, respectively. $[min^{-1}]$

h_{qi2} and h_{qi} – mass transfer coefficients of hydrophilic particles from upward to downward liquid flows in zone i, (i=p or f). $[min^{-1}]$

i – represents the zones (CSTR (c), pulp with plug flow (p), and froth (f))

k, k_2 – fraction of hydrophobic particles that after detachment goes to the downflow in the pulp and froth, respectively. dimensionless

k_{ac} – particle-bubble attachment rate constant in the well-mixed zone. $[min^{-1}]$

k_{af6}, k_{af7} – particle-bubble attachment rate constants of free hydrophobic particles in the downflow and upflow, respectively, in the froth. $[min^{-1}]$

k_{ap3}, k_{ap4} – particle-bubble attachment rate constants of the free downflow and upflow hydrophobic particles, respectively, in the pulp. $[min^{-1}]$

l – lumped parameter system (LPS)

p – pulp zone

ss – steady state

x_6, x_7 – free hydrophobics concentration in froth liquid downflow and upflow. $[kg.m^{-3}]$

Chapter 1

Introduction

1.1 An introduction to column flotation process

The process of transforming an ore to final valuable minerals (metals) includes a coherent chain of processes. This series of processes includes crushing, grinding, physical and chemical separating, flotation, regrinding and re-floating followed by filtering and drying to produce the final concentrate of valuable material. Column flotation, which is only responsible for physical treatment of ores, is part of the cleaning process in the mining industry (see Figure 1.1).

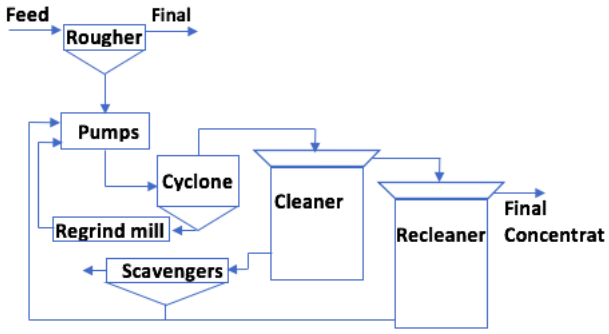

Figure 1.1: Copper cleaner/recleaner flotation plant [1].

The main goal of a flotation column unit is to improve the recovery and/or final grade of product to its highest possible level, and the other alternative to achieving this is to use a mechanical flotation cell. An important step to achieve this goal is to understand the involving variables that affect the operation performance significantly and control them. The control of column flotation has attracted some attention in the last few years [2]. Froth flotation is a commonly used method for a selective separation of valuable minerals (metals) from useless minerals (gangues) based on differences in surface properties. First, pneumatic flotation cells (air sparking through the porous bottom) were introduced by G.M. Callow in 1915 [3]. In this configuration, the air flowed horizontally with a cross-current flow with the slurry flow. This process was further tested by Town and Flynn in 1919 and was widely used in the industry from 1920-1930 [4]. This process was further replaced by a impeller-type flotation device. Modern flotation columns were developed in Canada in the early 1960s [5].

The column flotation dynamic characteristics are of major importance for the regulation of product quality. In particular, the column flotation geometry [4] favours a more quiescent environment in comparison to the mechanical cell, which improves the product quality and grade. Moreover, it requires less footprint since the need for long banks of conventional cells is eliminated. Not only that, this separation technique needs lower capital and maintenance costs and is more efficient and easier to implement for monitoring and controlling purposes in comparison to mechanical cell flotation. Also, this geometry provides an option to recycle the products to improve the quality and provides a deeper froth zone, which favours an increase in residence time in the froth zone and a further increase in separation quality. Column flotation

has three phases including solid (mineral particles), liquid (water), and gaseous (air) and three zones including pulp, froth, and interface. Figure 1.2 shows a three-phase column flotation system, which consists of three different zones. The froth zone is the topmost layer with more bubbly flow, and is called the cleaning zone. The pulp zone is the bottom zone and is called the collection zone. It is a diluted slurry where particle collection is considered to occur by the collision between particles and bubbles. The middle zone, called the interface layer, is between the froth and the pulp zones and it is the place where the interaction between the collection and cleaning zones occurs. At the interface, particle transport occurs in both directions.

Main column flotation separation processes are realized as downward slurry flow throughout the collection zone and a rise up of the air stream (as small bubbles) through the column, as seen in Figure 1.2.

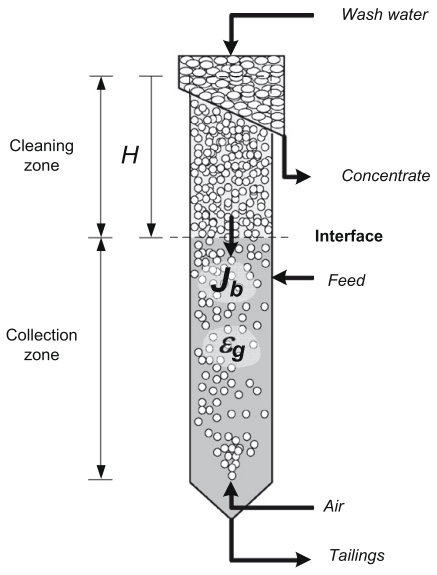

Figure 1.2: Schematic of a three-phase column flotation [6].

The primary transport of particle is from the collection zone to the cleaning zone by attachment to the bubbles, while transport of particles by entrainment into the froth phase is usually of negligible importance in the column. Some of the main physical sub-processes taking place in column flotation (see Figure 1.3) can be described as follows:

1. A collision occurs between the hydrophobic and hydrophilic solid particles and the air bubbles.

2. After the collision, the liquid film between hydrophobic particle and bubble thins out so that attachment happens, and eventually ruptures, leading to the attachment phenomenon.

3. The solid-liquid-gas interface on the surface of the air bubble moves to establish a stable bubble-particle aggregate.

4. From here, the aggregate rises to form the froth phase which can be collected in the launder.

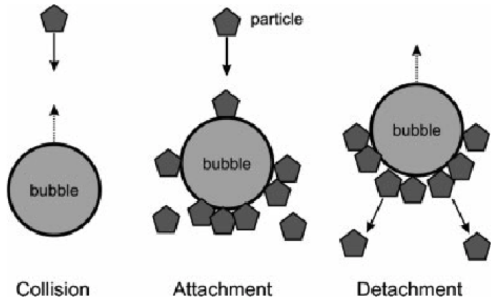

Figure 1.3: Collision, attachment and detachment phenomena.

In contrast to the hydrophobic particles, hydrophilic particles do not attach to

the air bubbles but remain in the flotation pulp. Besides the main sub-processes, some other simultaneous sub-processes such as 'entrainment of gangue into the froth zone' and 'coalescence of bubbles' occur regularly in a flotation column. As a result of coalescence of bubbles, particles detach and drop back from froth zone to the pulp zone with bias water even if the froth is not saturated with particles [7]. The detachment of valuable particles from bubbles impacts the recovery across the froth phase. The following mechanisms demonstrate how minerals travel through the flotation apparatus by entrainment:

- Particles are transported in a bubble lamella form in a thin hydrodynamic layer of water around the bubble (boundary layer theory) [8].
- Particles are transported in a wake of a rising bubbles (bubble wake theory).
- Particles go to the froth from the pulp by a swarm of ascending bubbles. Bubbles are slowed down and crowded in the interface of froth and pulp. Some suspended minerals may drop back and some may be squeezed and push up by bubble swarm due to the buoyancy force (bubble swarm theory) [9].

Although the mining industry faced several operational changes and improvements since 1960, the full potential of this unit operation has not been fully exploited due to the complexity of the process. Nowadays, in order to maximize the production at a lower operating cost under volatile metal market conditions, generating an accurate model and designing an optimal model-based controller of the system is of a high interest.

Effect of particle size on recovery: Several studies have shown that available industrial flotation technology is effective over a size range of approximately 15 to 150 microns and cannot refine very fine and very coarse particles by flotation. The well-known 'elephant curve' shows particles outside of critical size range in industry using conventional flotation equipment are rejected to the tailing [10] (see Figure 1.4 [4]). For fine particles (naturally occurring or generated after grinding) in order to increase the recovery (to increase the bubble/particle collision rate, which means to increase the probability of attachment), the design of equipment should be changed to provide more retention time. Therefore, we need to make smaller bubbles (micro or nano-bubbles) to increase the total surface area of air in order to increase the flotation rate or increase the gas flow rate. On the other hand, the recovery decreases for more coarse particles due to excessive turbulence, which induces detachment. In this case, the mechanical cell environment (due to increased agitation) is not suitable for the separation of coarse particles, and column flotation provides less agitated area. For particles greater than 200 microns, the strength of the bubble/particle attachment decreases [4]. The split-feed process is used sometimes in order to pre-separate smaller and coarser particles to improve the recovery [11–13].

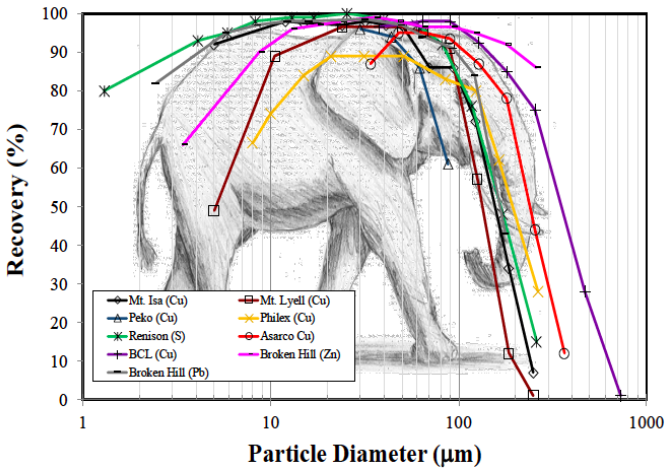

Figure 1.4: Conventional flotation data for industrial sulphide flotation circuits.

1.2 An introduction to monitoring, estimation, and control of column flotation

Application of modern control theory includes methods for process identification, online monitoring, state estimation, and prediction techniques [14] to reach the main objective of the flotation process control, which is the maximization of the concentrate grade and recovery without losing process stability [15]. Although the concentrate grade can be continuously measured using an on-stream analyzer, the only way to define the recovery is through estimation from a material balance. In order to relate important aspects of monitoring, estimation, and control of column flotation process, one needs to address the application related features of column flotation process, such as measurements and/or control.

Measurement: Basically, on-line instruments may not always exist or would

be expensive. For example, using X-ray fluorescence (XRF), which is known as a conventional technique to measure the composition of the stream for online measurement would be expensive to maintain and have low sampling rates with lengthy delays for analysis. Moreover, during offline laboratory analyzes, the structure of the froth changes and therefore alters the grade and recovery of the product [16, 17]. One possible benefit of the results of the offline measurement is that it can be used as initial guesses for the online estimator and to minimize the error between the model predicted and measured recovery over time.

For measuring froth depth, methods using floats or pressure gauges and recently temperature or conductivity profiles are commonly used in industrial applications [18]. Another important variable for the optimization of column flotation is bias which is defined as the 'net downflow water' [7], or 'difference between tailing water and the feed water' [19]. Measuring bias by using flow meters and density meters is difficult [6], while measuring bias using the temperature [20] and conductivity [19] profiles have been reported.

Another measurement technique is machine vision, which was introduced to froth flotation systems in the late 1980s [21]. Machine vision has been proposed as an ideal non-intrusive technique to rapidly and accurately extract meaningful information relating to the performance of the froth phase in flotation process such as grade and recovery of the valuable particle in the concentrate. Despite being challenging, many attempts have been done to link performance factors such as mass recovery rate and concentrate grade with measurable attributes of the froth phase [21–23].

Estimation: An important fact to consider is that measurements using hard-

ware sensors for a complex and harsh environment of froth flotation is very challenging. Therefore, a cheap, reliable, and fast alternative is an attractive option to be explored [24]. In particular, the important features of bubble surface area flux measurements are related to bubble size estimation which is reported in [25, 26]. In the same view, for the on-line measurements the estimation of bubble surface area flux and bias techniques have not been successfully developed. In this thesis, we address this issue of on-line real time estimation of important dynamic characteristics of froth flotation.

Control: Control of column flotation is not a trivial task due to the lack of accurate measurements, non-linear dynamics and high interaction among variables [27]. Automatic control and optimization should be applied in a hierarchical manner using the process variables with a strong effect on the grade and recovery, including froth depth, bias, and gas fraction. In the literature, three essential levels of process control have been studied including 1) instrumentation or base level flotation control, 2) intermediate flotation control or regulating control, and 3) optimizing flotation or supervisory control [6, 28]. At the base level, set points of feed, wash water, tailing, and air flowrates are manipulated variables. These manipulated variables are then utilized at the intermediate control level as variables for controlling the essential dynamics of the froth flotation column, such as froth depth, bias, gas fraction, or bubble surface area flux [6]. At the top level of the control structure is the supervisory control realization, which is often based on fuzzy rules [29]. As expected the advanced control strategies require data validation, state estimation and monitoring design, and the ability to handle the faults in the system.

Computer control strategies and systems applied to column flotation process typically target bias, froth depth, grade, recovery, and gas holdup using feedback control by manipulating variables such as the flow of feed, air, and water, as well as reagent addition [30]. Along the line of applied controller designs, three types of controllers may be identified as being used frequently in column flotation column operations. These are feedforward controllers to address disturbance rejection, as it can be anticipated that froth flotation column will be exposed to a variety of disturbances, nonlinear controllers to address nonlinearities in the systems, and multivariable controller designs to address interactions among multiple inputs and controlled outputs [6]. Along these designs, one way to take into account process nonlinearities is to use a qualitative knowledge of the process in the form of empirical modelling which describes nonlinearities. Then, PID controllers can be adapted for nonlinear control purposes based on such models. In the same vein, the attempts to improve existing industrial nonlinear controllers by adding heuristic control and adding logic rules have been attempted. However, the results cannot be extrapolated outside the range covered by the empirical data used to develop the model.

modelling: Flotation is a complex process due to the existence of large number of variables, which can be grouped in three categories of 'Feed Characteristics', 'Physicochemical Factors', 'Hydrodynamics'. Since the 1930s, numerous mathematical models have been reported [22, 31, 32]. Primarily, classical flotation models were developed and then with the development and application of computer techniques in flotation process modelling, the development of soft computing based models started [33]. The existence of approximately 100 variables which affect the flotation process

[34, 35] makes the flotation modelling a very complex real time process. Therefore, up to now no purely theoretical models have been developed.

1.3 Terminology

In this section, important terminology are introduced in order to facilitate understanding and description of column flotation and its control, and monitoring.

Interface level (L1): This variable shows the distance from bottom of the column to the position of the pulp-froth interface. It determines the height of cleaning and the collection zones. This level can be consequently translated to the mean pulp residence time. It needs to be controlled at a constant level for stable column operation.

Gas holdup (ϵ): The volumetric fraction of gas in the considered zone of the column (cleaning or collection).

$$\epsilon(\%) = \frac{Volume\ of\ bubbles}{Total\ volume} \times 100 \tag{1.1}$$

Wash water: One of the important characteristic features of column flotation is the addition of a fine spray of water on the surface of the overflowing product (concentrate). Wash water, besides having a stabilizing effect on the froth, it washes out the hydrophilic particles (that might be entrained to the froth phase) back to the pulp zone. This is a reason to call the froth zone the cleaning zone.

Bias rate: Wash water splits and one part of it moves down. The net downward water stream is called the bias [7]. The bias rate is positive if it moves down and negative if it moves up. The positive bias rate increases the grade and is desirable for the plant. Moreover, an excessive amount of bias decreases the residence time in the cleaning zone, which is non-desirable for the process. On the other hand, the high bias values might cause increased froth mixing and result in drop back of collected particles [36].

$$J_b = J_{ww} - J_{wc} \tag{1.2}$$

where J is the superficial velocity (volumetric flow rate divide by the column cross sectional area), b is bias, ww is the water that goes down as the wash water and wc water that goes up to the concentrate.

Frothers: The chemical reagents applied in flotation process to both reduce the bubble size and improve bubble stabilization and produce a stable froth in the column.

Collectors: The chemical reagents applied in flotation process to increase selectivity to enhance attachment between the mineral and bubbles by selectively making the mineral surface hydrophobic.

Kinetics: Fundamentally, flotation kinetics depend on the probability of collision, the probability of attachment and the probability of detachment between bubble

and particles. For better performance, particles of the valuable mineral should have a higher probability of attachment and low probability of detachment along with sufficient mineral liberation.

True flotation and entrainment mechanisms: A mineral particle is considered to be separated by true flotation if it rises up to the froth zone and later in the launder by attaching to the bubbles. In contrast, an entrainment mechanism is defined as a nonselective transport mechanism of separating suspended minerals [37, 38].

Grade and recovery: Efficiency of separation in column flotation is directly related to the recovery and grade of the valuable particle, which can be affected by many factors. These factors can be related to the chemistry (reagent), equipment (geometry, air flow rate, and impeller rate), or operation categories (feed rate and type, particle size, density and PH of the slurry). The efficiency of separation given by grade and recovery is defined as:

$$Grade(A)\ in\ the\ concentrate =$$

$$100 \times \frac{Amount\ of\ particle\ A\ in\ the\ concentrate\ (outlet)}{Total\ amount\ of\ solids\ in\ the\ concentrate\ (A+B+C+...)}$$

$$Recovery(A) = \frac{Amount\ of\ particle\ A\ in\ the\ concentrate\ (outlet)}{Amount\ of\ particle\ A\ in\ the\ feed\ (inlet)} \tag{1.3}$$

Note the concept of 'grade' applies to all other streams as well, not just the concentrate, while 'recovery' is typically only used for the concentrate.

Soft sensor: An equation which is used to predict or estimate a given unmeasured variable as a function of other variables [2].

Manipulated variables and control variables: There are several contributions [7, 39] which have studied the effect of different manipulated variables on the controlled variables and have suggested certain input-output pairs for the control of a flotation column. It is seen that a strong interaction exists between the manipulated and controlled variables; for example, the wash water rate has a slow effect on the interface level, bias rate, air holdup, as well as recovery, but has a fast effect on the grade. Also, the tailings flow rate has a fast effect on the interface level and bias rate and a medium effect on air holdup, but a slow effect on grade and recovery. Another important control aspect is that the air flow rate has a fast effect on level and air holdup, but a slow effect on bias and a medium effect on grade and recovery.

Normally, the interface level is controlled by manipulating the tailings flow rate or the wash water rate. By using PIDs, manipulating with the tailings flow rate is simple compared to manipulating with wash water, which has a slow response on the interface level. It is known that because of the process interactions, the selection of the best pairing of controlled and manipulated variables is a determining factor for the prediction of grade and the success of the process control.

In addition to PID control of local objectives, a few studies have reported on the application of fuzzy control, gain scheduled control, dynamic matrix control, generalized predictive control, global predictive control [6], and model predictive control (MPC) [27, 40] for column flotation. However, all these control design strategies were based on data-driven low order linear models based on system identification [40] or

r[H]

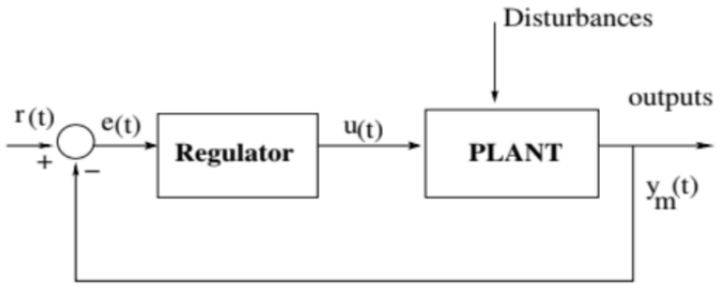

Figure 1.5: General representation of a feedback control system.

neural networks [27] and non were based on a fundamental model.

1.4 Problem formulation and framework

There are some unexplored issues to be addressed in the column flotation control design and the impact on its performance.

Operational performance is related to having control over the system in order to keep the system in the preferable operational region and/or to reach desired product grades and/or performance objectives while ensuring the stability of the hydrodynamic system. Concentrate and tailings grades are the main target variables in flotation processes. From the industrial point of view, optimum column flotation performance is related to the precise control of pulp level, flow rates, air sparging and accurate addition of reagents. It is natural to ask which type of controller can be designed to reach these goals? For the purpose of designing a controller that can help to reach these goals, one needs 1) to have a reliable dynamic model, 2) to ensure the stability of system (i.e. the controller does not make the system unstable), and

3) to ensure that the system can track some performance objective (e.g. grade in the product/concentrate) in an optimal manner. PI controller applied in the closed-loop does not guaranty stability of the system (higher than first-order system) and are usually used for stable systems.

Column flotation system is exposed to a variety of disturbances that can be known and unknown. In addition, it is difficult to maintain the quality of measurements as they are affected by high-frequency noise. In this thesis, a controller is designed to ensure tracking which means that the output of interest matches the reference trajectory so that a perfect tracking is achieved (the tracking error is zero). In this case, controller design achieves tracking of constant reference modelled signals and rejecting disturbances, while the closed-loop system stability is guaranteed.

The ideal solutions for high-quality control are model based controllers such as the optimal controller designs. Although optimal controller (OC) has been successfully implemented in many processes, so far the common control approach in flotation plant is knowledge-based (fuzzy logic, supervisory, and PID). A few works have reported the design of OC for column flotation, but they use a low order model based on system identification of the system [40] or neural network [27]. Having this in mind, a detailed fundamental model is developed in this thesis, and an optimal controller is designed based on this fundamental model. In addition, this thesis addresses the question of how the state-of-the-art column flotation control realization is close to successful application of OC. It is shown that the limits of the application of OC are not related to the control algorithm but difficulties in: 1) having reliable dynamic models, 2) state estimation, 3) having good measurements.

1.4.1 Objectives and challenges

The primary goal of this work is on-line model-based monitoring, estimation and control of a column flotation. To address this goal, the following scope of work is considered:

1. Developing fundamental models representation of column flotation

2. Exploring ensemble Kalman filter (EnKF) based state estimators: In practice, some essential properties for monitoring and control purposes cannot be measured explicitly (for example, the amount of metal extracted from ore at the column exit); instead they must be estimated from available measurements. This thesis explores the use of an ensemble Kalman filter (EnKF) as a tool for state estimation.

3. Exploring optimal controller design

    - A proper evaluation and control of the bubble distribution, gas holdup, and solid concentration through the column is developed which will offer new insight for flotation column monitoring and control.
    - In addition to the estimation and monitoring developments in this work, a model-based optimal control is designed. The main point is that the optimal control design ensures closed-loop stability and improved performance.
    - Exploring the complexity captured in a complex three-phase system with a coupling of one set of ODEs and two sets of PDEs.

1.4.2 Novelty and key challenges

1. The new proposed mathematical model has been tailored for unique column flotation pilot apparatus in the mineral processing lab at the University of Alberta. The pilot plant is unique since a mixer has been added to the column flotation geometry.

2. In previous modelling and simulation efforts in the literature, it was assumed that a flotation column consists of a series of well-mixed CSTRs. However, in reality, the froth is not perfectly mixed. Hence, the proposed model is an interconnection of a continuous stirred tank reactor (CSTR) which models the mixing section in the lower compartment, and two transport-reaction tubular reactor models with negligible diffusion terms in the pulp and froth zones.

3. The model accounts for the bubble interactions manifested as appearance and disappearance.

4. The model accounts for the recycle flow on top of the column from upflow to downflow.

5. The application of EnKF in column flotation system is novel.

6. The model's insights for gas holdup and solid concentration profiles through the column will offer new possibilities for flotation column control.

7. The application of OC in a system of coupled ODE and two transport-reaction hyperbolic PDEs is novel and solving this system is not trivial.

1.4.3 Thesis outline

The thesis is organized as the collection of three primary chapters and a chapter on conclusions, aside from this introductory chapter:

Chapter 2: *Mineral Flotation Column Model : A Dynamic Framework for Three Phase Hybrid Flotation Column*

The chapter focuses on the modelling of column flotation process in mineral processing. A comprehensive dynamic three-phase computational model is developed to include micro-scale and macro-scale sub-processes. This model accounts for bubble interaction effects. The mathematical model of the continuous separation process in the column flotation apparatus is given by the mass balances in the control volumes in each zones. The dominant phenomena of mass transfer are given by convective transport terms (as a result of the fluid motions), and the volume mass sources (sinks) are modelled as a result of chemical reactions or interphase mass transfer (solid-liquid-gas bubbles). These convection-reaction type models can help in a qualitative analysis of the response of the process to the manipulated inputs and process disturbances.

Chapter 3: *Modelling and Boundary Optimal Control Design of Hybrid Column Flotation*

The focus of this chapter is on the development of a boundary optimal control design for the column flotation. In particular, the complex distributed parameter system of three - phase column flotation is described by sets of nonlinear coupled conservation laws model given by hyperbolic partial differential equations (PDEs) and ordinary differential equations (ODEs). The controller design is based on linearized version of the model proposed in Chapter 2, and optimal boundary full state feedback control

law is constructed for coupled ODE-PDE system.

Chapter 4: *Monitoring and State Estimator Design of Column Flotation with Fundamental Dynamic Models*

The chapter addresses the study of monitoring and state estimation in the column flotation processes. In particular, the two-phase and three-phase models of the column flotation are utilized for deterministic and stochastic observer design. Furthermore, the two phase model is used in Luenberger observer design and it has been linked to experimental findings from the literature. In the case of the three-phase model, the ensemble Kalman filter is utilized since the model complexity did not allow for the design of the deterministic observer.

Chapter 5: *Conclusions and Recommendations* This chapter summarizes the research effort in this thesis and provides conclusions and guidance for future developments.

It should be noted that this thesis is based on the paper-format and therefore, it follows the rules set by Faculty of Graduate Studies and Research (FGSR) at University of Alberta. Hence, to maintain the paper-based format required by FGSR and to ensure thesis completeness, some parts of the chapters might contain repetition. Consequently, the overlap is not removed in order to provide smooth flow of the thesis to the readers and ease the understanding of the material.

Chapter 2

A dynamic model for a three phase hybrid column flotation system

Abstract A comprehensive novel hybrid dynamic fundamental model with Danckwerts' boundary conditions at the pulp/froth interface has been developed for a continuous flotation column. The model accounts for three phases, namely the water, gas, and solid particles (hydrophobic and hydrophilic), in one space dimension. The modelling framework is based on three subsystems, including a well-mixed reactor and two plug-flow reactors representing pulp (collection) and froth (cleaning) zones that are interconnected through the boundaries. The model considers the micro-scale processes taking place in the column, such as bubble-particle attachment and bubbles coalescence. The resulting mathematical model is a coupled set of nonlinear hetrodirectional hyperbolic partial differential equations for the pulp and the froth and a set of ordinary differential equations for the well-mixed zone. The movement between phases are given by liquid upflow, liquid downflow, and gas upflow. An important parameter in this simulation is the bubble size, which directly affects the gas holdup, and consequently the distributions of all states, including the concentration of at-

tached minerals through the column. Validation of the model is provided by testing its predictions against experimental data for two-phase systems. Finally, the effect of some important parameters such as gas flow rate, agitation, particle size on gas holdup, distributions of value minerals, grade, recovery, and attachment/detachment rates have been studied.

2.1 Introduction

2.1.1 Scope

A flotation column is a device that combines slurry with injected air bubbles and wash water, creating the conditions for separation of value minerals from gangue minerals in an ore based on differences in their hydrophobicity. Column flotation has wide applications in the mineral processing industry, including metallic, non-metallic ores and coal, as well as in wastewater treatment. Prior to its introduction into the flotation column, the feed slurry is treated with a collector to selectively make particles hydrophobic and attach to air bubbles. Therefore, hydrophobic minerals (valuable) and hydrophilic particles (gangue), where both are suspended in a liquid, will be separated selectively. These bubble-particle aggregates rise up to the top of the column and generate the froth phase (foam), which is rich in selected minerals. Froth carries the valuable minerals that are usually removed in the launder. However, hydrophilic particles that are not attached to the bubble stream settle and exit the column and form the tailing.

After analyzing over 4000 installed flotation columns, [41] reported that the trends in the application of column flotation varied by type, commodity and geographical

region. In the coal industry in Australia, and later in the USA and China, the phosphate industry in the USA and Brazil, and the iron ore industry in Brazil, column flotation is largely the dominant flotation technology. Within the base metals industry, flotation columns are generally accepted worldwide as smaller capacity cleaners. Although the flotation column was patented in Canada in the 1960s, reported by [7], the full potential of this complex separation equipment has still not been fully exploited. In North America, there has been an increasing tendency to install mechanical flotation cells rather than flotation columns. [41] state that the application of these columns remains limited by unanswered questions related to operational performance and the availability of reliable models of the process.

Dynamic modelling and simulation are two major tools for systematic process analysis that leads to better process control and potential increase in operational profitability. Empirical models are not general and can only be used for a narrow range of operation; therefore, it would be preferable to develop and use fundamental models. However, due to the complexities of the subprocesses involved in the operation of column flotation, such as particle/bubble attachment, detachment, and bubble coalescence, the task of building an appropriate dynamic model is very challenging. Currently, a dynamic three-phase mathematical model that can accurately describe dynamic column flotation unit operation and be used for control and monitoring has not yet been developed. Dynamic three-phase mathematical models for flotation columns in the literature account for specific situations; for example, only for particle interactions between the upward air and the downward liquid flows, neglecting the interaction between bubbles and particles in the upward liquid phase entrained by the bubbles [42, 43]. These three phases - upflow air, upflow liquid and downflow

liquid - should be coupled. Moreover, previous models do not account for the effect of mass transfer between upflows and downflow liquid [42–44]. Furthermore, in previous models, the column is modelled as a series of mixed reactors for the sake of simplicity [43, 44], and not as plug flow reactors. Moreover, the current available industrial flotation technology is effective over the size range of 15 to 150 microns of particles [11]. In this work, we consider the dense flow setting motivated by the desire to increase particle size separation range.

Significant to note that Stokes number (St), which represents a ratio of inertia to drag forces, is an important parameter in fluid-particle flows. St is useful to demonstrate the tendency of a particle to follow or deviate from the streamline. Particles having the small Stokes number follow the streamline and particles with large Stokes number deviate from the stream line [45, 46]. Stokes number which is a function of Reynolds number (Re), particles and bubble sizes (D_p and D_b), and liquid and particle densities (ρ_l, ρ_p) is defined as follows:

$$St = \frac{1}{9}\frac{\rho_p}{\rho_l}(\frac{D_p}{D_b})^2 Re \tag{2.1}$$

Flow with high St is categorized as dense flows in which the particle motion is controlled by collisions or continuous contact between particles and/or bubbles (the classical example of a collision dominated flow is fluidized bed in which the particles are suspended by the fluid and collide with each other and/or with the vessel wall). The fact of the limitation in particle size separation range, yet considering the effect of particle velocity on having a stable Stokes number for separation process, were a motivation to modify the apparatus geometry by addition of a mixer to the column geometry to extend the refining range. Mechanical flotation cells, due to the pres-

ence of mixers, provide enhanced particle-bubble collision through agitation, while flotation columns have a large quiescent zone that enables fractionation. In addition to enhanced bubble-particle collision, the use of an impeller in the well-mixed section also results in the production of fine bubbles which are favourable for fine particles attachment, while the quiescent area of the column is favourable for the separation of coarser minerals. In this regard, in order to expand the range of particle separation, and to combine the advantages of both types of flotation approaches, a novel hybrid flotation column has been constructed and is being tested by our group at University of Alberta. Therefore, there is still room for the flotation column and its modelling, for the purpose of control and monitoring, improvement.

2.1.2 Related work

The availability of a good mathematical model is necessary for the purpose of control and monitoring of the flotation process [46]. Numerous models have been presented to describe the flotation process, mostly mechanical flotation cells from macroscopic and microscopic points of view [47]. Generally, dynamic modelling of the flotation process can be categorized in two different ways: soft computing rules-based and phenomenological models [31]. Soft computing rules-based models are empirical models. According to the literature available, the most commonly-used soft computing methods in flotation processes and plants modelling are artificial neural networks [48], followed by fuzzy logic [49], genetic algorithms [50], support vector machines [22], decision trees and hybrids of these methods. Although setting clear boundaries is often not possible, phenomenological models of the flotation process can be classi-

fied as; Fundamental (based on first principle models e.g. Probabilistic, Kinetic, and Population-balance) and hybrid (based on both experimental data and first principle models). Initially, the first principle flotation models were developed analytically from the conservation of mass and the mechanisms related to bubble-bubble and bubble-particle interactions occurring in the mechanical flotation cells. In contrast, the empirical models are realized by adjusting the parameters of a mathematical relation to fit the existing experimental data. Hybrid models are determined with a mix of empirical and fundamental relationships [51].

The advantage of using empirical models is that only inputs and outputs data must be collected for the model development and less process knowledge is required. Therefore, they have a range of application limited to the specific operational condition under which they are developed. Yet fundamental models can be applied to a wider range of applications and provide a physical understanding of the process to predict concentrate grade and value recovery. While these models can also be used to analyze the process, they may be difficult to develop because particular relationships can either be unknown or impossible to isolate.

Although several first principles models have been published for mechanical cells [22, 32, 52–55], very few fundamental dynamic column flotation models have been proposed in the literature. Some of these models can be classified as micro-scale models [7, 56–59], implying that they were developed to estimate design parameters for a column flotation system, such as particle velocity [60], gas dispersion [61, 62], etc. As an example, well predicted the relative residence time between particles and liquid in a co-current mono-dispersed system using the particle slip velocity in hindered settling derived by [63]. In parallel with the fundamental models, [39, 49] have

focused on the development of soft computing based models.

Among the few reported models on column flotation, [42] provided the first reports on modelling of this unit operation. A steady state model with constant flux and gas holdup was developed to describe the concentration profiles of mineral, gangue and locked solids along the column based on axially-dispersed plug flow model of bubble and slurry phases. Further, several kinetic models have been developed to study the flotation rate based on pulp and froth dynamics [44, 64–67]. In these models, particle-bubble attachment and detachment are modelled as kinetic processes. In particular, the model proposed by [44] is based on material balance, a first-order kinetic assumption for attachment/detachment, and a vertical combination of CSTRs-in-series with the ability to handle pulp level variations. Nevertheless, a mean bubble diameter in every simulation cell is used and none of the micro-scale physical mechanisms such as bubble collision, attachment, and detachment have been considered.

In 1997, [43] presented a simultaneous solution for the air and solid phases through the column based on a population balance (PB) model. The model was based on the microscopic and macroscopic description of pulp and froth zones in which bubble coalescence and loading have been considered. A distribution of bubble sizes, particle sizes, and particle types were used. Attachment and detachment rates in Cruz's model were defined by the probability of attachment and detachment of particles from the bubbles. The column was modelled based on a vertical combination of a perfectly mixed zones. PB based modelling has been explored further to capture dynamic changes in bubble properties by bursting and coalescence in the froth phase [68]. Further studies on a relatively new research area of computational fluid dynamic - population balance (CFD-PB) simulation of bubble columns were conducted

by [69], whereas the studies were only for a two-phase system (water and air). [70] developed a new PB method for modelling bubble size distribution in two phase bubble column type reactors, which are used in many different chemical processes. Recently, [71] applied CFD for modelling of the drainage liquid in the froth. More recently, [72] set up a hyperbolic system based on the simple model published by [64] including only a froth zone and a collection zone. In this work, the flux functions are linear and velocities and gas holdup are constant over time and space. [73] took a step further and developed a simple dynamic model of two scalar conservation laws with a constant and discontinuous flux for the slurry and solids volume fractions. The model is of triangular nature since one equation can be solved independently of the other.

Among the various published contributions, some researchers concentrated on the modelling of recovery for the flotation process. The overall recovery of a mineral is a function of its recovery in both pulp and froth zones [74] which depends strongly on the knowledge of particle and liquid residence time and the flow regime [60]. It has been shown by [75] that recovery in the pulp phase is largely driven by the floatability properties of the ore, the bubble surface area, and the residence time of the particles in the pulp zone. In the froth phase, recovery is more a function of the time that particles spend in the froth, which is also a function of froth volume and froth mobility, the bubble coalescence rate, and the degree of liquid drainage from the froth [76].

The novel contributions of this chapter are: 1) a novel dynamic fundamental model for a hybrid column flotation process which accounts for bubble-particle bubble-bubble interactions is derived; 2) the hybrid column flotation process is modelled

as a series of two plug flow reactors (PFRs) and a continuous stirred tank reactor (CSTR) to represent a flotation column with a modified geometry which means a mixer has been added to the column geometry; 3) Dankwerts' boundary condition has been applied at the pulp and froth interface; 4) the model has an ability to handle different classes of bubble sizes and accounts for both macroscopic and microscopic mass transfer phenomena for hydrophobic and hydrophilic particles in the form of attached and free in the entrainment or downflow; 5) it accounts for the bubble appearance and breakage as well as temporal and spatial variation of gas holdup and fluxes.

The remainder of this paper is structured as follows: In Section 2, the column flotation process is described and modelled as a system of nonlinear coupled hyperbolic PDE-ODE system and a Dankwerts' type of boundary condition at the pulp/froth interface has been applied. Then, the state space description of the hybrid model for the modified column flotation geometry is obtained in Section 3. Section 4 addresses the numerical solution to the system of coupled PDE-ODE. The temporal spatial evolution of the system of nonlinear conservative hyperbolic PDE-ODE has been illustrated in Section 5, and the transport rate of each particles across the interface has been calculated and demonstrated in the same section. Here, the analysis of possible steady states has been provided and the effect of gas flow rates on grade and recovery of the system has been demonstrated. Finally, Section 6 provides conclusions.

2.2 Mathematical model

2.2.1 Hybrid column flotation and volumetric flows

A common column flotation apparatus consists of two zones, the pulp (collection) and the froth (cleaning) zones. However, in the unique unit operation considered in this work a mixer has been added to the bottom of the column (see Figure 2.1). The column geometry is modified by our group to expand the range of particle separation and to unify the advantages of both types of flotation approaches (mechanical cell and column flotation). Mechanical flotation cells, due to the presence of mixers, provide enhanced particle-bubble collision through agitation, while flotation columns have a large quiescent zone that enables fractionation. In addition to enhanced bubble-particle collision, the use of an impeller in the well-mixed section also results in the production of fine bubbles which are favourable for fine particles attachment, while the quiescent area of the column is favourable for the separation of coarser minerals.

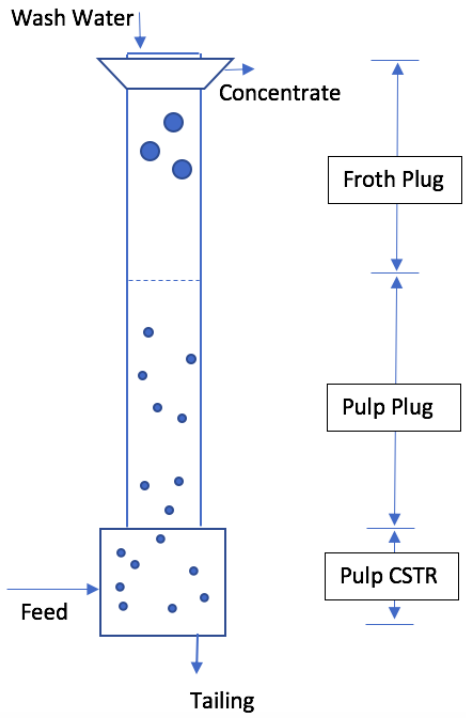

Figure 2.1: Conceptual presentation of the hybrid flotation column.

Figure 2.2: Experimental presentation of the hybrid flotation column.

The overall goal of the modelling is to capture the input to output relationships for a particular target application which can be grade and/or recovery of the value product. In this paper, in order to account for all relevant transport processes in the column, a dynamic model for a hybrid flotation column is developed that accounts for upward slurry, downward slurry, and rising air dynamics. The upward liquid phase is added to describe the effect of entrainment and the downward liquid phase is added to describe the effect of drainage on the column flotation dynamic process. Figure 2.1 illustrates the schematic of the hybrid flotation column geometry with a well-mixed zone added to a constant cross-sectional area column. The corresponding conceptual model of the flotation column indicating the volumetric flows of the feed Q_f, wash water Q_w, tailing Q_t, entrainment (upflow) Q_e, drainage (downflow) Q_r, gas Q_g and the spatially and temporal varying gas holdup $\epsilon(z,t)$. The model is comple-

mented with a population balance based model for bubble coalescence (appearance and breakage). In addition, the microscale processes happening in the column such as bubble-particle collision, attachment, as well as hydrodynamic forces of liquid and mass transfer between upflows and the downflow are considered. The comprehensive dynamic model is developed as an interconnection of three different subsystems (zones). Under the well-mixed assumption, the subsystem with the mixer is considered as a continuous stirred tank reactor (CSTR). The pulp and froth zones in the column are considered as two plug flow reactors (PFRs) in series. This is under the assumption of perfect radial mixing and no axial mixing.

In this study, the model structure shown in Figure 3.2 divides the flotation process into eight compartments: 1) slurry or liquid phase in the CSTR zone, 2) gas phase in the CSTR, 3) slurry phase, downflow in the pulp zone, 4) slurry phase, upflow in the pulp, 5) gas phase in the pulp, 6) slurry phase, downflow in the froth zone, 7) slurry phase, upflow in the froth, 8) gas phase in the froth. A solid particle can be in any of the eight compartments based on its state, e.g., attached to bubbles in the CSTR, pulp or froth zones, or detached (free) in the slurry upflow, or slurry downflow in the pulp or froth.

As illustrated in Figure 3.2(a), the dynamic mathematical model for hydrophobic particles is developed considering the bubble/particle attachment and detachment, as well as the gas and liquid transport phenomena. After collision and contact between the bubbles and minerals, hydrophobic minerals attach to the bubbles and form bubble-particle aggregates. These aggregates reach the top of the column and overflow from the top of the column as the product. Wash water sprayed from above provides cleaning action by washing down entrained particles [36, 77]. Therefore, the

interaction between rising bubbles, entrained particles, and downflow slurry leads to mass transfer of particles between the liquid and air phases as well as between the upward and downward liquid flows. The dominant phenomena of mass transfer are given by convective transport terms (as a result of the fluid motions), and the volume mass sources (sinks) are modelled as a result of physical reactions or interphase mass transfer. Moreover, the dynamic changes in bubble properties by coalescence and bursting are considered. The rates of these dynamic changes are defined based on the probabilities of interaction of different size classes of bubbles. One of the important parameters is the bubble size, which directly affects the distributions of gas holdup and consequently velocities and other states in the column.

As illustrated in Figure 3.2(b), it is assumed that there is no attachment between hydrophilic particles and bubbles and they entrained by the liquid flows. Moreover, the mass transfer between the liquid upflow and downflow due to differences in the concentration of particles in these two flows is also considered.

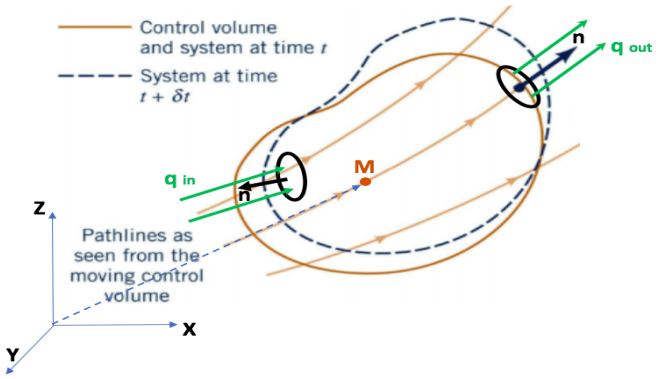

Figure 2.3: Reynolds transport theorem (RTT) schematics.

Using the Reynolds transport theorem (RTT), a mass balance based nonlinear

model presenting the reaction term in the transport-reaction model is defined for hydrophobic (valuable) and hydrophilic (gangue) particles, for each subsection. If X is a variable that varies both temporally and spatially, a scalar conservation equation in a one-dimensional domain is

$$\frac{1}{Lv}\frac{\partial X(z,t)}{\partial t} + \frac{1}{L}\frac{\partial X(z,t)}{dz} = \frac{D}{Lv}\frac{\partial^2 X(z,t)}{\partial^2 z} + \frac{gen. - cons.}{Lv} \tag{2.2}$$

where $Pe = Lv/D$, Peclet number, is a dimensionless number which defines the ratio of convection rate to the diffusive transport rate. D is the diffusion constant. In the system of column flotation under study, the Peclet number has a relatively large value so the inverse of it is a negligible term in comparison to the other terms. Therefore, equation 2.2 takes the form of a nonlinear hyperbolic PDE.

In this three-phase system, first order kinetics are used to describe the attachment/detachment of solid particles to/from the gas-bubbles (A $\underset{k_d}{\overset{k_a}{\rightleftharpoons}}$ B, where k_a is the attachment rate constant and k_d the detachment rate constant). A steady pulp/froth interface level is assumed. As reported in [7], this can be achieved by manipulating feed and tailing rates (which gives fast response) or wash water (slow response).

Finally, the mathematical model involves a set of linear ODEs representing concentrations in the CSTR zone and two sets of PDEs representing the spatial distribution of concentrations in the pulp and froth zones. In order to model the gas holdup dynamics, a set of nonlinear hyperbolic PDEs is developed to represent the air fraction distribution throughout the column (see equations 3.15, 3.17). These dynamic equations for the air and solid species concentration are solved simultaneously, and it shows the bubble-bubble and bubble-particle interactions throughout the column.

The slip velocity $u_s = v_g \pm v_l$ is defined as the velocity of gas phase relative to the

liquid phase. The average velocities, v_g and v_l, at each cross-sectional area are used. The $\pm$ sign refers to countercurrent or concurrent flow respectively. $v_g = Qg/(A\epsilon)$ and $v_l = (Qe - Qr)/(A(1-\epsilon))$ are assumed to be functions of volumetric flow rates, column cross sectional area, and gas volumetric fraction (holdup). Since gas holdup is temporal and spatial varying, velocities as functions of gas holdup also change over time along the column height.

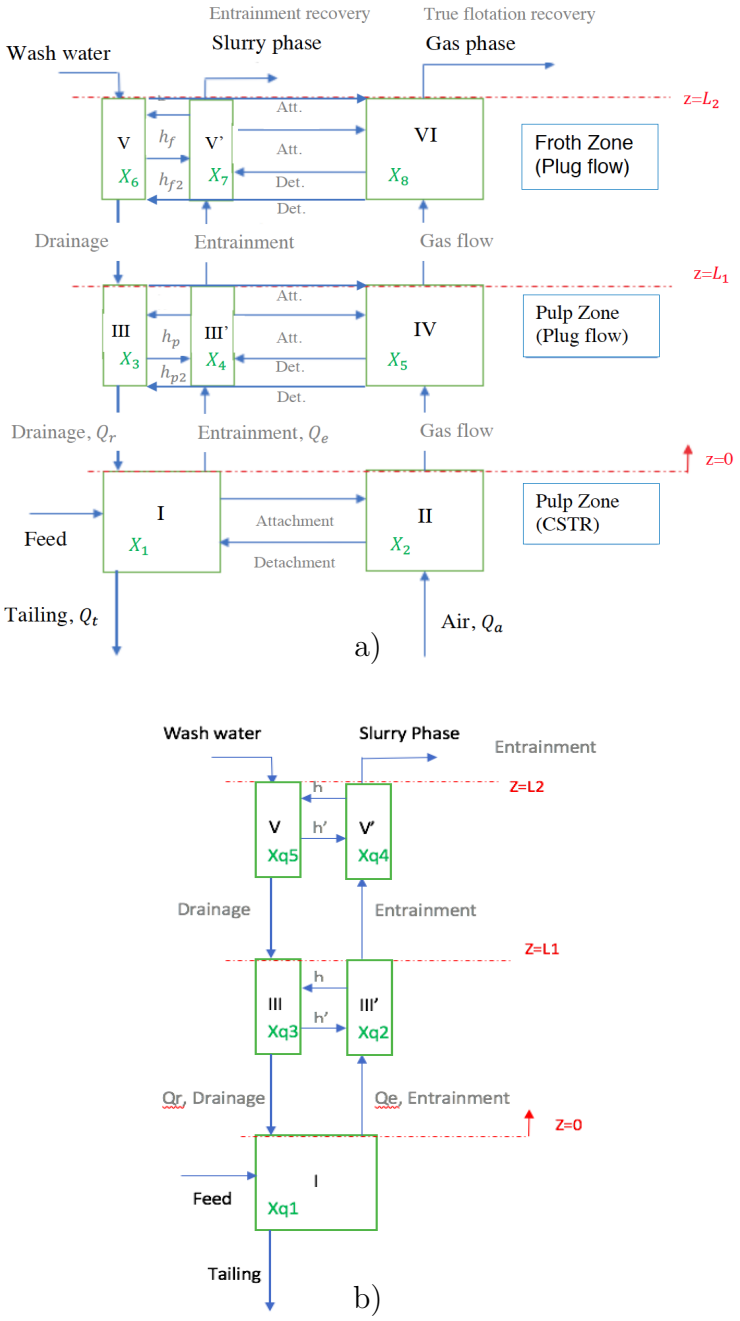

Figure 2.4: Schematic of mass transfer phenomena in a three-phase flotation column for a) hydrophobic, b) hydrophilic particles.

2.2.2 Particle models in the CSTR

For the CSTR, we apply the conservation mass balance (equation 2.2) with negligible diffusion to obtain models for hydrophobic particles in a three-phase well-mixed zone (see Figure 3.2). The state variables in the CSTR are concentrations of value mineral attached to the bubbles, $x_2(t)$, free in the liquid phase, $x_1(t)$, and free gangue particles in the liquid, $x_{q1}(t)$.

$$\frac{dx_1}{dt} = \frac{Q_f x_{1,0} - (Q_t + Q_e)x_1 + Q_r x_3(0,t)}{V_c(1-\epsilon_c)} - k_{ac}x_1 + k_{dc}x_2 \tag{2.3}$$

$$\frac{dx_2}{dt} = -\frac{Q_a x_2}{V_c \epsilon_c} + k_{ac}x_1 - k_{dc}x_2 \tag{2.4}$$

Hydrophilic particle model in the well-mixed zone is given by equation 2.5.

$$\frac{dx_{q1}}{dt} = \frac{Q_f x_{q1,0} - (Q_t + Q_e)x_{q1} + Q_r x_{q3}(0,t)}{V_c(1-\epsilon_c)} \tag{2.5}$$

2.2.3 Particle models in the pulp

The state variables in the pulp are concentrations of value minerals attached to the bubbles, $x_5(z,t)$, free in the upflow, $x_4(z,t)$, free in the downflow, $x_3(z,t)$, free gangue particles in the downflow, $x_{q3}(z,t)$, in the upflow, $x_{q2}(z,t)$, and finally gas holdup, $\epsilon_p(z,t)$.

Mass transfer between particles in counter-current upward and downward flows can be formulated as $h\Delta C$, where h is the mass transfer coefficient between upflows and downflow and ΔC is the difference between concentration of particles in these flows. Another factor that has been introduced in the modelling is the solid dropback factor k, which defines the fraction of solids drop back to the downflow liquid.

Hydrophobic particle models in the pulp are given by:

$$\frac{\partial x_3}{\partial t} = \frac{Q_r}{A\alpha_p(1-\epsilon_p)}\frac{\partial x_3}{\partial z} - k_{ap3}x_3 + kk_{dp}x_5 + h_p(x_4 - x_3) \quad (2.6)$$

$$\frac{\partial x_4}{\partial t} = \frac{-Q_e}{A(1-\alpha_p)(1-\epsilon_p)}\frac{\partial x_4}{\partial z} - k_{ap4}x_4 + (1-k)k_{dp}x_5 - h_{p2}(x_4 - x_3) \quad (2.7)$$

$$\frac{\partial x_5}{\partial t} = -\frac{Q_a}{A\epsilon_p}\frac{\partial x_5}{\partial z} + k_{ap3}x_3 + k_{ap4}x_4 - k_{dp}x_5 \quad (2.8)$$

with the associated boundary conditions that are linked to the states of the froth and the CSTR:

$$B.C.\ at\ z = L_1,\ \frac{\partial x_3(L_1,t)}{\partial z} = -K_{63}(x_6(L_1,t) - x_3(L_1,t)) \quad (2.9)$$

$$B.C.\ at\ z = 0,\ x_4(0,t) = x_1(t) \quad (2.10)$$

$$B.C.\ at\ z = 0,\ x_5(0,t) = x_2(t) \quad (2.11)$$

Models for hydrophilic particle in the pulp are given by

$$\frac{\partial x_{q3}}{\partial t} = \frac{Q_r}{A\alpha_p(1-\epsilon_p)}\frac{\partial x_{q3}}{\partial z} - h_{qp}(x_{q3} - x_{q2}) \quad (2.12)$$

$$\frac{\partial x_{q2}}{\partial t} = \frac{-Q_e}{A(1-\alpha_p)(1-\epsilon_p)}\frac{\partial x_{q2}}{\partial z} + h_{qp2}(x_{q3} - x_{q2}) \quad (2.13)$$

with the associated boundary conditions that are linked to the states of the froth and the CSTR:

$$B.C.\ at\ z = L_1,\ \frac{\partial x_{q3}(L_1,t)}{\partial z} = -K_{q35}(x_{q5}(L_1,t) - x_{q3}(L_1,t)) \quad (2.14)$$

$$B.C.\ at\ z = 0,\ x_{q2}(0,t) = x_{q1}(t) \quad (2.15)$$

2.2.4 Particle models in the froth

Models for hydrophobic particles in the froth and interface zones follow the schematic of Figure 3.2. The state variables for the froth zone are the concentration of value

particles free in the upflow, $x_7(z,t)$, free in the downflow, $x_6(z,t)$, attached to bubbles, $x_8(z,t)$, concentration of free gangue particles in the upflow, $x_{q4}(z,t)$, in the downflow, $x_{q5}(z,t)$, and the gas holdup, $\epsilon_f(z,t)$.

$$\begin{aligned}
\frac{\partial x_6}{\partial t} &= \frac{(Q_r+Q_w)}{A\alpha_f(1-\epsilon_f)}\frac{\partial x_6}{\partial z} - k_{af6}x_6 + k_2k_{df}x_8 + h_f(x_7-x_6) && (2.16)\\
\frac{\partial x_7}{\partial t} &= \frac{-Q_e}{A(1-\alpha_f)(1-\epsilon_f)}\frac{\partial x_7}{\partial z} - k_{af7}x_7 + (1-k_2)k_{df}x_8 + ... && (2.17)\\
&... \quad -h_{f2}(x_7-x_6)\\
\frac{\partial x_8}{\partial t} &= \frac{-Q_a}{A\epsilon_f}\frac{\partial x_8}{\partial z} + k_{af6}x_6 + k_{af7}x_7 - k_{df}x_8 && (2.18)
\end{aligned}$$

with associated boundary conditions that are linked to the states of the pulp.

$$B.C.\ \ at\ \ z=L_1,\ \ \frac{\partial x_7(L_1,t)}{\partial z} = -K_{47}(x_4(L_1,t)-x_7(L_1,t)) \qquad (2.19)$$

$$B.C.\ \ at\ \ z=L_1,\ \ \frac{\partial x_8(L_1,t)}{\partial z} = -K_{58}(x_5(L_1,t)-x_8(L_1,t)) \qquad (2.20)$$

We have made the assumption that some part of the flow is recycled back to the column at the top. Therefore, the boundary condition at the top of the column is modified as $x_6(L_2,t) = \beta x_7(L_2,t)$. In this modelling framework, we assume that $\beta = 0.5$ of the concentration of free hydrophobic particles on top of the column is returning to the downflow. This modelling framework permits to account for the top recycle of hydrophobic particles which impacts overall dynamics of the entire column.

Hydrophilic particle models in the froth/interface are

$$\frac{\partial x_{q5}}{\partial t} = \frac{(Q_r + Q_w)}{A\alpha_f(1-\epsilon_f)}\frac{\partial x_{q5}}{\partial z} - h_{qf}(x_{q5} - x_{q4}) \tag{2.21}$$

$$\frac{\partial x_{q4}}{\partial t} = \frac{-Q_e}{A(1-\epsilon_f)(1-\alpha_f)}\frac{\partial x_{q4}}{\partial z} + h_{qf2}(x_{q5} - x_{q4}) \tag{2.22}$$

$$B.C.\ \ at\ \ z = L_2,\ \ x_{q5}(L_2, t) = 0 \tag{2.23}$$

$$B.C.\ \ at\ \ z = L_1,\ \ \frac{\partial x_{q4}(L_1, t)}{\partial z} = -K_{q24}(x_{q2}(L_1, t) - x_{q4}(L_1, t)) \tag{2.24}$$

2.2.5 Gas holdup model

Gas holdup models (given as equations 4.23-2.30) account for the bubble coalescence in the pulp and froth zones. These models represent the changes of gas fraction between bubbles of different size classes that are proportional to the number of collisions between those bubbles and other bubble size classes in the system. In the present work, bubbles are categorized into $n = 3$ discrete size classes for convenience, but there is no conceptual restriction on the number of bubble size classes.

$$\frac{\partial \epsilon_{p,n}(z,t)}{\partial t} = -v_{\epsilon,n,p}\frac{\partial \epsilon_{p,n}(z,t)}{\partial z} - \mathcal{D}_{p,n}(z,t) + \mathcal{A}_{p,n}(z,t) \tag{2.25}$$

$$B.C.\ \ at\ \ z = 0,\ \ \epsilon_{p,n}(0,t) = \epsilon_{c,n}(t) \tag{2.26}$$

$$\epsilon_p(z,t) = \sum_{n=1}^{3} \epsilon_{p,n}(z,t) \tag{2.27}$$

$\mathcal{A}_{p,n}(z,t)$ and $\mathcal{D}_{p,n}(z,t)$ in equation 4.23 are measures of how many interactions result in coalescence in each bubble size class.

Gas fraction evolution in the froth and interface are modelled as equation 3.17.

$$\frac{\partial \epsilon_{f,n}(z,t)}{\partial t} = -v_{\epsilon,n,f}\frac{\partial \epsilon_{f,n}(z,t)}{\partial z} - \mathcal{D}_{f,n}(z,t) + \mathcal{A}_{f,n}(z,t) \tag{2.28}$$

$$B.C.\ \ at\ \ z = L_1,\ \ \frac{\partial \epsilon_f(L_1,t)}{\partial z} = -K_\epsilon(\epsilon_{p,n}(L_1,t) - \epsilon_{f,n}(L_1,t)) \tag{2.29}$$

$$\epsilon_f(z,t) = \sum_{n=1}^{3} \epsilon_{f,n}(z,t) \tag{2.30}$$

The total gas holdup used in the above equations is the summation of gas holdup of the three bubbles size classes (see equations 2.27 and 2.30). Computation of gas holdup propagation through the column requires the determination of the velocity of swarm of bubbles in each bubble size classes. In this work, the terminal velocity of a single bubble proposed by [78] and applied by [44] to calculate the rising velocity of the swarm of bubbles. The velocity of each bubble size classes in each zone, $v_{\epsilon,n,i}$, has been calculated using the mean diameter of each of the three bubble size classes using the following set of equations. Solid particles give a slurry viscosity μ_i which has an opposite effect on the bubble rise velocity.

$$\begin{aligned} v_{\epsilon,n,i} &= \frac{\Gamma_i((1+3.36C_cDb_n^2)^{0.5}-1)^2}{2C_cDb_n} \\ \Gamma_i &= \frac{g(\rho_{l,i}-\rho_{g,i})}{9\mu_i} \\ C_c &= 110 + 260(1-exp(-0.11c));\ \ c \leqslant 6cm^3/100l \end{aligned} \tag{2.31}$$

In the present work, it is assumed that the total increase/decrease in the volume fraction of bubbles can be defined as a physical reaction term. The approaches taken in the works of [79], [42], and further extended and applied by [43] are considered to define an adequate mathematical representations of coalescence events. These terms are measures of how many interactions results in coalescence (result in appearance

and breakage) in each bubble size classes that could be applied to the entire column. Therefore, the total rise in the gas holdup of bubbles in the size class n due to bubble coalescence with bubbles of smaller size classes, can be quantified using

$$\mathcal{A}_{i,n} = 0.5 \sum_{j}^{Nl} \phi_{i,n-j,j} \frac{\epsilon_{n-j}\epsilon_j}{\sum_{l}^{Nl} \frac{\epsilon_l Db_{n-j}^3 Db_j^3}{Db_n^3 Db_l^3}} \tag{2.32}$$

The total decline in bubbles holdup in the size class n due to collision with bubbles of all size classes is

$$\mathcal{D}_{i,n} = \sum_{j}^{Nl} \phi_{i,n,j} \frac{\epsilon_n \epsilon_j}{\sum_{l}^{Nl} \epsilon_l \frac{Db_j^3}{Db_l^3}} \tag{2.33}$$

Nl is the total number of discrete size classes in the distribution, $l \neq 0$. The collision success factor, ϕ, is an empirically defined parameter which is a function of the colliding bubble sizes or other factors such as type or amount of flotation reagents. Some flotation reagents may effect the bubble surface in a way that promote coalescence, which is undesirable and decreases the effective bubble surface area.

$$\phi_{i,n,j} = \frac{\xi_{i,n,j}}{(Db_n + Db_j)^2} \tag{2.34}$$

In the pulp section, it is assumed that the probability of bubble coalescence is higher than the probability of bubble breakage, $\mathcal{A}_{p,n} > \mathcal{D}_{p,n}$. However, in the froth section it is assumed that the probability of breakage is higher than the probability of coalescence, $\mathcal{A}_{f,n} < \mathcal{D}_{f,n}$.

Efforts of Smoluchowski in considering particle aggregation to be equivalent to a series of chemical reactions, is the basis for our today understanding of the process of particle collisions in fluids [80]. The coagulation of colloidal particles is considered as a two-step process. The first is the collision of particles and the second is the

attachment process. In flotation, detachment is considered as the third process. The attachment and detachment rates, for each bubble size classes, in the CSTR zone have been calculated using the formula presented by [46] and later on applied by [81, 82] which can be represented as equations 2.36-2.54. The process of particle collision is governed by physical factors such as particle, velocities and sizes of particles and bubbles, densities of particle and fluid, diffusion, temperature, fluid shear. Whether the particle will attach to the bubble depends on conditions at the interface between fluid and particles, surface charges and potentials, etc. The particle-bubble detachment is determined by the attachment forces minus detachment forces. If the particles are randomly distributed through the fluid, their collision frequency (number of collisions per unit volume per unit time) is a function of gas flow rate, rise and fluctuating velocities, and sizes of particles and bubbles. Particles detachment frequencies depend on introduced turbulences.

$$k_{ac} = \mathcal{Z}_1 p_c p_a p_s \tag{2.35}$$

$$k_{dc} = \mathcal{Z}_2 p_d \tag{2.36}$$

where, the collision frequency, $\mathcal{Z}_1$, detachment frequency, $\mathcal{Z}_2$, probability of bubble-particle collision, p_c, probability of bubble-particle attachment, p_a, probability of bubble-particle aggregate stability, p_s, and probability of bubble-particle detachment,

p_d are given by [82–88] as follows:

$$\mathcal{Z}_1 = 30\frac{Q_a(U_b^2+U_p^2)^{1/2}}{\pi d_b^2 V_{cell}\nu_b}(\frac{d_p+d_b}{2})^2 \tag{2.37}$$

$$\mathcal{Z}_2 = 2^{\frac{1}{2}}\mathcal{E}^{1/3}(d_p+d_b)^{\frac{-2}{3}} \tag{2.38}$$

$$p_c = 3sin^2\theta_t exp(\mathcal{H})\frac{d_p}{d_b} \tag{2.39}$$

$$\mathcal{H} = 3K_3 cos\theta_t(ln\frac{d_b}{d_p}-1.8) - \frac{9K_3(\frac{2}{3}+\frac{cos^3\theta_t}{3}-cos\theta_t)}{\frac{6d_p sin^2\theta_t}{d_b}} \tag{2.40}$$

$$p_a = sin^2(2arctan\ exp(-t_{ind}\frac{2(v_p+v_b)+v_b(\frac{d_b}{d_b+d_p})^3}{d_b+d_p})) \tag{2.41}$$

$$p_d = \frac{1}{1+\frac{F_{at}}{F_{det}}} \tag{2.42}$$

$$p_s = 1-p_d \tag{2.43}$$

$$K_3 = v_b(\rho_p-\rho_{sl})d_p^{\frac{2}{9}}d_b\nu_l \tag{2.44}$$

The bubble rise velocity, v_b, and particle velocity, v_p are:

$$v_b = (\frac{4gd_b}{3c_d})^{\frac{1}{2}} \tag{2.45}$$

$$v_p = \frac{Q_{e,pc}-Q_{r,pc}}{0.16^2} \tag{2.46}$$

$$c_d = 0.28\frac{(1+0.0921\Phi^{\frac{1}{2}}+1)}{(1+0.0921\Phi^{\frac{1}{2}}-1))^2} \tag{2.47}$$

$$\Phi = max(1.14\times 10000, \frac{4}{3}\frac{\rho_{sl}^2 g d_b^2}{\mu_{sl}^2}) \tag{2.48}$$

$$t_{ind} = 100 * d_p^{0.99} \tag{2.49}$$

Generalized Sutherland equation:

$$\frac{F_{at}}{F_{det}} = 3\frac{1-cos\theta_d\gamma}{g(\rho_p-\rho_{sl}*(\frac{1}{2}+\frac{3}{4}cos\frac{\theta_d}{2}))}\frac{1+\frac{d_p}{d_b}}{d_p^2} \tag{2.50}$$

The relative turbulent fluctuating velocities of bubbles, U_b, and the relative turbulent

fluctuating velocities of particles, U_p are:

$$U_b = 0.33(\mathcal{E}^{\frac{4}{9}} \frac{d_b^{\frac{7}{9}}}{\nu_l^{\frac{1}{3}}} \frac{\rho_g - \rho_{sl}}{\rho_{sl}})^{\frac{1}{3}} \tag{2.51}$$

$$U_p = 0.33(\mathcal{E}^{\frac{4}{9}} \frac{d_p^{\frac{7}{9}}}{\nu_l^{\frac{1}{3}}} \frac{\rho_p - \rho_{sl}}{\rho_{sl}})^{\frac{1}{3}} \tag{2.52}$$

$$\mathcal{E} = 0.8 * \frac{P}{\rho_l V} \tag{2.53}$$

$$P = \rho_{sl} * P_0 * N^3 * D_l^5 \tag{2.54}$$

where $\mathcal{E}$ is the turbulent dissipation energy, $[\frac{W}{kg}]$. It is assumed that only 80 % of the maximum power input is used. P is power dissipation in a stirred vessel . P_0 is a dimensionless power number, D_l is the impeller diameter, N is the number of impeller revolutions per second, V is the volume swept by the impeller, ρ_l is the liquid density, ν_l is the liquid viscosity, and γ is the liquid surface tension, $\frac{N}{m}$. θ_t is the the maximum possible collision angle of the particle on the surface of the bubble beyond which collision is prevented, θ_d is the detachment angle [88].

To calculate final values of attachment and detachment rates, k_{ac} and k_{dc}, the following averaging method has been applied.

$$k_{ac} = \frac{k_{ac,1}\epsilon_{c,1} + k_{ac,2}\epsilon_{c,2} + k_{ac,3}\epsilon_{c,3}}{\epsilon_{c,1} + \epsilon_{c,2} + \epsilon_{c,3}} \tag{2.55}$$

$$k_{dc} = \frac{k_{dc,1}\epsilon_{c,1} + k_{dc,2}\epsilon_{c,2} + k_{dc,3}\epsilon_{c,3}}{\epsilon_{c,1} + \epsilon_{c,2} + \epsilon_{c,3}} \tag{2.56}$$

where $\epsilon_{c,n}$, $n = 1, 2, 3$ represents gas holdup for each of the three bubble size classes in the CSTR/well-mixed zone.

2.2.6 Interface boundary conditions

In the previous reported works it is assumed that the concentration of particles below and above the interface are equal. Therefore, the typical Dirichlet type of boundary condition has been implemented:

$$x_3(L_1,t) = x_6(L_1,t);\ x_4(L_1,t) = x_7(L_1,t);\ x_5(L_1,t) = x_8(L_1,t) \tag{2.57}$$
$$x_{q3}(L_1,t) = x_{q5}(L_1,t);\ x_{q2}(L_1,t) = x_{q4}(L_1,t)$$

However, in this work, boundary conditions at the interface has been modified to the Danckwerts' boundary condition:

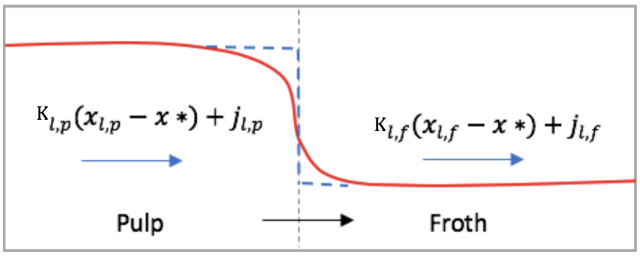

Figure 2.5: Schematic of concentration profile across the interface, x^* is the concentration at the interface

$$j_{l,p} + K_{l,p}(x_{l,p} - x^*) = j_{l,f} + K_{l,f}(x_{l,f} - x^*) \tag{2.58}$$

Figure 2.5 illustrates the associated exchange of fluxes at the interface. It is assumed that the driving force for movement of the particles just above the interface (froth

side) is both gradient-driven and linear while the driving force for the movement of particles just below the interface (pulp side) is of a linear type which means the gradient-driven flux in the pulp, $j_{l,p}$, in equation 2.58 is negligible. It is also assumed that transfer coefficients of the particles below and above the interface are equal; $K_{4,p} = K_{7,f} = K_{47}$; $K_{5,p} = K_{8,f} = K_{58}$; $K_{q2,p} = K_{q4,f} = K_{q24}$. Therefore, the general form of boundary condition at the interface as demonstrated in equation 2.58, will be simplified for each states as in equations 2.9, 2.14, 2.19, 2.20, 2.24, 2.29. The modification of boundary conditions are proposed according to the fact that the flow in the pulp side of the interface lifts the particles to the interface, after the particles pass through the interface as a barrier, they move to the froth side. However, at the interface between the CSTR and pulp still of the Dirichlet type and they are well-posed to guarantee existence of smooth solutions.

2.3 Grade and Recovery

Efficiency of separation in column flotation is directly related to the recovery and grade of the value particle, which can be affected by many factors. In particular, the expression for mineral recovery is defined as ratio of the amount of valuable particle in the outlet and the amount of valuable particles in the feed, and is given as follows:

$$\begin{aligned} Recovery(A) &= 100 \times \frac{Amount\ of\ particle\ A\ in\ the\ concentrate\ (outlet)}{Amount\ of\ particle\ A\ in\ the\ feed\ (inlet)} \\ &= 100 \times \frac{Q_a x_8|_{z=L_2} + Q_c x_7|_{z=L_2}}{Q_f x_{1,0}} \end{aligned} \tag{2.59}$$

Along the same line, the grade of valuable particle in the concentrate outlet stream is calculated as:

$$Grade(A)\ in\ the\ concentrate =$$

$$= 100 \times \frac{Amount\ of\ particle\ A\ in\ the\ concentrate\ (outlet)}{Total\ amount\ of\ solids\ in\ the\ concentrate\ (A+B+C+...)}$$

Hence, the grade expression is based on concentration and is calculated as the concentration ratio of valuable minerals to the summation of concentrations of other minerals in the concentrate (in this case attached and free hydrophobic and free hydrophilic particles), as follows:

$$Grade(A)\ in\ the\ concentrate = 100 \times \frac{Q_a x_8|_{z=L_2} + Q_c x_7|_{z=L_2}}{Q_a x_8|_{z=L_2} + Q_c x_7|_{z=L_2} + Q_c x_{q4}|_{z=L_2}} \quad (2.60)$$

Note the concept of 'grade' applies to all other streams as well, not just the concentrate, while 'recovery' is typically only used for the concentrate.

2.4 Matrix representation of the model

The matrix representation for the well-mixed zone, given that $\hat{X}_1 = \begin{bmatrix} x_1 & x_2 & x_{q1} \end{bmatrix}^T$, is:

$$\begin{aligned} \frac{d\hat{X}_1}{dt} &= \hat{A}_1\hat{X}_1 + \hat{B}_1 \quad (2.61) \\ \hat{A}_1 &= \begin{bmatrix} \frac{-(Q_t+Q_e)}{V_c(1-\epsilon_c)} - k_{ac} & k_{dc} & 0 \\ k_{ac} & -k_{dc} - \frac{Q_a}{\epsilon_c V_c} & 0 \\ 0 & 0 & \frac{-(Q_t+Q_e)}{(1-\epsilon_c)V_c} \end{bmatrix} \\ \hat{B}_1^T &= \begin{bmatrix} \frac{Q_f x_{1,0}+Q_r x_3(0,t)}{V_c(1-\epsilon_c)} & 0 & \frac{Q_f x_{q1,0}+Q_r x_{q3}(0,t)}{V_c(1-\epsilon_c)} \end{bmatrix} \end{aligned}$$

In the pulp, $\hat{X}_2 = \begin{bmatrix} x_3 & x_4 & x_5 & x_{q2} & x_{q3} \end{bmatrix}^T$, and

$$\frac{\partial \hat{X}_2}{\partial t} = -V_2 \frac{\partial \hat{X}_2}{\partial z} + \hat{A}_2 \hat{X}_2 \tag{2.62}$$

$$\hat{A}_2 = \begin{bmatrix} -k_{a3p} - h_p & h_p & kk_{dp} & 0 & 0 \\ h_{p2} & -k_{a4p} - h_{p2} & (1-k)k_{dp} & 0 & 0 \\ k_{ap3} & k_{a4p} & -k_{dp} & 0 & 0 \\ 0 & 0 & 0 & -h_{qp2} & h_{qp2} \\ 0 & 0 & 0 & h_{qp} & -h_{qp} \end{bmatrix}$$

$V_2 = diag(\begin{bmatrix} \frac{-Qr}{A\alpha_p(1-\epsilon_p)} & \frac{Qe}{A(1-\alpha_p)(1-\epsilon_p)} & \frac{Qa}{A\epsilon_p} & \frac{-Qr}{A\alpha_p(1-\epsilon_p)} & \frac{Qe}{A(1-\alpha_p)(1-\epsilon_p)} \end{bmatrix})$ which presents a matrix with diagonal elements while off diagonal elements are zero. In equation 2.62, velocity terms denote the direction of the transport (positive velocity refers to the transport from the top of the column to the bottom, and negative represents transport from the bottom to the top).

In the froth zone, $\hat{X}_3 = \begin{bmatrix} x_6 & x_7 & x_8 & x_{q4} & x_{q5} \end{bmatrix}^T$, and

$$\frac{\partial \hat{X}_3}{\partial t} = -V_3 \frac{\partial \hat{X}_3}{\partial z} + \hat{A}_3 \hat{X}_3 \tag{2.63}$$

$$\hat{A}_3 = \begin{bmatrix} -k_{a6p} - h_f & h_f & k_f k_{df} & 0 & 0 \\ h_{f2} & -k_{a7f} - h_{f2} & (1-k_f)k_{df} & 0 & 0 \\ K_{af6} & K_{a7f} & -k_{df} & 0 & 0 \\ 0 & 0 & 0 & -h_{qf2} & h_{qf2} \\ 0 & 0 & 0 & h_{qf} & -h_{qf} \end{bmatrix}$$

$V_3 = diag(\begin{bmatrix} \frac{-(Qr+Qw)}{A\alpha_f(1-\epsilon_f)} & \frac{Qe}{A(1-\alpha_f)(1-\epsilon_f)} & \frac{Qa}{A\epsilon_f} & \frac{Qe}{A(1-\alpha_f)(1-\epsilon_f)} & \frac{-(Qr+Qw)}{A\alpha_f(1-\epsilon_f)} \end{bmatrix})$.

2.5 Numerical method

In the governing system of differential equations (PDEs) and ordinary differential equations (ODEs) the independent variables are time $t > 0$ and height $z \in \mathbb{R}$. The unknowns are the gas holdup $\epsilon \in [0, 1)$ and mass concentration of attached and free hydrophobic and hydrophilic solids through the column. All 16 states (unknowns) in the column are functions of z and t and 3 states (unknowns) in the CSTR are functions of t. The temporal and spatial varying gas holdup accounts for the coalescence of possibly varying three size classes of bubbles in pulp and froth. The analysis of possible steady states represent the stationary modes of operation of a flotation column without changing control parameters. The resulting steady states are layers of concentrations of bubbles for different bubble size classes, concentrations of attached (separated) and free particles (hydrophobic and hydrophilic) through the column.

The numerical simulation of the hybrid three phase model of boundary coupled hetero-directional hyperbolic PDE-ODE system has been conducted. The initial set of simulation studies was performed by numerically integrating the model given by equations 2.61, 2.62 and 2.63, using backward Euler discretization in space and forward in time such that the numerical stability of the simulation is preserved (see Figure 2.6).

In this method, approximately $600,000$ iterations were needed to reach the convergence to the operational steady state. During the computation process, an arbitrary initial gas holdup, attached and free hydrophobic particles concentration profiles, free hydrophilic particles concentration profiles, as well as initial velocities are assumed. Gas holdup, concentration of attached and free hydrophobic particles, and

concentration of free hydrophilic particles, as well as velocities are updated in each iteration to achieve convergence to the steady state.

The rate of transport of particles across the interface is calculated by multiplying the concentrations and propagation velocities of each states at the interface and is given by

$$f_{x3} = \frac{Q_r}{A\alpha_p(1-\epsilon_p(L_1,t))}x_3(L_1,t) \tag{2.64}$$

$$f_{x4} = \frac{-Q_e}{A(1-\alpha_p)(1-\epsilon_p(L_1,t))}x_4(L_1,t) \tag{2.65}$$

$$f_{x5} = \frac{Q_a}{A\epsilon_p(L_1,t)}x_5(z,t) \tag{2.66}$$

$$f_{x6} = \frac{Q_r+Q_w}{A\alpha_f(1-\epsilon_f(L_1,t))}x_6(L_1,t) \tag{2.67}$$

$$f_{x7} = \frac{-Q_e}{A(1-\alpha_f)(1-\epsilon_f(L_1,t))}x_7(L_1,t) \tag{2.68}$$

$$f_{x8} = \frac{-Q_a}{A\epsilon_f(z,t)}x_8(z,t) \tag{2.69}$$

$$f_{xq2} = \frac{-Q_e}{A(1-\alpha_p)(1-\epsilon_p(L_1,t))}x_{q2}(L_1,t) \tag{2.70}$$

$$f_{xq3} = \frac{Q_r}{A\alpha_p(1-\epsilon_p(L_1,t))}x_{q3}(L_1,t) \tag{2.71}$$

$$f_{xq4} = \frac{-Q_e}{A(1-\epsilon_f(L_1,t))(1-\alpha_f)}x_{q4}(L_1,t) \tag{2.72}$$

$$f_{xq5} = \frac{Q_r+Q_w}{A\alpha_f(1-\epsilon_f(L_1,t))}x_{q5}(L_1,t) \tag{2.73}$$

2.6 Results and Discussion

A hydrophobic mineral in a flotation column is collected through two processes: particle-bubble attachment and/or entrainment of the particle within the boundary layers and wake of the bubble. Figure 2.6(a) demonstrates the spatiotemporal prop-

agation of the concentration of attached particles to bubbles in the pulp and froth and illustrates how the arbitrary initial profile is transported across the column and washes out over time in approximately twelve minutes (which is the approximate residence time of the column). Along the same lines, the evolution of the CSTR states (see Figure 2.6(b)) influences the state evolution through the boundary condition and propagates through the column and after approximately twenty five minutes reaches the steady-state profile. As can be seen from the propagating wave from the bottom to the top of the column, the hyperbolic PDE characteristics describing the velocity of propagation are nonlinear, which means that gas holdup increases in velocity along the column. The observed increasing trend of attached hydrophobic particle concentration in the CSTR in Figure 2.6(b) is as expected. This accumulation over the time is due to the slower motion of the particle-bubble aggregates.

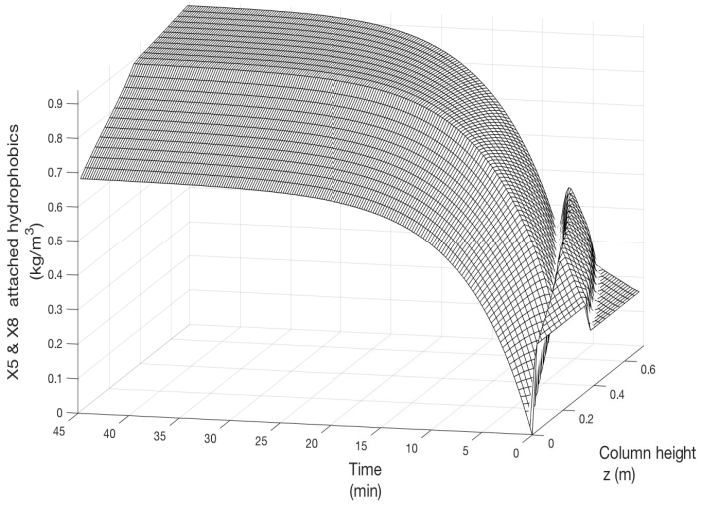

a)

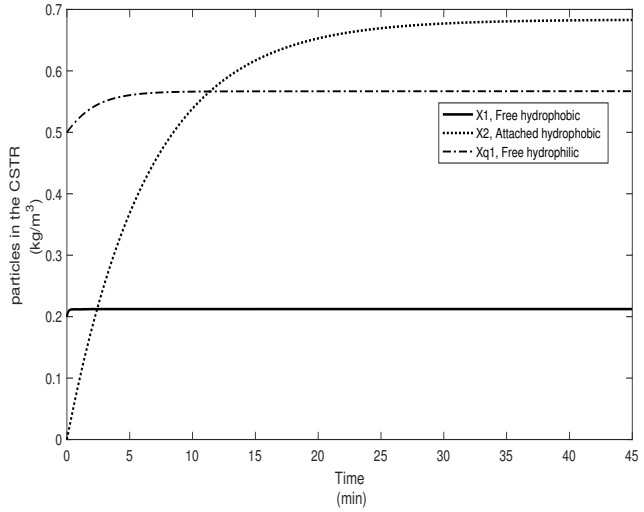

b)

Figure 2.6: a) The concentration of attached hydrophobic particles through the column, b) the concentration of attached, free hydrophobic and free hydrophilic particles in the well-mixed zone.

Figure 2.7(a) illustrates the spatiotemporal concentration propagation of the free

hydrophobic particles which are subject to entrainment. Figure 2.7(b) shows evolution of valuable particles dropped down from the entrainment or detached from bubbles. The residence time for the free hydrophobic particles, in both upward and downward flows, are much less than the residence time for the attached particles. In other words, facilitated transport of the attached particles by the bubbles is related to many factors such as the attachment/detachment rates of particles to/from the bubbles, bubble size classes and bubble velocities, etc. On the other hand, the amount of free particles transported in the entrainment is smaller in comparison to the amount of attached particles, which is more desirable from the practical point of view to separate more valuable particles selectively, than by entrainment which contains some gangue particles as well, in the free form.

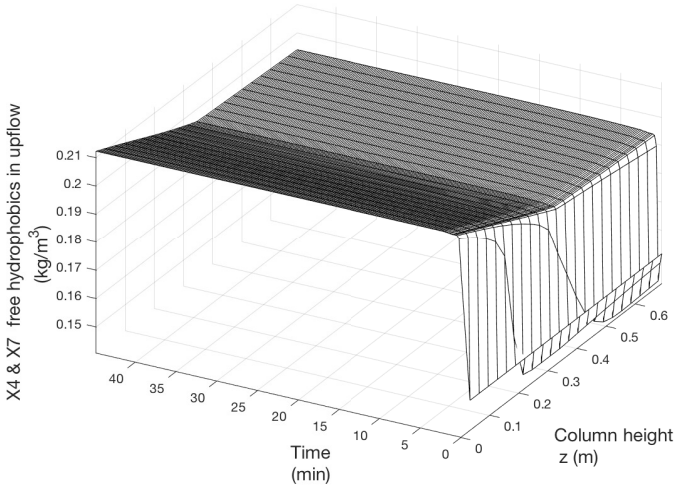

a)

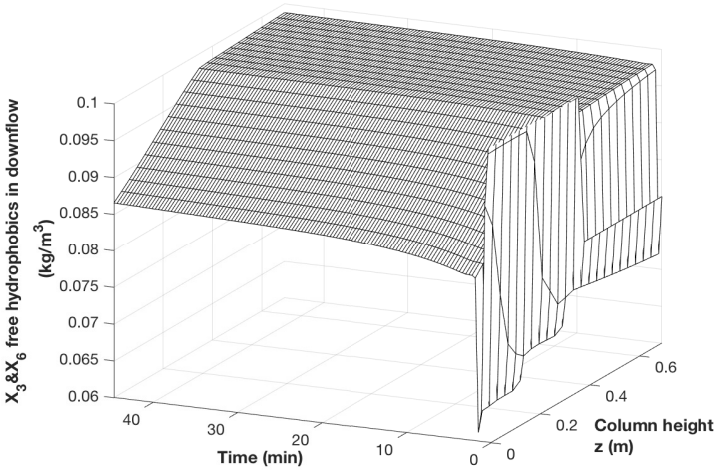

b)

Figure 2.7: a) The concentration of free hydrophobic particles through the column in downflow, b) in upflow.

Figure 2.8 demonstrates the propagation of hydrophilic minerals removal (drain-

ing) to the downflow due to the cleaning effect of wash water. This phenomenon tends to promote froth stability.

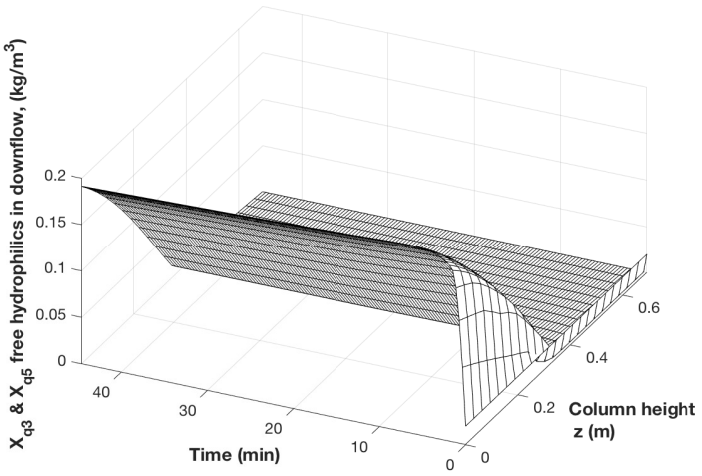

Figure 2.8: The concentration of free hydrophilic particles through the column in downflow.

Figure 2.9 shows the temporal-spatial propagation of gas holdup of three different bubble size classes through the column height, separately. The figure illustrates that there are interactions between bubbles in a bubble swarm. The results are under the assumption that the diameters of the three bubble classes in the froth are greater than those of in the pulp, yet constant in each zone. Among all the states in the column, gas holdup (see Figure 2.9) and consequently the attached particles to the bubble, X_8 (see Figure 2.6) are the slowest.

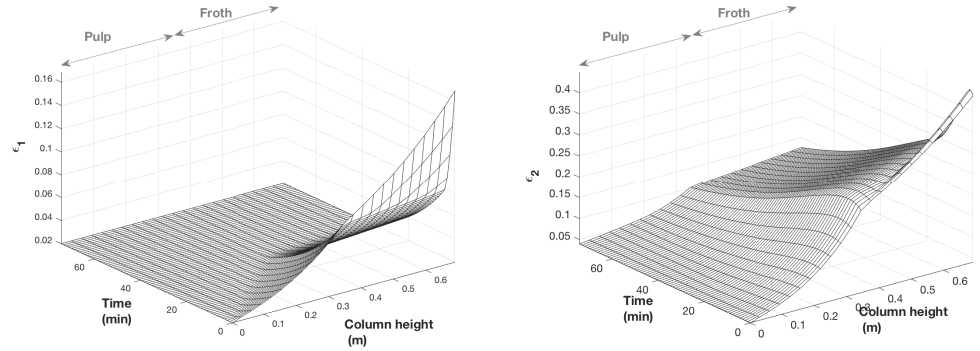

a)

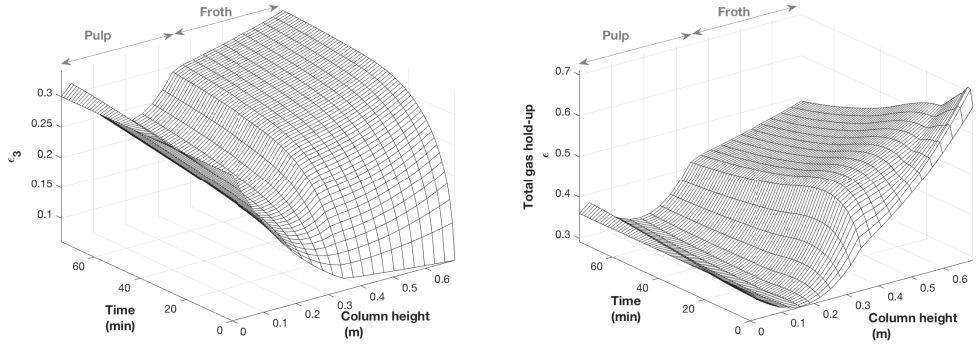

b)

Figure 2.9: Propagation of gas holdup for three bubble size classes (left(a), left(b), right(a)) and total gas holdup through the column (right(b))

At the steady state, the concentration of attached hydrophobic particles increases, while the concentration of free hydrophobic particles in the upflow decreases, through the column from the pulp to the froth. From the froth to the pulp, the concentration of free hydrophobic particles in the downflow decreases (see Figure 2.10).

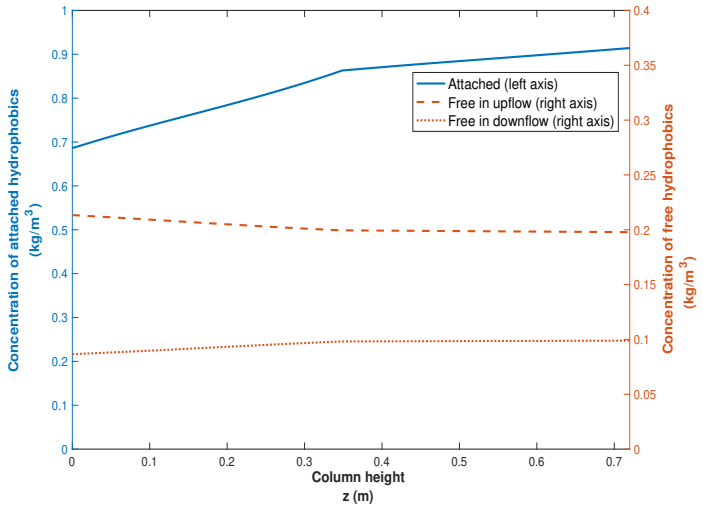

Figure 2.10: The steady state propagation of hydrophobic particles concentration through the column with Danckwerts' boundary conditions at the interface

Figure 2.11 shows the temporal propagation of recovery and grade of hydrophobic particles in the concentrate (in the hybrid flotation column and its conventional flotation column), separately. The figure illustrates that grade of value minerals in the concentrate at the top of the column (using equation 2.60) increase over time and reaches its final value of 79% (out of 100%) after almost 25 mins. Moreover, recovery increases to its maximum value of 75% in 25 minutes. This simulation has been done for mineral pair with densities of $4200 kg/m^3$ and $2600 kg/m^3$.

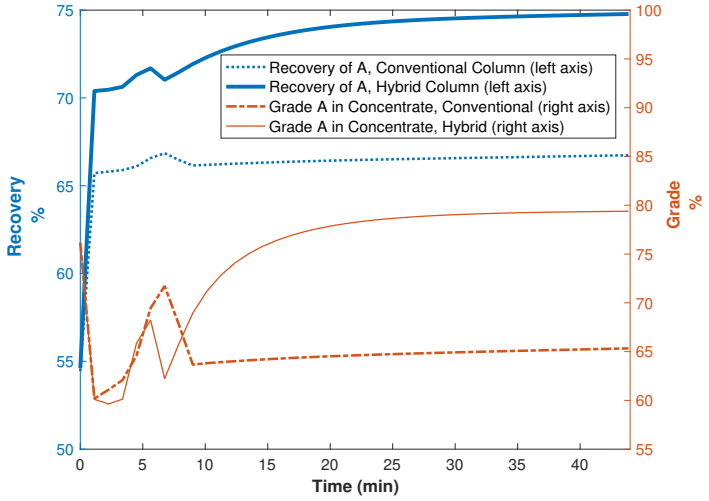

Figure 2.11: Propagation of recovery and grade of hydrophobic particles in the concentrate in a hybrid flotation column vs a conventional flotation column .

Since, the hybrid column is investigated, one needs to compare its performance to a conventional column. In this regard, the result of hybrid column with the simulation results of the conventional column in which no well-mixed section is incorporated is compared (see Figure 2.11). Figure 2.11 shows the positive effect of the addition of CSTR to the geometry of the column and simulation results demonstrate that both grade and recovery increases in this case due to the mixing in the CSTR section of the hybrid column.

Figure 2.12 illustrates that the gas holdup of bubbles in smallest size class reaches almost a constant value throughout the column, the gas holdup of bubbles in the middle and the largest size classes increases up to the top of the column. The figure also demonstrates the reliability of the simulated results in this work. The steady state simulated profile of the gas holdup through the column (of the same condition)

is very close to the empirical data determined by [43] through a series of conductivity measurements.

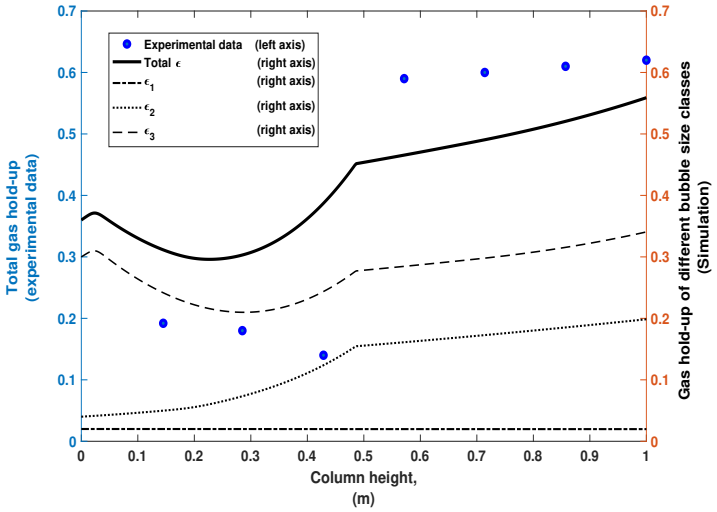

Figure 2.12: The steady state propagation of gas holdup through the column with Danckwerts' boundary condition at the interface; Experimental data for gas holdup obtained through the conductivity measurement by Cruz 1997 is used for model verification (Simulation is conducted for the same conditions: $Q_a = 0.002m^3/min$, initial $\epsilon_c = [0.02, 0.02, 0.2]$, constant froth depth)

Since Danckwerts' boundary condition is applied at the interface, the model accounts for time varying fluxes crossing the interface, and the transport rate across the interface over time is calculated (see Figure 2.13). Experimental validation for the transport gradient at the interface is difficult to be realized in practice, this is the reason why the Dankwerts' boundary condition is proposed as the most general boundary condition to capture the transport across the froth/pulp interface.

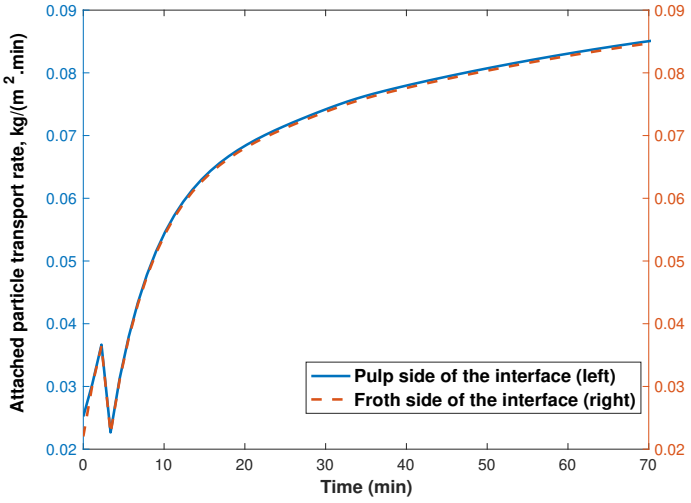

Figure 2.13: Transport rate of attached hydrophobic particles across the interface.

2.6.1 Effect of gas velocity

Although it is not experimentally validated for this system, the correlation proposed by [89] relating gas holdup in the well-mixed zone to gas velocity, impeller specifications, and fluid properties is used:

$$\epsilon_c = 0.25(\frac{P_g}{V_l})^{0.27} u_g^{0.525}(1+\psi)^{-0.85} \tag{2.74}$$

$$P_g = 0.65P(1+\frac{u_g}{ND_l})^{-1}(1+0.5*\psi)^{0.4}$$

$$P = N_p \rho_{sl} N^3 D_l$$

where ψ is the average solid volume fraction, P_g is the gas power consumption, P is the power consumption in Watts, N is the revolutions per second, N_p is the power consumption constant, D_I is the impeller diameter, V_l is the liquid or slurry volume and u_g is the superficial gas velocity.

Figures 2.14-2.16 illustrate the effect of superficial gas velocity (1.2438, 2.4874,

4.9751, 5.9701 m/min) on gas holdup profiles, the grade and recovery of the valuable minerals in the column (at a fixed impeller rate, 105 rpm, and frother concentration) by applying equation 2.74.

Gas flow has a pronounced impact on the gas holdup through the column. As the gas flow rate increases, ϵ increases (see Figure 2.14). This is expected as the bubble rise velocity (relative to a stationary observer) is decreased. However, increasing the gas flow will decrease the maximum gas velocity that can be tolerated for operation to remain in the desired bubbly flow regime. Therefore, above the maximum gas velocity limit, instead of the desirable bubbly flow regime, the operation will move to churn-turbulent or slug flow regimes (see [7]).

In this case, as the gas flow rate increases the grade decreases (see Figure 2.15). This decrease can be explained as more gangue particles can be entrained to the top of the column. In contrast, the recovery versus gas rate increases (see Figure 2.16) about 3 percentage points rise, which is not a significant value.

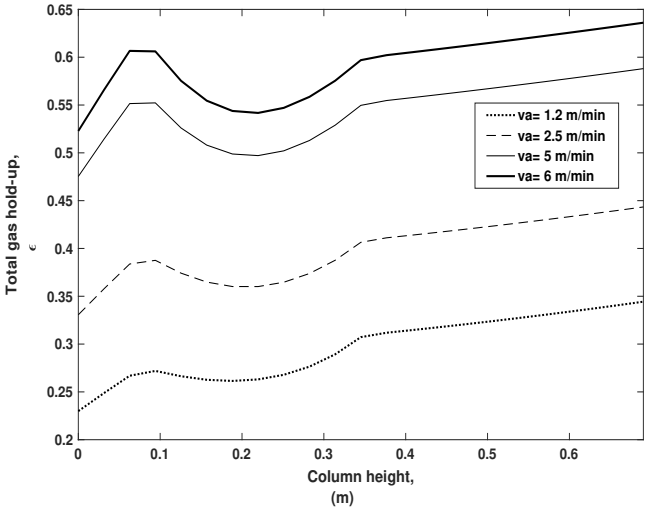

Figure 2.14: Gas holdup versus gas rate

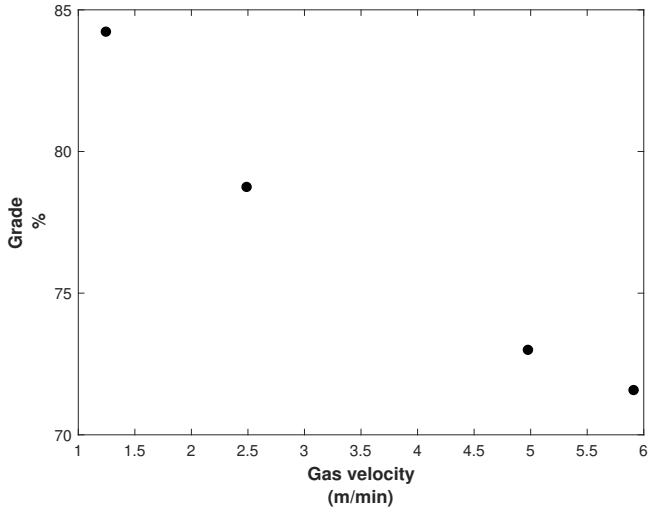

Figure 2.15: Grade versus gas rate.

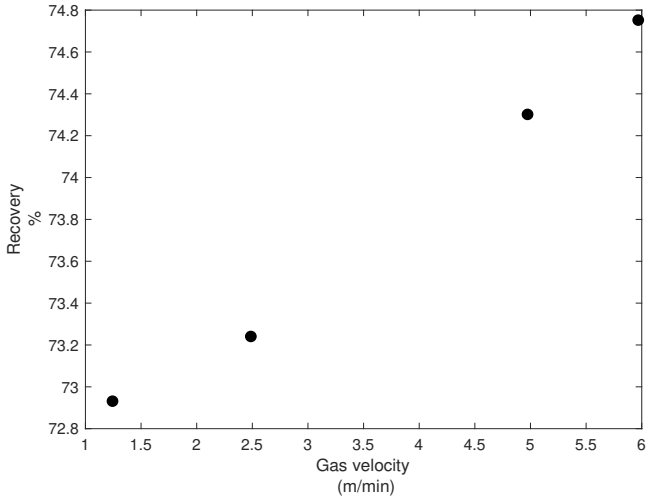

Figure 2.16: Recovery versus gas rate.

2.6.2 Effect of agitation

In this hybrid proposed flotation column configuration, agitation in the well-mixed zone is employed to facilitate bubble dispersion, and to form a homogeneous slurry. Agitation which is manifested as the speed of the impeller greatly impact outcomes from numerical simulations.

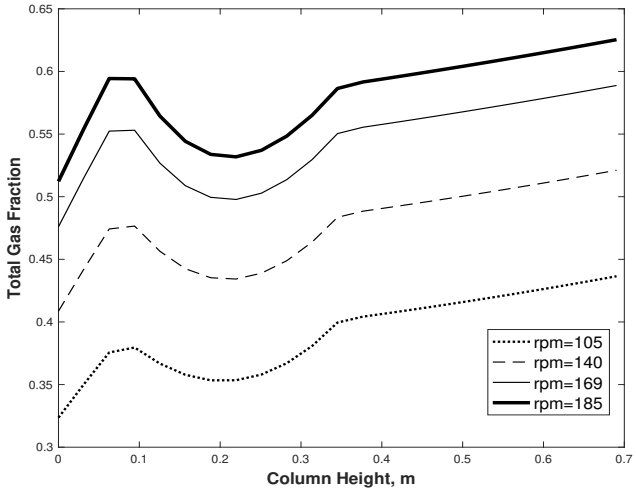

Figure 2.17: Effect of agitation on the steady state total gas holdup profile through the column.

Figures 2.17 - 2.19 illustrate the effect of agitation (105, 140, 169, 185 rpm) on the total gas holdup, attached and free hydrophobic particle concentration profiles as well as the grade and recovery of the valuable minerals in the column (at a fixed gas flow rate of 0.4975 $\frac{m}{min}$ and frother concentration) by applying equation 2.74.

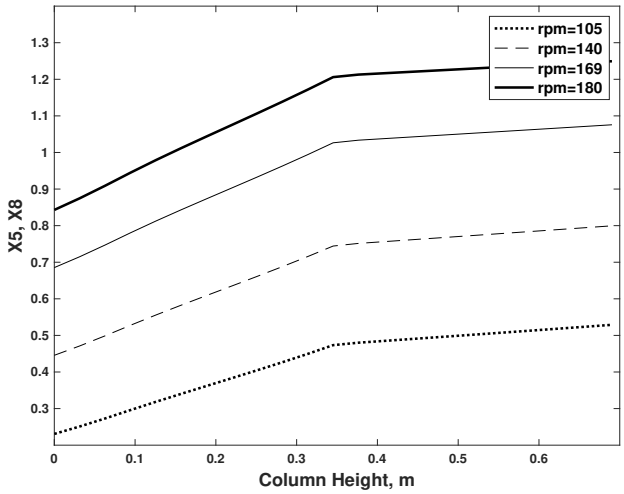

Figure 2.18: Effect of agitation on the steady state profile of attached hydrophobic particles concentration through the column.

Studies reveal that increasing impeller speed and consequently decreasing bubble sizes, at constant gas flow rate increases the total gas holdup through the column at steady state (see Figure 2.17). Thus the concentration of attached value particles through the column (see Figure 2.18) as well as the recovery (see Figure 2.19) increases by increasing the agitation of well-mixed zone.

Agitation causes the formation of fine bubbles, and promotes particle-bubble collision, so increases the value (hydrophobic) recovery (see Figure 2.19). However fine bubbles typically adversely affect grades due to more water that is carried to the froth by the finer bubbles .

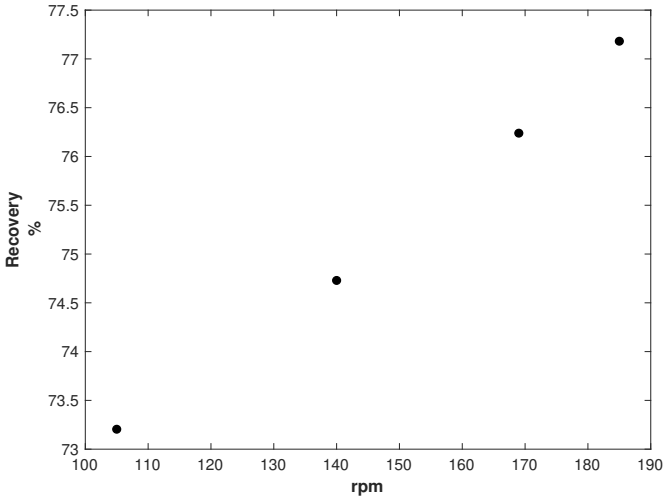

Figure 2.19: Effect of agitation on the recovery.

Figures 2.18 and 2.19 demonstrate the positive effect of agitation on the concentration of attached valuable minerals and recovery in a hybrid flotation column. These figures as well as Figure 2.11 illustrate that based on the modelling effort, addition of a mixer to the geometry of the column enhances its performance in comparison to a conventional one. Moreover, as it is illustrated in figures 2.20-2.22 by increasing agitation (manifested as RPM = 100 to 170) both attachment and detachment rates increase. The increase in the attachment rate is due to the mixer presence in the CSTR zone which provides enhanced particle-bubble collision. In addition, the use of an impeller in the well-mixed section results in the production of fine bubbles which are favourable for fine particles attachment. However, increasing the impeller speed, and consequently agitation, increases the detachment rate and may cause some of the attached particles to detach from the bubbles.

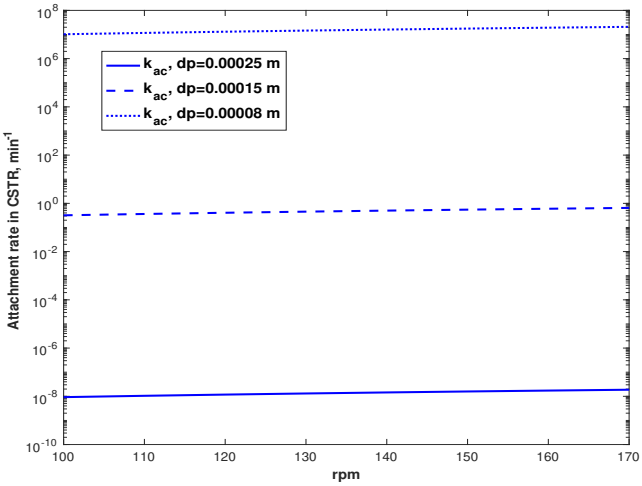

Figure 2.20: Effect of agitation and particle size on the attachment rate in CSTR.

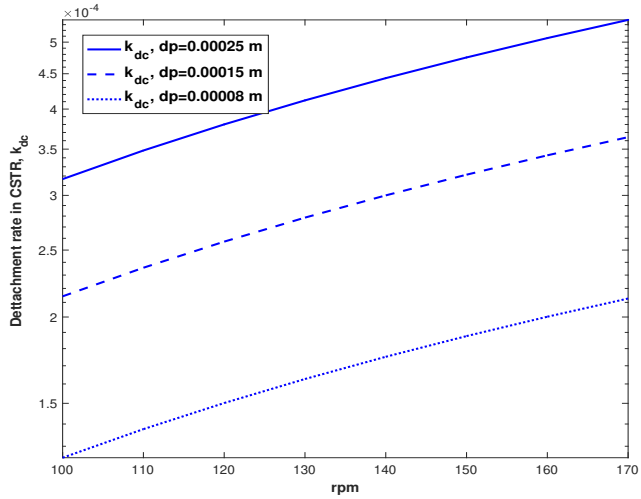

Figure 2.21: Effect of agitation and particle size on the detachment rate in CSTR.

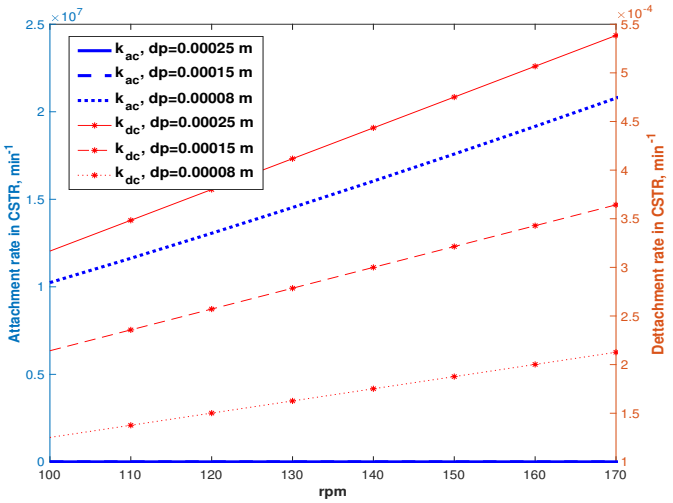

Figure 2.22: Effect of agitation and particle size on the attachment and detachment rate in CSTR.

Moreover, modelling analysis demonstrates that the hybrid flotation column is effective over a size range of 80 to 250 microns of particles. Since in this range the considered parameters are physically meaningful and simulation results are easily realizable and reproducible. This can approve the initial motivation to construct a modified column flotation geometry by addition of a mixer to the column geometry to expand the range of particle separation, and to unify the advantages of both types of flotation approaches, column and mechanical cell. Impeller in the well-mixed section produces fine bubbles which are favourable for fine particles attachment, while the quiescent area of the column is favourable for the separation of coarser minerals.

2.6.3 Industrial relavent case study (Galena/Quartz)

In this section, we provide simulation results for the separation of Galena/Quartz (Galena is the valuable mineral) with the specific densities of $7600 kg/m^3$ and $2650 kg/m^3$.

The Galena/ Quartz with the ratio of 10:90 is applied to be a more industrial realistic ore composition and we are providing the insight through the simulation study conducted for the separation of these two minerals. Figure 2.23(a) demonstrates the spatiotemporal propagation of the concentration of attached Galena particles to bubbles in the pulp and froth and illustrates how the arbitrary initial profile is transported across the column and washes out over time in approximately thirteen minutes. Along the same lines, the evolution of the CSTR states (see Figure 2.23(b)) influences the state evolution through the boundary condition and propagates through the column and after approximately twenty minutes reaches the steady-state profile.

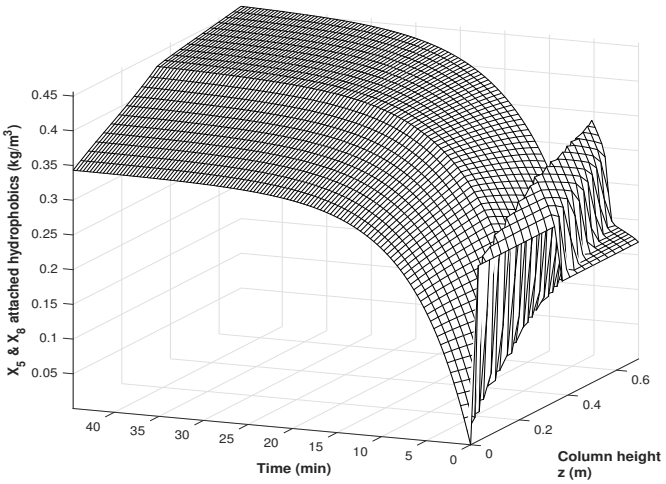

a)

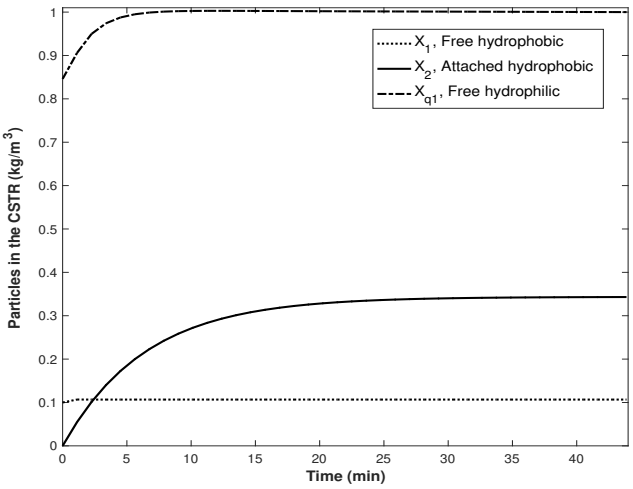

b)

Figure 2.23: a) The concentration of attached Galena through the column, b) the concentration of attached, free Galena and free Quartz in the well-mixed zone.

At the steady state, the concentration of attached hydrophobic particles increases,

while the concentration of free hydrophobic particles in the upflow decreases, through the column from the pulp to the froth. From the froth to the pulp, the concentration of free hydrophobic particles in the downflow decreases (see Figure 2.24).

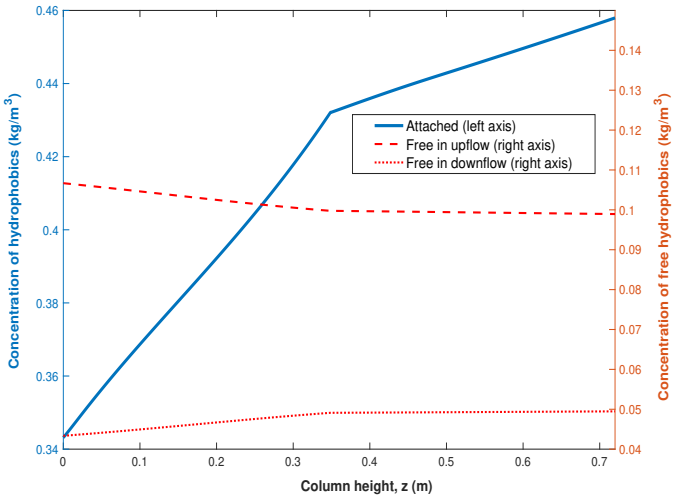

Figure 2.24: The steady state propagation of Galena concentration through the column with Danckwerts' boundary conditions at the interface.

Figure 2.25 shows the temporal propagation of recovery and grade of Galena particles in the concentrate (in the hybrid flotation column), separately. The figure illustrates that grade of Galena in the concentrate at the top of the column increase over time and reaches its final value of almost 40% after $25mins$. Moreover recovery increases to its maximum value of almost 75% in 25 minutes.

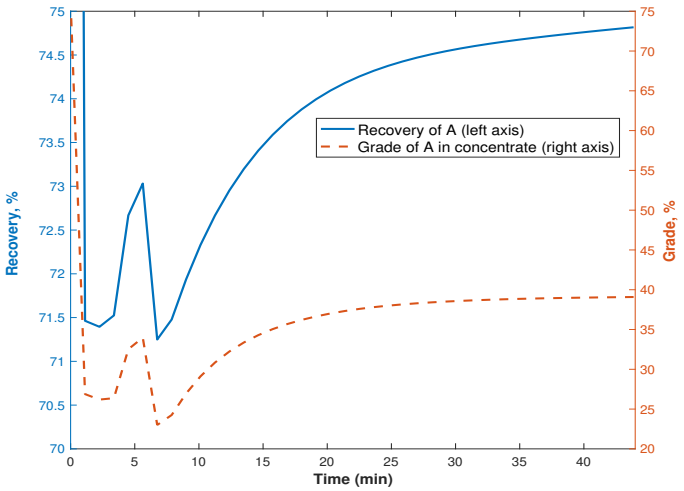

Figure 2.25: Propagation of recovery and grade of Galena in the concentrate in a hybrid flotation column

2.7 Conclusion

A three-phase dynamic model of the boundary coupled hetero-directional hyperbolic PDE-ODE system representing continuous column flotation has been developed and applied to a hybrid flotation column with a mechanically agitated section (represented by a CSTR) at the bottom and a conventional column setup above it. In solving the system of equations in the pulp zone, the boundary conditions were given by the CSTR concentrations. At the base of the froth, which represents the interface between the froth and the pulp zones, a Dankwerts' boundary condition was applied. Using this model, the gas holdup, free and attached hydrophobic particles concentrations, as well as free hydrophilic particles concentration profiles are simulated. The results has been validated by comparing the simulated results with previously published experimental results in the literature for conventional flotation columns (see

Fig 2.10). We have shown that the proposed method is capable of being extended to different column conditions and well predicts the system over a wide range of operating conditions, different ranges of bubble sizes, mass transfer and reaction rates, as well as equal/unequal bubble sizes in the pulp and froth sections with different classes of bubbles sizes. Finally, the effect of gas flow rate and agitation on the gas holdup, concentration of minerals, grade, recovery and attachment/detachment rates are demonstrated in this work.

Chapter 3

Modelling and Boundary Optimal Control Design of Hybrid Column Flotation

Abstract A three-phase continuous hybrid flotation column that seeks to obtain the benefits of both mechanical cells and flotation columns is modelled as the interconnection of a CSTR representing the well-mixed zone and two plug-flow reactors (PFR) representing pulp and froth zones. The plant model accounts for the micro-scale processes such as bubble-particle collision and attachment, the appearance and breakage of bubbles. This complex distributed parameter system (DPS) is described by sets of nonlinear coupled conservation counter-current hyperbolic partial differential equations (PDEs) and one set of ordinary differential equations (ODEs). The dynamic conservation law based model for the continuous hybrid flotation column including a well-stirred, pulp (bubbly), and froth zones is utilized in an optimal model-based controller design. This modern state-of-the-art controller synthesis needs to account for optimality, stability, and performance. The controller design utilizes a linear model obtained by linearization at operating steady states of interest. A full-state

optimal feedback control law is designed and controller performance has been demonstrated through a numerical simulation of physically meaningful and relevant plant operating conditions. The LQR-based optimal controller outperforms PI-based controller in terms of stabilizing states by returning the states to the steady state after a perturbation in the initial condition.

3.1 Introduction

Column flotation is an efficient separation process to separate valuable mineral(s) from ore(s) based on the differences in minerals hydrophobicity. Modern flotation columns were developed in Canada in the early 1960s [5] and since their commercial application in 1980s [7], they have been used in a rather broad range of applications: the mineral processing industry including metallic, non-metallic ores, as well as in wastewater treatment processes. Technological advantages of this separation technique over conventional mechanical flotation cells include simplicity of construction, low energy consumption, higher recovery and product grade [90]. In general, minerals, water and air are fed in the lower part of the column. Subsequently, the transport of the material and minerals includes the transport of hydrophobic particles attached to the bubbles, which propagate in an attached form from the pulp to the froth zone, and the liquid up-flow and down-flow, in its free form, and is affected by the hydrodynamics of the inflow and outflow streams. Note that the net downward flow of liquid represents the so-called bias of the flotation column. Column flotation is a complex distributed parameter system (DPS) that involves three phases of solid particles, gas or air bubbles, and liquid flows (up-flow and down-flow).

The main operational objective of column flotation process is to maximize the grade

and/or recovery of valuable mineral(s) while keeping the other variable above a threshold value and the main objective of column flotation control is to maintain its required operational level despite disturbances in the operation. However, large variations in the feed concentrations and several other hydrodynamical disturbances reduce the grade and recovery of column operation. Therefore, control strategies and system analysis applied to column flotation typically target down-flow, froth depth, grade, recovery, and gas hold up by manipulating variables such as the flow of feed, air, and wash-water, and reagent addition [6, 15]. Currently, a common control approach in flotation plants is the knowledge-based (e.g. fuzzy logic or supervisory) control realization, despite the fact that computational cost of the rule-based control for such a complex system is high [29]. Model-based control design has the potential to provide improved performance while ensuring stability of the hydrodynamic system. Due to a large number of variables and subprocesses the modelling of the flotation process is complex [31]. Although setting clear boundaries is often not possible, models of the flotation process can be classified as fundamental (based on first principles models, e.g. probabilistic, kinetic, and population-balance), empirical (statistical models derived from experimental data) and hybrid (based on both experimental data and first principle models). First principles models employ the conservation of mass and the mechanisms related to bubble-bubble and bubble-particle interactions occurring in the mechanical flotation cells. In contrast, empirical modelling is realized by adjusting the parameters in a regression relationship to provide the best fit to the existing data, with considerable flexibility in choosing the functional form of the regression relationship. Hybrid models are determined with a mix of empirical and fundamental relationships [51].

Although several models have been proposed for mechanical froth flotation cells [22, 47, 55], there are only a few dynamic models proposed for the column flotation process in the literature that can be used for model-based controller design applications. These models try to connect the hydrodynamic process conditions (interfacial area of bubbles, bubble size distribution, and particle size distribution) to mineral recovery and provide an improvement to the theoretical understanding of column flotation [43, 91], [64, 69]. Some of these models can be classified as micro-scale models [57, 59], implying that they were developed to estimate design parameters for a column flotation system, such as particle velocity [60], gas dispersion [61, 62], and not for use in process control.

Initial modelling efforts for column flotation include the work of Sastry and Lofftus [64] and Cruz [43], who proposed a population balance based model for the flotation column process. This model was based on the microscopic and macroscopic description of pulp and froth zones in which bubble coalescence and loading have been considered and a distribution of bubble sizes, particle sizes, and particle types were also used. Non-constant attachment and detachment rates in Cruz [43] model were defined by the probability of attachment and detachment of particles from the bubbles. The column was modelled based on a vertical combination of a perfectly mixed aeration zone, a perfect-CSTR-in-series lower collection zone, a single perfectly mixed feed zone, a perfect mixers-in-series upper collection zone, the interface, and three plug flow volumes including stabilized froth, wash water, and draining froth. This dynamic simulator of the column flotation system did not have the ability to handle pulp level variations or to account for pressure effects in the gas phase. On the other hand, the model proposed by Bouchard et al. [44] is based on macroscopic

descriptions of pulp and froth phases, material balance, and a first-order kinetic assumption for attachment/detachment. This model uses a CSTRs-in-series approach with the ability to handle pulp level variations and account for pressure effects in the gas phase. In addition, a mean bubble diameter in every simulation cell is used and the physical mechanisms of collision, attachment, and detachment have not been considered separately in determining the attachment and detachment rate constants. In Tian, et al.[72] a hyperbolic transport-reaction system based on the model published by Sastry and Lofftus [64] is considered, which accounts only for froth and collection zones. The current modelling effort which is along the modelling development associated with this work is presented in [73] and they considered conservative hyperbolic PDEs in physically meaningful lab setting [92].

Flotation is generally effective over a size range of approximately 15 to 150 microns of mineral particles [11]. Mechanical flotation cells provide enhanced particle-bubble collision through agitation, while flotation columns have a large quiescent zone that enables fractionation. In this regard, in order to expand the range of particle separation, and to combine the advantages of both types of flotation approaches, our group has constructed and is testing a novel hybrid flotation column. In addition to enhanced bubble-particle collision, the use of an impeller in the well-mixed section also results in the production of smaller bubbles, which is favourable for the attachment of fine particles, while the quiescent area of the column is favourable for the separation of coarser minerals. In this work, we present a model for the purpose of modelling and control of this hybrid flotation column. Note that the term 'hybrid' in this work implies that a CSTR is added to the flotation column geometry. The three-phase dynamic model for the hybrid column accounts for the coupling of a

nonlinear hetero-directional system of hyperbolic PDEs-ODE in which the upward and downward liquid flows represent flows of free particles, respectively. The gas flow represents the flow of attached hydrophobic particles to the bubbles. The model accounts for three regions of well-mixed (CSTR), pulp (collection) and froth (cleaning) as well as microscale processes taking place in the column, such as bubble-particle collisions and attachments and the hydrodynamic forces in the liquid.

The hybrid flotation column is an example of a transport-reaction system, and typically, in-domain actuation is applied for the purpose of controlling such systems (e.g. heating the fixed bed reactor through the jacket along the column). Developing controller design for such models representing these systems is challenging and has received some attention in the literature [93]. However, in most transport-reaction systems (including column flotation), control actuation is applied at the boundaries of the system, which increases the complexity of the design further. The mathematical difficulty of solving boundary control problems is associated with dealing with the point actuation (at the boundary); to solve the control problem for these systems, we have transferred the actuation to in-domain actuation [94]. However, there is limited published research in the area of optimal control for this type of system. Moghadam, et al.[94] considered the optimal control of coupled ODEs and hyperbolic PDEs with uni-directional transport in a two-phase contactor with a constant transport velocity. The novelty of this contribution, besides the derivation of a dynamic fundamental model for a hybrid column flotation process which accounts for bubble-particle bubble-bubble interactions, is extending the framework of designing an optimal control formulation available in the literature [94], to the novel hybrid column flotation model which represents a three-phase hetero-directional transport

system where the velocity matrix in the transport operator is spatially and temporally varying along the column height (see Figure 2.16).

We provide a systematic general procedure for the design of a full state optimal controller regarding the coupling of nonlinear hetero-directional system of hyperbolic PDE-ODE. We consider 1) a boundary coupled hetero-directional nonlinear hyperbolic PDE-ODE system that allows the inclusion of various transport interactions, 2) systematic dynamical analysis of the linearized model, 3) design of optimal feedback operators for the system of coupled PDE-ODE system by solving Riccatti matrix operator equations. Accordingly, optimal control gains of the ODE subsystem given by a finite dimensional model and infinite dimensional hetero-directional hyperbolic PDEs are coupled and solved simultaneously. In this sense, one can explore optimality of the state evolution and control effort evolution that is compartmentalized in different sections of the column reaction system. In addition, we provide a comparison with non-model based (PI) controllers, and we point out advantages of the proposed design.

Thus, the major contribution of this work is the investigation of the control of a novel hybrid column flotation process and the development of an optimal controller for a boundary coupled hetero-directional nonlinear hyperbolic PDE-ODE system.

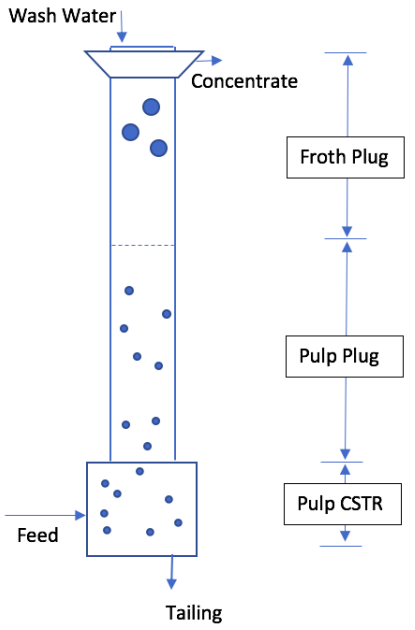

Figure 3.1: Model presentation

This paper is structured as follows: In section 1, the column flotation process is described and in section 2 is modelled as a system of nonlinear coupled PDE-ODEs, and a linearized state-space description for the system is obtained. Section 3 addresses the state feedback regulator design problem. The profile of the linearized system is illustrated and parameters for regulators are designed and calculated in detail in section 4, and the simulation results are shown to demonstrate the controller performance. Finally, section 5 provides conclusions from the study.

3.2 Model development for hybrid column flotation

3.2.1 Hybrid column

A common column flotation apparatus consists of two zones; the pulp (collection) and the froth (cleaning) zones. The hybrid column we consider is unique since an impeller has been added to the column flotation geometry (see Figure 3.1).

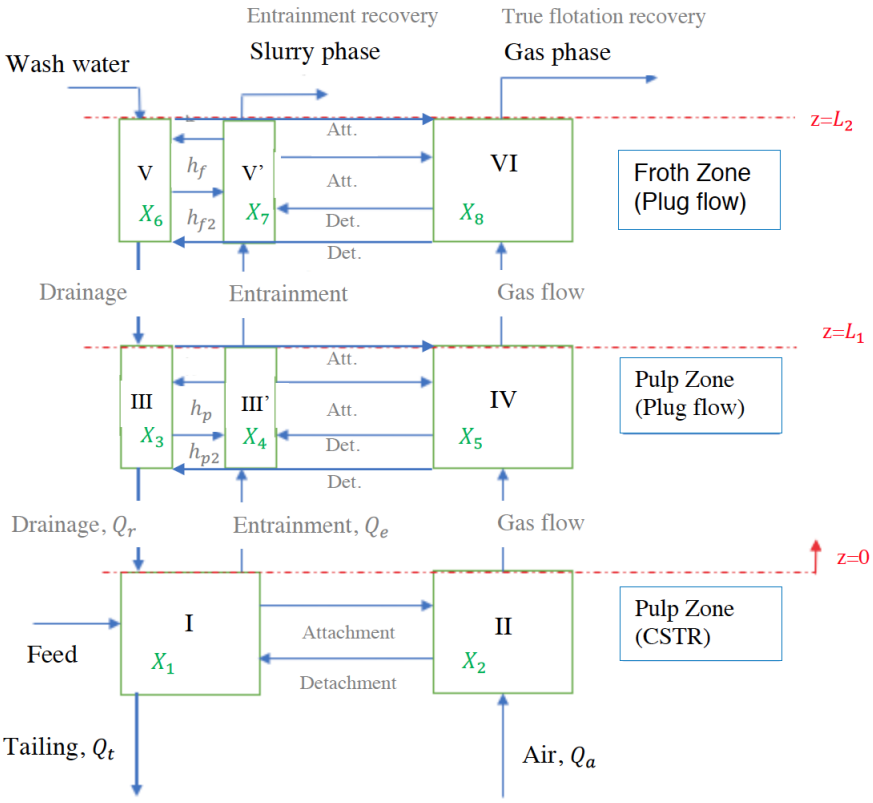

Figure 3.2: Schematic of a three-phase column flotation system considering the transport of hydrophobic particles

Assuming perfect mixing, the compartment with the agitation is considered as

a continuous stirred tank reactor (CSTR). On the other hand, the collection zone (pulp) and the bubbly zone (froth) in the column section are considered as two plug flow reactors (PFRs) in series; in which we assume perfect radial mixing and no axial mixing (along the direction of the flow). In this modelling framework, the effect of axial dispersion is neglected in comparison to the flow of the fluid. A seminal paper by Sastry and Lofftus in 1988 [64], reveals that for estimating the degree of dispersion in flotation columns, the Peclet number for plug flow conditions is considered to be infinite.

The dynamic mathematical model has been developed considering bubble-particle attachment and detachment, as well as the gas and liquid transport phenomena. The process can be considered as a counter-current flow system. The air injected by a sparger at the bottom of the column forms bubbles that rise up through the column length. Slurry that contains the particles of the ore is introduced in the agitated section. After collision and contact between the bubbles and minerals, hydrophobic minerals attach to the bubbles and form bubble-particle aggregates. The valuable minerals, i.e. hydrophobic particles, are transported to the top of the column by the bubbles and finally overflow from top of the column as the product (concentrate). The purpose of the wash water above the overflow level is to wash down entrained (hydrophilic) particles back to the froth zone [36, 77]. Therefore, the interaction between rising bubbles, entrained particles, and down-flow slurry leads to mass transfer of the particles between the water and air phases as well as between the upward and downward water flows. The mass transfer processes of attachment and detachment of particles to and from the bubbles are treated as kinetic processes or reactions.

3.2.2 Modelling

We present a three-phase fundamental dynamic model based on physical principles for a continuous (in contrast to the batch production) hybrid column flotation process that includes a well-mixed section. The model extends the modelling contributions in the literature [43, 44, 73, 79]. However, the novelty of this contribution is that it has been tailored for a hybrid column flotation, accounts for a CSTR added to the column geometry, includes transport-reaction conservation laws and accounts for macro- and micro-scale processes including bubble interactions, mass transfer between up-flow, down-flows. As illustrated in Figure 3.2, this process is modelled as an interconnection of three different subsystems, including a CSTR, which represents a well-mixed zone, and two plug flow transport reactors, representing pulp and froth zones. In addition, the model is augmented by considering the microscale processes taking place in the column, such as bubble-particle collisions and attachments as well as hydrodynamic forces. In particular, the modelling accounts for the three phases: solid particles, gas (air bubbles), and liquid in the froth zone. The three flows in the system are the gas upward flow, liquid up-flow and liquid down-flow. A solid particle can be found in any of the eight compartments (I, II, III, III', IV, V, V', VI), based on its state, e.g. attached to the bubbles (gas phase) as X_2 in the CSTR, X_5 in the pulp, and X_8 in the froth zone. A solid particle can be free (not attached) in the downward liquid flow as X_3 in the pulp or as X_6 in the froth or as X_1 in the CSTR, or as X_4 or X_7 in liquid phase up-flow, in the pulp or froth zones, respectively.

In addition, a mass balance-based nonlinear model representing the reaction term in the transport-reaction system is defined for valuable particles, hydrophobic, for

each compartment. The assumption of regulated and constant pulp/froth interface position, i.e. level, is applied in this modelling setting. As reported in previous studies [7], the most important factors in level regulation are the feed and tailing flow rates, which are kept constant in this modelling and control framework. The resulting model equations, system of nonlinear hyperbolic partial differential equations (PDEs) and ordinary differential equations (ODEs) have been solved using Euler integration backward in space and forward in time such that the numerical stability of the simulation is preserved.

A three-phase model for hydrophobic particles in the CSTR

The state variables for the CSTR model are concentration of valuable minerals attached to the bubbles, $X_2(t)$, and free in the liquid phase, $X_1(t)$. A mass balance over the CSTR control volume, a lumped parameter system (LPS), provides:

$$\frac{dX_1}{dt} = -\frac{(Q_t + Q_{ep})X_1}{V_c(1-\epsilon_c)} - K_{ac}X_1 + K_{dc}X_2 + \frac{Q_f X_{1,0}}{V_c(1-\epsilon_c)} \tag{3.1}$$

$$\frac{dX_2}{dt} = -\frac{Q_a X_2}{V_c \epsilon_c} + K_{ac}X_1 - K_{dc}X_2 \tag{3.2}$$

where $X_{1,0}$ denotes the input (concentration of free particles) into the CSTR, and the balance of the flow rates provides the following relationship for the stationary operating processes, $Q_f + Q_r = Q_t + Q_e$ (see Notation list).

Hydrophobic particles model in the pulp zone

The state variables for the pulp or collection zone are the concentrations of valuable mineral attached to the bubbles, $X_5(z,t)$, free in the up-flow, $X_4(z,t)$, and free in the down-flow, $X_3(z,t)$. The transport hyperbolic PDEs are used to describe the

evolution of transport in both directions. The transport of attached and free valuable materials in the air and up-flow streams is linked to the states of the CSTR by the boundary conditions:

$$\frac{\partial X_3}{\partial t} = \frac{Q_{rp}}{A_c \alpha_p (1-\epsilon_p)} \frac{\partial X_3}{\partial z} - K_{ap3} X_3 + k K_{dp} X_5 + \\ + h(X_4 - X_3) \tag{3.3}$$

$$B.C.\ at\ z = L_1 \qquad X_3(L_1, t) = X_6(L_1, t) \tag{3.4}$$

with $X_3(z,t)$ being the state that represents particles transported downwards and is defined on the height range of $[0, L_1]$. Therefore, the concentration of the attached and free valuable materials transported upwards are:

$$\begin{aligned} \frac{\partial X_4}{\partial t} &= -\frac{Q_{ep}}{A_c(1-\alpha_p)(1-\epsilon_p)} \frac{\partial X_4}{\partial z} - K_{ap4} X_4 + \\ &+ (1-k) K_{dp} X_5 - h'(X_4 - X_3) \end{aligned} \tag{3.5}$$

$$\frac{\partial X_5}{\partial t} = -\frac{Q_a}{A_c \epsilon_p} \frac{\partial X_5}{\partial z} + K_{ap3} X_3 + K_{ap4} X_4 - K_{dp} X_5 \tag{3.6}$$

with the associated boundary conditions that are linked to the states of the CSTR:

$$B.C.\ at\ z = 0 \qquad X_4(0,t) = X_1(t) \tag{3.7}$$

$$B.C.\ at\ z = 0 \qquad X_5(0,t) = X_2(t) \tag{3.8}$$

The states $X_4(z,t)$ and $X_5(z,t)$ are also defined on $[0, L_1]$. At this point, there is a coupling of the CSTR dynamics to the underlying transport PDE through the boundary conditions, so that the dynamics of the CSTR concentration drive the boundary states evolution for the transport of the upward ($X_4(z,t)$ and $X_5(z,t)$) and downward ($X_3(z,t)$, driven by the state $X_6(z,t)$ from the froth zone) particles.

Hydrophobic particles model in the froth and interface zones

The state variables for the froth zone are concentration of valuable minerals attached to the bubbles ($X_8(z,t)$), free valuable minerals in the up-flow ($X_7(z,t)$), and free valuable minerals in the down-flow ($X_6(z,t)$) with associated boundary conditions.

$$\begin{aligned} \frac{\partial X_6}{\partial t} &= \frac{(Q_{rf}+Q_w)}{A_c\alpha_f(1-\epsilon_f)}\frac{\partial X_6}{\partial z} - K_{af6}X_6 + k_2K_{df}X_8 + \\ &+ h_f(X_7 - X_6) \end{aligned} \tag{3.9}$$

$$B.C. \quad at\ z = L_2 \qquad X_6(L_2,t) = \eta(t) \tag{3.10}$$

where the conditions at the top of the column are associated with the wash water input $\eta(t)$. The upward transport includes free and attached particles, which is coupled to the pulp zone by boundary conditions and is given as:

$$\begin{aligned} \frac{\partial X_7}{\partial t} &= -\frac{Q_{ef}}{A_c(1-\alpha_f)(1-\epsilon_f)}\frac{\partial X_7}{\partial z} - K_{af7}X_7 + \\ &+ (1-k_2)K_{df}X_8 - h'_f(X_7 - X_6) \end{aligned} \tag{3.11}$$

$$\frac{\partial X_8}{\partial t} = -\frac{Q_a}{A\epsilon_f}\frac{\partial X_8}{\partial z} + K_{af6}X_6 + K_{af7}X_7 - K_{df}X_8 \tag{3.12}$$

$$B.C.\ at\ z = L_1;\ X_7(L_1,t) = X_4(L_1,t) \tag{3.13}$$

$$B.C.\ at\ z = L_1;\ X_8(L_1,t) = X_5(L_1,t) \tag{3.14}$$

Gas-holdup model for froth and pulp zones

In this section, we describe gas fraction models in the pulp and froth zones, in which gas holdup variations propagate both temporally and spatially along the column height. The model accounts for the bubble coalescence and breakage of three bubble

size classes in the pulp, and three bubble size classes in the froth.

$$\frac{\partial \epsilon_{p,n}(z,t)}{\partial t} = -v_{\epsilon,n,p}\frac{\partial \epsilon_{p,n}(z,t)}{\partial z} - \mathcal{D}_{p,n}(z,t) + \mathcal{A}_{p,n}(z,t); \tag{3.15}$$

$$\frac{\partial \epsilon_{f,n}(z,t)}{\partial t} = -v_{\epsilon,n,f}\frac{\partial \epsilon_{f,n}(z,t)}{\partial z} - \mathcal{D}_{f,n}(z,t) + \mathcal{A}_{f,n}(z,t) \tag{3.16}$$

$$\epsilon_{p,n}(0,t) = \epsilon_{c,n}(t), \quad \epsilon_p(z,t) = \sum_{n=1}^{3} \epsilon_{p,n}(z,t) \tag{3.17}$$

$$\epsilon_{f,n}(L_1,t) = \epsilon_{p,n}(L_1,t), \quad \epsilon_f(z,t) = \sum_{n=1}^{3} \epsilon_{f,n}(z,t) \tag{3.18}$$

The total gas hold-up is a summation of the gas hold-ups of the three bubbles size classes. In the present work, based on the approaches taken in the works of Sastry,[42, 79] extended and applied by Cruz [43], the total increase/decrease in the volume fraction of bubbles is mathematically defined by defining the total rise, $\mathcal{A}_{p,n}(z,t)$, and the total decline, $\mathcal{D}_{p,n}(z,t)$, statistically as measures of how many interactions results in coalescence in each bubble size class n that could be applied to the entire column.

In the system of equations 3.1, 3.2, 3.3, 3.5, 3.6, 3.9, 3.11 and 3.12, the grade and recovery of the froth overflow (the concentrate or product flow) is controlled by three inputs: the slurry composition at the top of the column, $U_1 = \eta$, which is linked to the wash water flow rate, the feed composition, $U_2 = X_{1,0}$, and air flow rate, $U_3 = Q_a$, which will be considered in the full state feedback control design.

The state space model of the CSTR can be written in a matrix format as:

$$\frac{\partial}{\partial t}\begin{bmatrix} X_1 \\ X_2 \end{bmatrix} = \begin{bmatrix} \frac{-(Q_t+Q_{ep})}{V_c(1-\epsilon_c)} - K_{ac} & K_{dc} \\ K_{ac} & -K_{dc} - \frac{Q_a}{\epsilon_c V_c} \end{bmatrix}\begin{bmatrix} X_1 \\ X_2 \end{bmatrix} + \tag{3.19}$$

$$+ \begin{bmatrix} \frac{Q_f X_{1,0}}{V_c(1-\epsilon_c)} \\ 0 \end{bmatrix}$$

It is assumed that $K_{ac} = GU_3^m$ where, $m = 0.45$ and $G = 8.08$, and $U_2 = X_{1,0}$. Therefore, equation 3.19 can be rewritten as

$$\begin{aligned} \frac{\partial X_1}{\partial t} &= (\frac{-(Q_t + Q_{ep})}{V_c(1-\epsilon_c)} - GU_3^m)X_1 + K_{dc}X_2 + \\ &+ \frac{Q_f U_2}{V_c(1-\epsilon_c)} \end{aligned} \tag{3.20}$$

$$\frac{\partial X_2}{\partial t} = GU_3^m X_1 - (K_{dc} + \frac{U_3}{V_c\epsilon_c})X_2 \tag{3.21}$$

The compact model of the transport PDE-ODE interconnection given in the state space format for the froth zone is

$$\frac{\partial}{\partial t}\begin{bmatrix} X_6 \\ X_7 \\ X_8 \end{bmatrix} + \Lambda_1 \frac{\partial}{\partial z}\begin{bmatrix} X_6 \\ X_7 \\ X_8 \end{bmatrix} = \Gamma_1 \begin{bmatrix} X_6 \\ X_7 \\ X_8 \end{bmatrix} \tag{3.22}$$

while equations for the collection zone or pulp zone can be written in the state space format as

$$\frac{\partial}{\partial t}\begin{bmatrix} X_3 \\ X_4 \\ X_5 \end{bmatrix} + \Lambda_2 \frac{\partial}{\partial z}\begin{bmatrix} X_3 \\ X_4 \\ X_5 \end{bmatrix} = \Gamma_2 \begin{bmatrix} X_3 \\ X_4 \\ X_5 \end{bmatrix} \tag{3.23}$$

The transport and reaction matrices for equations 3.22 and 3.23 are defined as:

$$\Lambda_1 = \begin{bmatrix} \frac{-(Q_r+Q_w)}{A_c\alpha_f(1-\epsilon_f)} & 0 & 0 \\ 0 & \frac{Q_e}{A_c(1-\alpha_f)(1-\epsilon_f)} & 0 \\ 0 & 0 & \frac{Q_a}{A_c\epsilon_f} \end{bmatrix} \tag{3.24}$$

$$\Gamma_1 = \begin{bmatrix} -K_{af6} - h_f & h_f & k_2K_{df} \\ h'_f & -K_{af7} - h'_f & (1-k_2)K_{df} \\ K_{af6} & K_{af7} & -K_{df} \end{bmatrix} \tag{3.25}$$

$$\Lambda_2 = \begin{bmatrix} \frac{-Q_r}{A_c\alpha_p(1-\epsilon_p)} & 0 & 0 \\ 0 & \frac{Q_e}{A_c(1-\alpha_p)(1-\epsilon_p)} & 0 \\ 0 & 0 & \frac{Q_a}{A_c\epsilon_p} \end{bmatrix} \tag{3.26}$$

$$\Gamma_2 = \begin{bmatrix} -K_{ap3} - h & h & kK_{dp} \\ h' & -K_{ap4} - h' & (1-k)K_{dp} \\ K_{ap3} & K_{ap4} & -K_{dp} \end{bmatrix} \tag{3.27}$$

$$\frac{\partial}{\partial t}\begin{bmatrix} \epsilon_{p,n} \\ \epsilon_{f,n} \end{bmatrix} = \begin{bmatrix} \frac{V_{\epsilon,n,p}\partial}{\partial z} & 0 \\ 0 & \frac{V_{\epsilon,n,f}\partial}{\partial z} \end{bmatrix}\begin{bmatrix} \epsilon_{p,n} \\ \epsilon_{f,n} \end{bmatrix} + \begin{bmatrix} \mathcal{A}_{p,n} - \mathcal{D}_{p,n} \\ \mathcal{A}_{f,n} - \mathcal{D}_{f,n} \end{bmatrix} \tag{3.28}$$

Finally, the boundary and initial conditions for the PDEs and ODEs are given by:

$$X_4(0,t) = X_1(t);\ X_5(0,t) = X_2(t);\ X_3(L_1,t) = X_6(L_1,t) \tag{3.29}$$

$$X_7(L_1,t) = X_4(L_1,t);\ X_8(L_1,t) = X_5(L_1,t);\ X_6(L_2,t) = \eta(t) \tag{3.30}$$

$$X_1(0) = X_{1,0};\ X_2(0) = 0;\ X_3(z,0) = X_{3,0}(z) \tag{3.31}$$

$$X_4(z,0) = X_{4,0}(z);\ X_5(z,0) = X_{5,0}(z) \tag{3.32}$$

$$\epsilon_{p,n}(0,t) = \epsilon_{c,n}(t); \epsilon_{f,n}(L_1,t) = \epsilon_{p,n}(L_1,t) \tag{3.33}$$

$$\epsilon_{p,n}(z,0) = \epsilon_{p,n,0}(z); \epsilon_{f,n}(z,0) = \epsilon_{f,n,0}(z); \epsilon_{c,n}(0) = \epsilon_{c,n,0} \tag{3.34}$$

The coupling of the PDE-ODE system is provided through the boundaries between the CSTR and the pulp (linking the ODE system and the transport hyperbolic PDE) and through the boundary between the pulp and froth zones. For simplicity, we do not consider dropback of particles from the column to the CSTR, but there is no conceptual issue in including this phenomenon if required.

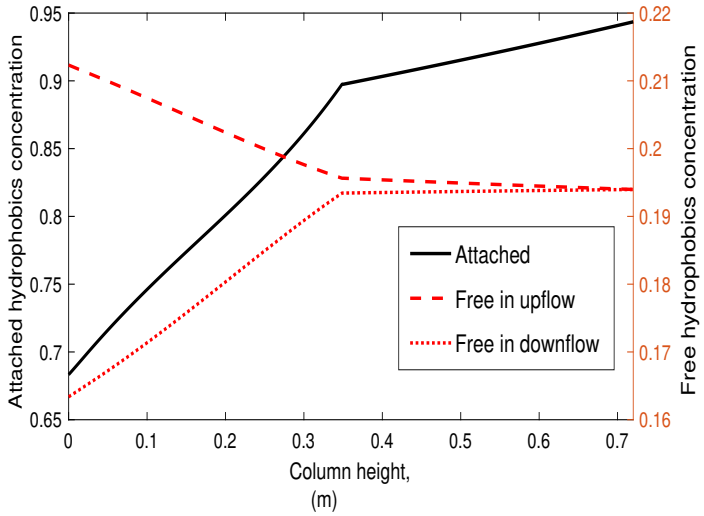

Figure 3.3: The steady state concentration profiles through the column obtained by the simulation of the full nonlinear model $X_{5ss}([0, L_1])$-$X_{8ss}([L_1, L_2])$: solid line, $X_{4ss}([0, L_1])$-$X_{7ss}([L_1, L_2])$: dashed line, $X_{3ss}([0, L_1])$-$X_{6ss}([L_1, L_2])$: dotted line.

3.2.3 Linearized model

The system of model equations developed above is nonlinear, and it is linearized around the steady state of interest to facilitate dynamic analysis and controller design. Note that the controller developed based on this linearized model is implemented on the nonlinear process. The equilibrium condition for the system is obtained by solving the set of nonlinear PDEs and ODEs for the plant model at steady state. With the given steady state inputs, the steady state spatial profiles of the gas hold up and concentration of particles in three forms, as attached, free upward, and free downward are illustrated in Figures 3.3 to 3.4. Hence, the linear system is obtained by defining the standard perturbation of the states around the steady state.

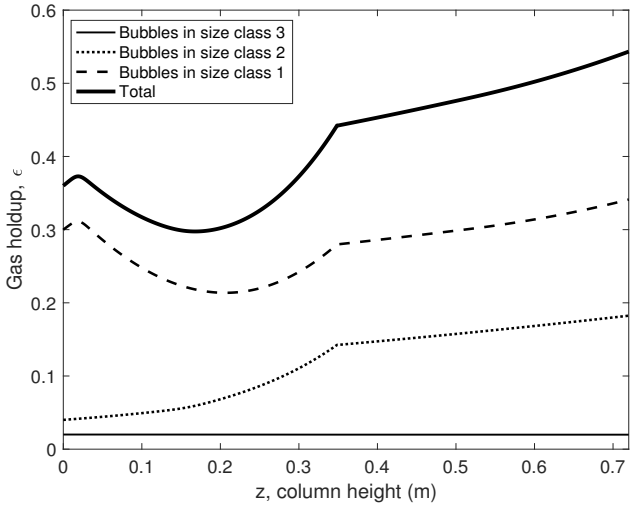

Figure 3.4: Schematic of the steady state gas hold up profiles through the column.

$$x_k(t) = X_k(t) - X_{kss}; \quad k = 1 \ \ to \ \ 2 \tag{3.35}$$

$$x_j(z,t) = X_j(z,t) - X_{jss}(z); \quad j = 3 \ \ to \ \ 8 \tag{3.36}$$

$$\tilde{u}_\nu(t) = U_\nu(t) - U_{\nu,ss}; \quad \nu = 1 \ \ to \ \ 3 \tag{3.37}$$

This provides the following linearized system of equations:

$$\frac{\partial}{\partial t}\begin{bmatrix} x_1 \\ x_2 \end{bmatrix} = \begin{bmatrix} A_{111ss} & A_{112ss} \\ A_{121ss} & A_{122ss} \end{bmatrix}\begin{bmatrix} x_1 \\ x_2 \end{bmatrix} + \begin{bmatrix} \frac{Q_f \tilde{u}_2}{V_c(1-\epsilon_c)} - GmU_{3ss}^{m-1}X_{1ss}\tilde{u}_3 \\ (GmU_{3ss}^{m-1}X_{1ss} - \frac{X_{2ss}}{\epsilon_c V_c})\tilde{u}_3 \end{bmatrix} \tag{3.38}$$

$$\frac{\partial x_3(z,t)}{\partial t} = V_3\frac{\partial x_3(z,t)}{\partial z} + A_{211}x_3(z,t) + A_{212}x_4(z,t) + \tag{3.39}$$
$$+ \quad A_{213}x_5(z,t)$$
$$\frac{\partial x_4(z,t)}{\partial t} = -V_4\frac{\partial x_4(z,t)}{\partial z} + A_{221}x_3(z,t) + \tag{3.40}$$
$$+ \quad A_{222}x_4(z,t) + A_{223}x_5(z,t)$$
$$\frac{\partial x_5(z,t)}{\partial t} = \frac{-U_{3ss}}{\epsilon_p A_c}\frac{\partial x_5(z,t)}{\partial z} + A_{231}x_3(z,t) + \tag{3.41}$$
$$+ \quad A_{232}x_4(z,t) + A_{233}x_5(z,t) - \frac{1}{\epsilon_p A_c}\frac{\partial X_{5ss}(z)}{\partial z}\tilde{u}_3$$
$$\frac{\partial x_6(z,t)}{\partial t} = V_6\frac{\partial x_6(z,t)}{\partial z} + A_{311}x_6(z,t) + A_{312}x_7(z,t) + \tag{3.42}$$
$$+ \quad A_{313}x_8(z,t)$$
$$\frac{\partial x_7(z,t)}{\partial t} = -V_7\frac{\partial x_7(z,t)}{\partial z} + A_{321}x_6(z,t) + \tag{3.43}$$
$$+ \quad A_{322}x_7(z,t) + A_{323}x_8(z,t)$$
$$\frac{\partial x_8(z,t)}{\partial t} = \frac{-U_{3ss}}{\epsilon_f Ac}\frac{\partial x_8(z,t)}{\partial z} + A_{331}x_6(z,t) + \tag{3.44}$$
$$+ \quad A_{332}x_7(z,t) + A_{333}x_8(z,t) - \frac{1}{\epsilon_f Ac}\frac{\partial X_{8ss}(z)}{\partial z}\tilde{u}_3$$

During linearization of the model given by equations 3.1-3.12, it is considered that $V_5 = \frac{U_3}{\epsilon_p A_c}$ and $V_8 = \frac{U_3}{\epsilon_f A_c}$ are the functions of the third input to the system ($Q_a = U_3$).

$$V_3 = \frac{Q_r}{A_c\alpha_p(1-\epsilon_p)};\ V_4 = \frac{Q_e}{A_c(1-\alpha_p)(1-\epsilon_p)} \tag{3.45}$$

$$V_5 = \frac{Q_a}{A_c\epsilon_p};\ V_6 = \frac{(Q_r+Q_w)}{A_c\alpha_f(1-\epsilon_f)} \tag{3.46}$$

$$V_7 = \frac{Q_e}{A_c(1-\alpha_f)(1-\epsilon_f)};\ V_8 = \frac{Q_a}{A_c\epsilon_f} \tag{3.47}$$

$$A_{111ss} = \frac{-1*(Q_t+Q_e)}{V_c(1-\epsilon_c)} - GU^m_{3ss} \tag{3.48}$$

$$A_{112ss} = K_{dc};\ \ A_{121ss} = GU^m_{3ss} \tag{3.49}$$

$$A_{122ss} = -K_{dc} - \frac{U_{3ss}}{\epsilon_c V_c} \tag{3.50}$$

$$A_{211} = -K_{ap3} - h;\ \ A_{212} = h;\ \ A_{213} = kK_{dp} \tag{3.51}$$

$$A_{221} = h';\ A_{222} = -K_{ap4} - h';\ A_{223} = (1-k)K_{dp} \tag{3.52}$$

$$A_{231} = K_{ap3};\ \ A_{232} = K_{ap4};\ \ A_{233} = -K_{dp} \tag{3.53}$$

$$A_{311} = -K_{af6} - h_f;\ \ A_{312} = h_f;\ \ A_{313} = k_2K_{df} \tag{3.54}$$

$$A_{321} = h'_f;\ A_{322} = -K_{af7} - h'_f \tag{3.55}$$

$$A_{323} = (1-k_2)K_{df};\ \ A_{331} = K_{af6} \tag{3.56}$$

$$A_{332} = K_{af7};\ \ A_{333} = -K_{df} \tag{3.57}$$

with the boundary conditions: $x_3(L_1,t) = x_6(L_1,t);\ x_4(0,t) = x_1(t);\ x_5(0,t) = x_2(t);\ x_6(L_2,t) = \eta(t);\ x_7(L_1,t) = x_4(L_1,t);\ x_8(L_1,t) = x_5(L_1,t)$.

Here, the domain of the states $x_3(z,t), x_4(z,t), x_5(z,t)$ is given on $z \in (0, L_1)$ while $(x_6(z,t), x_7(z,t), x_8(z,t))$ belong to $z \in (L_1, L_2)$ and hence the challenge is to represent the entire linear state space in a compact and unified setting. Hence, the extended state $x \in L_2(0, L_1) \oplus L_2(L_1, L_2) \oplus \mathbb{R}^n$ has been considered, where X are

real Hilbert spaces $L_2(0, L_1) \oplus L_2(L_1, L_2)$ with a defined inner product $\langle \cdot, \cdot \rangle$ and $\mathbb{R}^n$ is a real space. The input $u(t) \in U$, and the output $y(t) \in Y$; and U and Y are real Hilbert spaces. Equations 3.38-3.45 can be expressed in equivalent state space format as

$$\begin{aligned} \frac{\partial x_d}{\partial t}(z,t) &= V(z)\frac{\partial x_d}{\partial z}(z,t) + M(z)x_d(z,t) + \qquad (3.58) \\ &+ B_d(z)u(t) \\ \frac{\partial x_l}{\partial t}(t) &= Ax_l(t) + Bu(t) \qquad (3.59) \\ y(t) &= C(\cdot)[x_d(\cdot,t), x_l(t)]^T \qquad (3.60) \end{aligned}$$

augmented with the boundary conditions and initial conditions:

$$\begin{aligned} x_d &= [x_d^{\mathcal{F}}; x_d^{\mathcal{P}}] \qquad (3.61) \\ x_d^{\mathcal{F}}(L_1,t) &= x_d^{\mathcal{P}}(L_1,t); \;\; x_d^{\mathcal{P}}(0,t) = x_l(t) \qquad (3.62) \\ x_d(z,0) &= x_{d,0}(z); \;\; x_l(0) = x_{l,0} \qquad (3.63) \end{aligned}$$

$C(\cdot) = diag(C_d(\cdot), C_l)$, and $x_d(\cdot,t) = [x_6, x_7, x_8, x_3, x_4, x_5]^T$ and $x_l(t) = \begin{bmatrix} x_1 & x_2 \end{bmatrix}$. The input array $u = [\eta, \tilde{u}_2, \tilde{u}_3]$ will be considered in the full state feedback control design.

3.2.4 Boundary to in-domain input transformation

The interconnection of the system of hyperbolic PDEs and ODEs is considered as a boundary-controlled hyperbolic PDE system. In particular, the inputs are applied to the ODE system and by the boundary interconnection propagate to the pulp and the froth zones; however, one input is applied in the countercurrent direction at the top of the column (e.g. η). The manipulated inputs are wash water, air

flow rate, feed concentration and the controller variables are the spatial profiles of minerals. In order to change the inhomogeneous boundary condition for the PDE system to the new system with a homogeneous boundary condition, one can apply a state transformation by considering $\omega^{\mathcal{P}}(z,t) = x_d^{\mathcal{P}}(z,t) - \mathfrak{B}^{\mathcal{P}} x_l(t)$ and $\omega^{\mathcal{F}}(z,t) = x_d^{\mathcal{F}}(z,t) - \mathfrak{B}^{\mathcal{F}} x_d^{\mathcal{P}}(L_1,t)$ (we drop z-dependence in $\omega^{\mathcal{F}}(z,t) = \omega^{\mathcal{F}}(t)$ and $\omega^{\mathcal{P}}(z,t) = \omega^{\mathcal{P}}(t)$ in subsequent sections). In this way, the state of the CSTR given by the ODEs is linked to the spatial state of the pulp section by the $\mathfrak{B}$ operator, and from the interface of the pulp-froth section to the froth section. In other words, the spatial functions $\mathfrak{B}^{\mathcal{F}}$ and $\mathfrak{B}^{\mathcal{P}}$ represent two actuator distribution functions which link the finite dimensional CSTR state, $x_l(t)$ to $\omega^{\mathcal{P}}(z,t)$ and $x_d^{\mathcal{P}}(L_1,t)$ to $\omega^{\mathcal{F}}(z,t)$, respectively. Using this transformation, the control variable $U(t)$ can affect the PDEs throughout the entire column domain.

$$\begin{aligned} \dot{\omega}^{\mathcal{F}}(t) &= \dot{x}_d^{\mathcal{F}}(t) - \mathfrak{B}^{\mathcal{F}} \dot{x}_d^{\mathcal{P}}(L_1,t) && (3.64) \\ \dot{\omega}^{\mathcal{P}}(t) &= \dot{x}_d^{\mathcal{P}}(t) - \mathfrak{B}^{\mathcal{P}} \dot{x}_l(t) && (3.65) \\ \omega(0) &= \omega_0; \;\; \omega_0 = [\omega_0^{\mathcal{F}}; \;\; \omega_0^{\mathcal{P}}]; \;\; x_d = [x_d^{\mathcal{F}}; x_d^{\mathcal{P}}] && (3.66) \end{aligned}$$

where: $\omega_0^{\mathcal{P}} = x_{d,0}^{\mathcal{P}} - \mathfrak{B}^{\mathcal{P}} x_{l,0}$ and $\omega_0^{\mathcal{F}} = x_{d,0}^{\mathcal{F}} - \mathfrak{B}^{\mathcal{F}} x_{d,0}^{\mathcal{P}}(L_1)$. Hence, $\dot{\omega}^{\mathcal{F}}(t) = \dot{x}_d^{\mathcal{F}}(t) - \mathfrak{B}^{\mathcal{F}}(\omega^{\mathcal{P}}(L_1,t) + \mathfrak{B}^{\mathcal{P}} \dot{x}_l)$, so that the ODE dynamics couple to the froth and pulp zones in the column. Therefore, the result of this state transformation is a newly obtained infinite-dimensional state-space system of coupled DPS and LPS:

$$\begin{aligned} \dot{x}(t) &= \mathcal{A}x(t) + \mathcal{B}u(t) && (3.67) \\ y(t) &= \mathfrak{C}x(t) && (3.68) \end{aligned}$$

3.2.5 Boundary to in-domain input transformation

The interconnection of the system of hyperbolic PDEs and ODEs is considered as a boundary-controlled hyperbolic PDE system. In particular, the inputs are applied to the ODE system and by the boundary interconnection propagate to the pulp and the froth zones; however, one input is applied in the countercurrent direction at the top of the column (e.g. η). The manipulated inputs are wash water, air flow rate, feed concentration and the controller variables are the spatial profiles of minerals. In order to change the inhomogeneous boundary condition for the PDE system to the new system with a homogeneous boundary condition, one can apply a state transformation by considering $\omega^{\mathcal{P}}(z,t) = x_d^{\mathcal{P}}(z,t) - \mathfrak{B}^{\mathcal{P}} x_l(t)$ and $\omega^{\mathcal{F}}(z,t) = x_d^{\mathcal{F}}(z,t) - \mathfrak{B}^{\mathcal{F}} x_d^{\mathcal{P}}(L_1,t)$ (we drop z-dependence in $\omega^{\mathcal{F}}(z,t) = \omega^{\mathcal{F}}(t)$ and $\omega^{\mathcal{P}}(z,t) = \omega^{\mathcal{P}}(t)$ in subsequent sections). In this way, the state of the CSTR given by the ODEs is linked to the spatial state of the pulp section by the $\mathfrak{B}$ operator, and from the interface of the pulp-froth section to the froth section. In other words, the spatial functions $\mathfrak{B}^{\mathcal{F}}$ and $\mathfrak{B}^{\mathcal{P}}$ represent two actuator distribution functions which link the finite dimensional CSTR state, $x_l(t)$ to $\omega^{\mathcal{P}}(z,t)$ and $x_d^{\mathcal{P}}(L_1,t)$ to $\omega^{\mathcal{F}}(z,t)$, respectively. Using this transformation, the control variable $U(t)$ can affect the PDEs throughout the entire column domain.

$$\dot{\omega}^{\mathcal{F}}(t) = \dot{x}_d^{\mathcal{F}}(t) - \mathfrak{B}^{\mathcal{F}} \dot{x}_d^{\mathcal{P}}(L_1,t) \tag{3.69}$$

$$\dot{\omega}^{\mathcal{P}}(t) = \dot{x}_d^{\mathcal{P}}(t) - \mathfrak{B}^{\mathcal{P}} \dot{x}_l(t) \tag{3.70}$$

$$\omega(0) = \omega_0;\ \ \omega_0 = [\omega_0^{\mathcal{F}};\ \ \omega_0^{\mathcal{P}}];\ \ x_d = [x_d^{\mathcal{F}}; x_d^{\mathcal{P}}] \tag{3.71}$$

where: $\omega_0^{\mathcal{P}} = x_{d,0}^{\mathcal{P}} - \mathfrak{B}^{\mathcal{P}} x_{l,0}$ and $\omega_0^{\mathcal{F}} = x_{d,0}^{\mathcal{F}} - \mathfrak{B}^{\mathcal{F}} x_{d,0}^{\mathcal{P}}(L_1)$. Hence, $\dot{\omega}^{\mathcal{F}}(t) = \dot{x}_d^{\mathcal{F}}(t) - \mathfrak{B}^{\mathcal{F}}(\omega^{\mathcal{P}}(L_1,t) + \mathfrak{B}^{\mathcal{P}} \dot{x}_l)$, so that the ODE dynamics couple to the froth and pulp zones

in the column. Therefore, the result of this state transformation is a newly obtained infinite-dimensional state-space system of coupled DPS and LPS:

$$\dot{x}(t) = \mathcal{A}x(t) + \mathcal{B}u(t) \tag{3.72}$$

$$y(t) = \mathfrak{C}x(t) \tag{3.73}$$

The state transformations that transfer the boundary to in-domain actuations are achieved by considering:

$$x_3(z,t) = x_3^n(z,t) + B_3(z)x_6(L_1,t) \tag{3.74}$$

$$x_4(z,t) = x_4^n(z,t) + B_4(z)x_1(t) \tag{3.75}$$

$$x_5(z,t) = x_5^n(z,t) + B_5(z)x_2(t) \tag{3.76}$$

$$x_6(z,t) = x_6^n(z,t) + B_6(z)\eta \tag{3.77}$$

$$x_7(z,t) = x_7^n(z,t) + B_7(z)x_4(L_1,t) \tag{3.78}$$

$$x_8(z,t) = x_8^n(z,t) + B_8(z)x_5(L_1,t) \tag{3.79}$$

which provides a condition to calculate the boundary values of B_3, B_4, B_5, B_6, B_7, B_8.

$$x_3(L_1,t) = x_3^n(L_1,t) + B_3(L_1)x_6(L_1,t);\;\; x_3(L_1,0) = x_{3,0}^n + B_3(z)x_6(L_1,0);$$
$$x_3^n(L_1,t) = 0;\;\; B_3(L_1) = 1$$
$$x_4(0,t) = x_4^n(0,t) + B_4(0)x_1(t);\;\; x_4(z,0) = x_{4,0}^n + B_4(z)x_1(t);$$
$$x_4^n(0,t) = 0;\;\; B_4(0) = 1$$
$$x_5(0,t) = x_5^n(0,t) + B_5(0)x_2(t);\;\; x_5(z,0) = x_{5,0}^n + B_5(z)x_2(t);$$
$$x_5^n(0,t) = 0;\;\; B_5(0) = 1$$
$$x_6(L_2,t) = x_6^n(L2,t) + B_6(L_2)\eta(t);\;\; x_6(L_2,0) = x_{6,0}^n + B_6(z)\eta(0);$$
$$x_6^n(L_2,t) = 0;\;\; B_6(L_2) = 1$$
$$x_7(L_1,t) = x_7^n(L_1,t) + B_7(L_1)x_4(L_1,t);\;\; x_7(z,0) = x_{7,0}^n + B_7(z)x_4(L_1,0);$$
$$x_7^n(L_1,t) = 0;\;\; B_7(L_1) = 1$$
$$x_8(L_1,t) = x_8^n(L_1,t) + B_8(L_1)x_5(L_1,t);\;\; x_8(z,0) = x_{8,0}^n + B_8(z)x_5(L_1,0);$$
$$x_8^n(L_1,t) = 0;\;\; B_8(L_1) = 1$$

By introducing x_3 , x_4, x_5, x_6, x_7, x_8 with the above new state representations, one obtains the operators of the linear state space model. Assuming that $\mathfrak{B}$ exists, one can define a system that has a homogenous boundary condition and distributed actuation through the domain. Therefore, by taking $B_3(L_1) = 1$, $B_4(0) = 1$, $B_5(0) = 1$, $B_6(L_2) = 1$, $B_7(L_1) = 1$, $B_8(L_1) = 1$, and with the assumption of $\mathfrak{B}(z) = 1$, the

state space representation can be simplified as

$$\mathscr{F} = \begin{bmatrix} F_{11} & F_{12} & F_{13} & 0 & F_{15} & F_{16} \\ F_{21} & F_{22} & F_{23} & F_{24} & F_{25} & F_{26} \\ F_{31} & F_{32} & F_{33} & F_{34} & F_{35} & F_{36} \\ F_{41} & F_{42} & F_{43} & F_{44} & F_{45} & F_{46} \\ F_{51} & 0 & 0 & F_{54} & F_{55} & F_{56} \\ F_{61} & 0 & 0 & F_{64} & F_{65} & F_{66} \end{bmatrix} \tag{3.80}$$

$$\mathfrak{A} = \begin{bmatrix} A_{311} & 0 & 0 \\ A_{321} & A_{111ss} - A_{222} & A_{112ss} - A_{223} \\ A_{331} & A_{121ss} - A_{232} & A_{122ss} - A_{233} \\ -A_{311} & A_{212} & A_{213} \\ 0 & A_{222} - A_{111ss} & A_{223} - A_{112ss} \\ 0 & A_{232} - A_{121ss} & A_{233} - A_{122ss} \end{bmatrix} \tag{3.81}$$

$$A = \begin{bmatrix} 0 & 0 & 0 \\ 0 & A_{111ss} & A_{112ss} \\ 0 & A_{121ss} & A_{122ss} \end{bmatrix}; \quad B = \begin{bmatrix} 1 & 0 & 0 \\ 0 & \frac{Q_f}{V_c(1-\epsilon_c)} & -GmU_{3ss}^{m-1}X_{1ss} \\ 0 & 0 & GmU_{3ss}^{m-1}X_{1ss} - \frac{X_{2ss}}{\epsilon_c V_c} \end{bmatrix} \tag{3.82}$$

$$\bar{\mathscr{B}}_d = \begin{bmatrix} -1 & 0 & 0 \\ 0 & \frac{Q_f}{V_c(1-\epsilon_c)} & GmU_{3ss}^{m-1}X_{1ss} \\ 0 & 0 & GmU_{3ss}^{m-1}X_{1ss} - \frac{X_{2ss}}{V_c\epsilon_c} + \frac{1}{\epsilon_p Ac}\frac{\partial X_{5ss}(L_1)}{\partial z_p} - \frac{1}{\epsilon_f A_c}\frac{\partial X_{8ss}}{\partial z_f} \\ 1 & 0 & 0 \\ 0 & \frac{Q_f}{V_c(1-\epsilon_c)} & GmU_{3ss}^{m-1}X_{1ss} \\ 0 & 0 & -GmU_{3ss}^{m-1}X_{1ss} + \frac{X_{2ss}}{V_c\epsilon_c} - \frac{1}{\epsilon_p Ac}\frac{\partial X_{5ss}(z)}{\partial z_p} \end{bmatrix} \tag{3.83}$$

where $\mathscr{B}_{f1} = GmU_{3ss}^{m-1}X_{1ss} - \frac{X_{2ss}}{V_c\epsilon_c} + \frac{\partial X_{5ss}(L_1)}{\epsilon_p A_c \partial z_p} - \frac{\partial X_{8ss}}{\epsilon_f A_c \partial z_f}$, $\mathscr{B}_{f2} = -GmU_{3ss}^{m-1}X_{1ss} + \frac{X_{2ss}}{V_c\epsilon_c} - \frac{1}{\epsilon_p A_c}\frac{\partial X_{5ss}(z)}{\partial z_p}$, $\delta(L_1 - z)$ denotes a Dirac function which takes the value of the

state at the point L_1 within the domain $[0, l]$ ($l = L_1 + L_2$ being the total length of the column). It is assumed that the process is operated at a constant volume, which implies that a level controller is implemented. This state space representation accounts for infinite and finite dimensional systems. The operator $\mathcal{A}$ in Equation 3.72 generates an exponentially stable semigroup $T_{\mathcal{A}}(t)$ on $X \times R^2$, which means that the initial value problem for Equation 3.72 is well-posed and has a unique solution. Detailed expressions for the elements of $\mathscr{F}$ are provided in Appendix B.

3.3 Boundary optimal (LQ) regulator design of a hybrid system of coupled hyperbolic PDEs and ODEs

We used the proposed optimal control law to regulate the concentration of minerals in the CSTR, and their profiles in the pulp and the froth zones.

$$\begin{bmatrix} \dot{\omega}(t) \\ \dot{x}_l(t) \end{bmatrix} = \begin{bmatrix} \mathscr{F} & \mathfrak{A} \\ 0 & A \end{bmatrix} \begin{bmatrix} \omega(t) \\ x_l(t) \end{bmatrix} + \begin{bmatrix} \bar{\mathscr{B}}_d \\ B \end{bmatrix} u(t) \tag{3.84}$$

$$y(t) = \mathfrak{C} \begin{bmatrix} \omega(t) & x_l(t) \end{bmatrix}^T \tag{3.85}$$

with the following boundary and initial conditions:

$$\omega(0, t) = 0; \;\; x_l(0) = x_{l,0} \tag{3.86}$$

where the new infinite-dimensional state-space system has a spatial state of $\omega(\cdot, t)$ and a finite dimensional of $x_l(t)$ defined as follows:

$$\omega(t) = \begin{bmatrix} x_6^n & x_7^n & x_8^n & x_3^n & x_4^n & x_5^n \end{bmatrix}^T \tag{3.87}$$

$$x_l(t) = \begin{bmatrix} x_1 & x_2 \end{bmatrix}^T; \quad u(t) = \begin{bmatrix} \eta & \tilde{u}_2 & \tilde{u}_3 \end{bmatrix}^T \tag{3.88}$$

so that the combined state is a column vector, $x(t) = [\omega(t) \;\; x_l(t)]^T$. Considering the following infinite-time horizon quadratic objective function:

$$J(x_0, u) = \int_0^\infty (< \mathfrak{C}x(t), \mathcal{P}\mathfrak{C}x(t) > + < u(t), \mathcal{R}u(t) >)dt \tag{3.89}$$

$$\tag{3.90}$$

and the positive semidefinite operator $\mathcal{P}$:

$$\mathcal{P} = PI; \;\; P = \begin{bmatrix} P_{11} & P_{12} \\ P_{21} & P_{22} \end{bmatrix} \tag{3.91}$$

and the positive definite matrix R, one can consider the solution of the infinite horizon optimal control problem by solving

$$\min_{u(t)} J(x_0, u) = \int_0^\infty (< \mathfrak{C}x(t), \mathcal{P}\mathfrak{C}x(t) > + < u(t), \mathcal{R}u(t) >)dt \tag{3.92}$$

$$s.t. \dot{x}(t) = \mathcal{A}x(t) + \mathcal{B}u(t) \tag{3.93}$$

The minimization of the objective function results in solving the following operator Riccati equation (ORE):

$$(\mathcal{A}^*\mathcal{Q} + \mathcal{Q}\mathcal{A} + \mathfrak{C}^*\mathcal{P}\mathfrak{C} - \mathcal{Q}\mathcal{B}R^{-1}\mathcal{B}^*\mathcal{Q})x = 0 \tag{3.94}$$

$$u_{opt}(t) = \mathcal{K}x(t) \tag{3.95}$$

$$\mathcal{K} = -R^{-1}\mathcal{B}^*\mathcal{Q} \tag{3.96}$$

where the operator $\mathcal{A} + \mathcal{B}\mathcal{K}$ generates an exponentially stable C_0-semigroup, or, in other words, the closed-loop feedback structure through the gain $\mathcal{K}$ achieves the exponential stabilization of the system. Moreover, to solve the ORE, it is assumed that the solution is in the following form:

$$\mathcal{Q} = \begin{bmatrix} \phi_0 I & 0 \\ 0 & \psi_0 I \end{bmatrix} \tag{3.97}$$

where ϕ_0 and ψ_0 are non-negative diagonal and non-negative symmetric matrices containing spatial functions $\phi_0(z)$ and values ψ_0, respectively. By substituting for operators $\mathcal{A}$, $\mathcal{B}$, $\mathfrak{C}$ and $\mathcal{Q}$ in equation 3.94, one obtains:

$$\begin{bmatrix} \mathscr{F}^* & 0 \\ \mathfrak{A}^T & A^T \end{bmatrix} \begin{bmatrix} \phi_0 & 0 \\ 0 & \psi_0 \end{bmatrix} + \begin{bmatrix} \phi_0 & 0 \\ 0 & \psi_0 \end{bmatrix} \begin{bmatrix} \mathscr{F} & \mathfrak{A} \\ 0 & A \end{bmatrix} + .. \tag{3.98}$$

$$+ \begin{bmatrix} \mathscr{C}_d^* & 0 \\ \bar{\mathscr{B}}_d^* \mathscr{C}_d^* & \mathscr{C}_l^* \end{bmatrix} \begin{bmatrix} P_{11} & P_{12} \\ P_{21} & P_{22} \end{bmatrix} \begin{bmatrix} \mathscr{C}_d & \mathscr{C}_d \bar{\mathscr{B}}_d \\ 0 & \mathscr{C}_l \end{bmatrix} - ...$$

$$\begin{bmatrix} \phi_0 & 0 \\ 0 & \psi_0 \end{bmatrix} \begin{bmatrix} \bar{\mathscr{B}}_d \\ B \end{bmatrix} R^{-1} \begin{bmatrix} \bar{\mathscr{B}}_d^* & B^* \end{bmatrix} \begin{bmatrix} \phi_0 & 0 \\ 0 & \psi_0 \end{bmatrix} = 0 \tag{3.99}$$

so that matrix multiplication yields the following system of four equations:

$$\mathscr{F}^* \phi_0 + \phi_0 \mathscr{F} + \mathscr{C}_d^* P_{11} \mathscr{C}_d - \phi_0 \bar{\mathscr{B}}_d R^{-1} \bar{\mathscr{B}}_d^* \phi_0 = 0 \tag{3.100}$$

$$\phi_0 \mathfrak{A} + \mathscr{C}_d^* P_{11} \mathscr{C}_d \bar{\mathscr{B}}_d + \mathscr{C}_d^* P_{12} \mathscr{C}_l - \phi_0 \bar{\mathscr{B}}_d R^{-1} B^* \psi_0 = 0 \tag{3.101}$$

$$\mathfrak{A}^T \phi_0 + \bar{\mathscr{B}}_d^* \mathscr{C}_d^* P_{11} \mathscr{C}_d + \mathscr{C}_l^* P_{21} \mathscr{C}_d - \psi_0 B R^{-1} \bar{\mathscr{B}}_d^* \phi_0 = 0 \tag{3.102}$$

$$A^T \psi_0 + \psi_0 A + \mathfrak{B}^* \mathscr{C}_d^* P_{11} \mathscr{C}_d \mathfrak{B} + \mathscr{C}_d^* P_{21} \mathscr{C}_d \mathfrak{B} + \mathfrak{B}^* \mathscr{C}_d^* P_{12} \mathscr{C}_l + ... \tag{3.103}$$

$$... + \mathscr{C}_l^* P_{22} \mathscr{C}_l - \psi_0 B R^{-1} B^* \psi_0 = 0$$

Since equation 3.101 can be transformed to equation 3.102 by taking the transpose and vice versa, these two equations are not independent. Equation 3.100 can be converted to the following differential equation:

$$V \frac{d\phi_0}{dz} = M^* \phi_0 + \phi_0 M + C_d^* P_{11} C_d - \phi_0 \bar{\mathscr{B}}_d R^{-1} \bar{\mathscr{B}}_d^* \phi_0 \tag{3.104}$$

Therefore, the following set of equations needs to be solved to find ϕ_0:

$$V_6\frac{\partial\phi_{01}}{\partial z} = 2A_{311}\phi_{01} + P_{111} - \frac{\phi_{01}^2}{R_1} \tag{3.105}$$

$$-V_7\frac{\partial\phi_{02}}{\partial z} = 2A_{322}\phi_{02} + P_{112} - \phi_{02}^2((\frac{Qf}{V_c(1-\epsilon_c)})^2\frac{1}{R_2} + \Gamma_1^2\frac{1}{R_3}) \tag{3.106}$$

$$-V_8\frac{\partial\phi_{03}}{\partial z} = 2A_{333}\phi_{03} + P_{113} - \frac{\phi_{03}^2\Gamma_2^2}{R_3} \tag{3.107}$$

$$V_3\frac{\partial\phi_{04}}{\partial z} = 2A_{211}\phi_{04} + P_{114} - \frac{\phi_{04}^2}{R_1} \tag{3.108}$$

$$-V_4\frac{\partial\phi_{05}}{\partial z} = 2A_{222}\phi_{05} + P_{115} - \phi_{05}^2((\frac{Qf}{V_c(1-\epsilon_c)})^2\frac{1}{R_2} + \Gamma_1^2\frac{1}{R_3}) \tag{3.109}$$

$$-V_5\frac{\partial\phi_{06}}{\partial z} = 2A_{233}\phi_{06} + P_{116} - \frac{\phi_{06}^2}{R_3}\Gamma_3^2 \tag{3.110}$$

with boundary conditions:

$$\phi_{01}(L_1) = 0,\ \phi_{02}(L_2) = 0,\ \phi_{03}(L_2) = 0,\ \phi_{04}(0) = 0,\ \phi_{05}(L_1) = 0,\ \phi_{06}(L_1) = 0 \tag{3.111}$$

where $\Gamma_1 = GmU_{3ss}^{m-1}X_{1ss}$, $\Gamma_2 = GmU_{3ss}^{m-1}X_{1ss} - \frac{X_{2ss}}{V_p\epsilon_c} + \frac{1}{\epsilon_p A_c}\frac{\partial X_{5ss}(L1)}{\partial z_p} - \frac{1}{\epsilon_f A_c}\frac{\partial X_{8ss}}{\partial z_f}$, $\Gamma_3 = -GmU_{3ss}^{m-1}X_{1ss} + \frac{X_{2ss}}{V_c\epsilon_c} - \frac{1}{\epsilon_p Ac}\frac{\partial X_{5ss}(L1)}{\partial z_p}$.

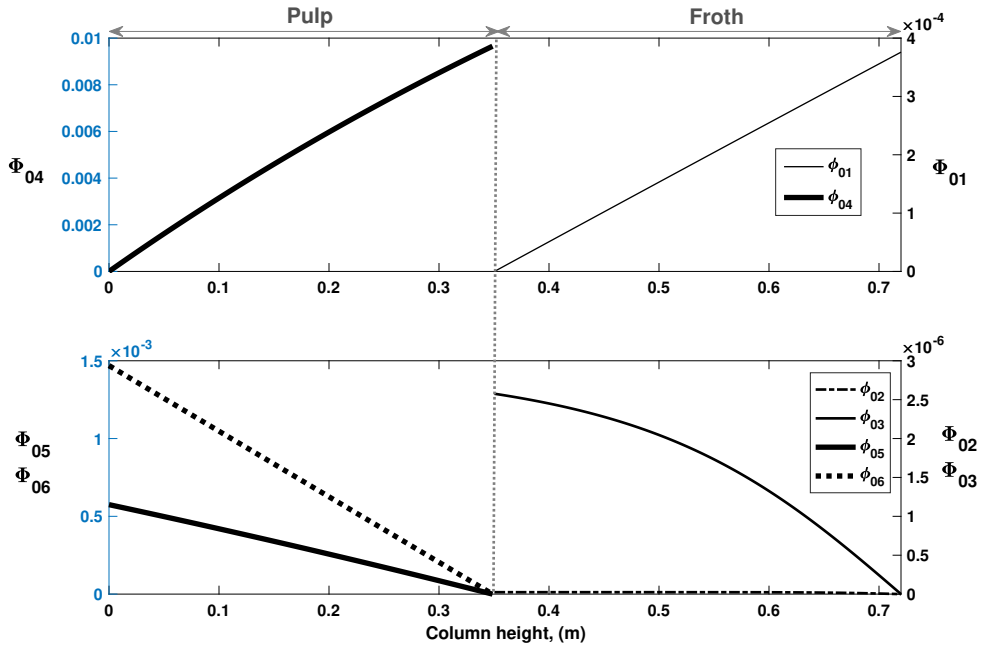

Figure 3.5: Spatial characteristics of the gain

The spatial characteristics of the gain, in the procedure of designing the LQ control law, is given in Figure 3.5. It should be noted that $\phi_1, \phi_2, \phi_3, \phi_4, \phi_5, \phi_6$ are positive gains related to the states $x_6, x_7, x_8, x_3, x_4, x_5$, respectively. It can be seen that the gains, Φ_{01} and Φ_{04}, associated with the states in the downflow, x_3 and x_6, are higher than the gains associated with the states in the upflows (entrainment and attached to the bubbles). In other words, from a practical point of view, it is more difficult to control the downflow than the upflows in the column flotation process. This is natural because the natural flow is the upward transport by the bubbles as the carrier and the downflow is effected only by a small flow of the wash water. Moreover, the actuation in the pulp zone (see Figure 3.5) requires stronger gain than in the froth zone, Φ_{01} and Φ_{04}. Φ_{03} and Φ_{06} are the spatial gains related to the attached

states in the froth and pulp, x_8 and x_5, respectively. Φ_{02} and Φ_{05} are the spatial gains related to the free entrained states, x_7 and x_4. By comparing these gains, it is clear that the control of attached particles is more difficult than the control of free entrained particles. Therefore, x_8 and x_5 require higher gains. We follow the algorithm proposed in [94] to solve differential algebraic DAE equations 3.104 - 3.110 in a systematic manner:

- First, positive definite symmetric matrices P_{11} and R are chosen in order to find the unique and non-negative solution of ϕ_0. Therefore, the matrix Riccati differential equation (equation 3.100) has been solved using the Euler integration method in space by solving a boundary value problem.

- After calculating ϕ_0, and choosing a guess for P_{12}, P_{22} is substituted by $P_{12}^* P_{11}^{-1} P_{12} + \epsilon I$, $\epsilon > 0$ in equation 3.104 to calculate ψ_0 and P_{12}. ([94] prove that there exists a positive symmetric P_{22} such that algebraic equations 3.102 and 3.104 simultaneously yield solutions P_{12} and ψ_0). Note that since equations 3.101 and 3.102 are the adjoint of each other and $P_{12} = P_{21}^*$, only one of these equations needs to be solved.

- Given P_{12} , a new $P22 > P_{12}^* P_{11}^{-1} P_{12} + \epsilon I$ is chosen and equation 3.102 and equation 3.104 are solved to find a new Ψ_0. The calculated P_{12} is such that the matrix P is positive and $Q = diag(\Phi_0, \Psi_0)$ (see Figure 3.5) is a non-negative solution of ORE.

- Finally, the state feedback operator can be calculated from

$$K = -R^{-1}[\bar{\mathscr{B}}_d^* \phi \quad B^* \psi] \tag{3.112}$$

Note that this solution exists if the finite-dimensional part is exponentially stabilizable and exponentially detectable.

- The LQR input can be calculated using

$$u_{opt} = Kx(t) \tag{3.113}$$

Remark: In this design, it is assumed that all states in the flotation column are measured, thus $C_d(z)$ is equal to $diag(1,1,1,1,1,1)$ and C_l is equal to $diag(1,1,1)$. However, one can apply spatial measurement and this will only change the evaluation of the above expressions and not the design procedure.

3.4 Results and discussion

To evaluate the performance of the control strategy, the designed feed-back controller has been applied to the original nonlinear system in closed loop. The nonlinear PDE-ODE system has been integrated numerically with the Euler method, backward in space and forward in time. We present representative simulations in this section, but have tested the controller for a variety of initial conditions. Details of the parameters used in the simulations are provided in Appendix C. In the simulation study, the following values were used as one representation of the initial conditions: $x_1(0) = 0.2\ kg/m^3$, $x_2(0) = 0$, $x_3(z,0) = 0.1066\ kg/m^3$, $x_4(z,0) = 0.18\ kg/m^3$, $x_5(z,0) = 0.3\ kg/m^3$, $x_6(z,0) = 0.08\ kg/m^3$, $x_7(z,0) = 0.18\ kg/m^3$, $x_8(z,0) = 0.2\ kg/m^3$. Note that the obtained steady state profiles are provided in Figures 3.3-3.4.

Finally, in order to account for a presence of noise which is associated with the real plant condition, we tested the controller performance when random noise was added

to the states and parameters (i.e. K_{ac}) of the plant model. For the design of the optimal controller, we chose positive definite

$P_{11} = diag(0.05, 0.0004, 0.0005, 0.0005, 0.000003, 0.000001)$, $R = diag(1, 1, 1)$, and $P_{12} = [0.05, 0, 0; 0, 0.025, 0; 0, 0, 0.14; 0.0001, 0, 0; 0, 0.1, 0; 0, 0, 0.001]$ and calculated the positive definite matrix $P_{22} = diag(1.1, 3335.9, 41.2)$. Moreover, the solution to equation 3.112 is the feedback controller gain.

Finally, in order to analyze the performance of the designed optimal controller, the rate of convergence of the system states after perturbation has been compared among these three cases: open-loop, controlled with model-based controller (LQR), and controlled with non-model-based (PI) controller.

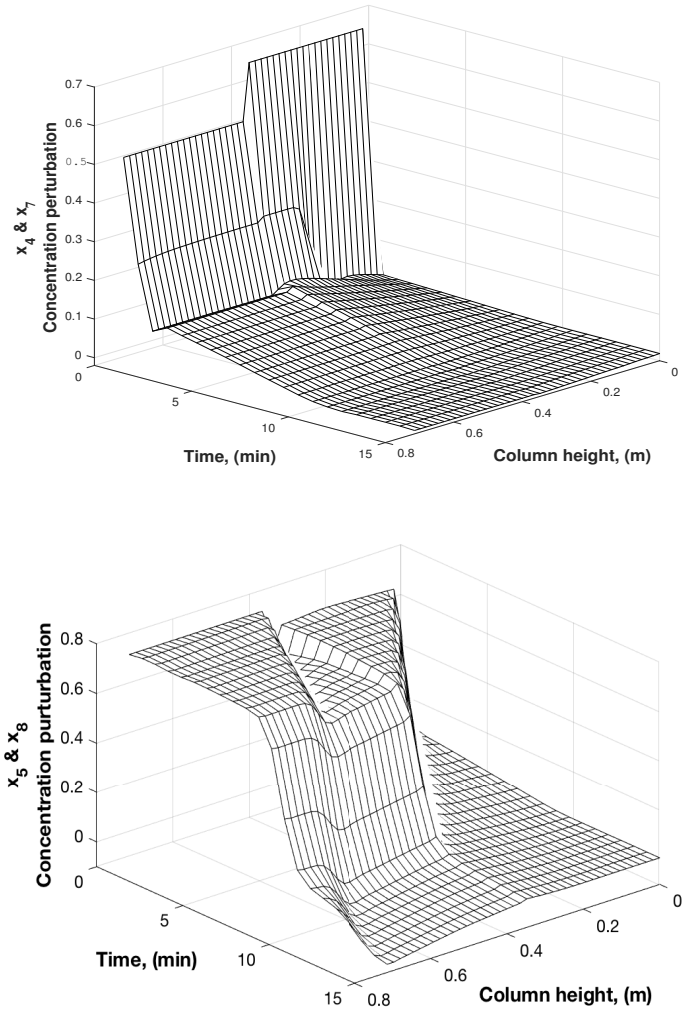

Figure 3.6: Concentration perturbation propagation of hydrophobic particles: free, x_4 and x_7, and attached, x_5 and x_8, in the pulp and froth.

Figure 3.6 (a) illustrates the spatiotemporal propagation of the free hydrophobic particles in the upflow (entrainment) through the column. Figure 3.6 (b) demonstrates the spatiotemporal propagation of concentration perturbation of attached hydrophobic particles to the bubbles in the pulp and froth zones after implement-

ing the LQR. Figure 3.6 illustrates how an arbitrary initial profile is stabilized after approximately 12 minutes (which is the approximate residence time of the column). Even though an LQR was designed to provide exponential stability of the system from any initial condition in a finite dimensional setting, the transport-reaction system, which is infinite dimensional, has a finite time governed by the slowest state after which exponential stabilization can be achieved. Among all the states in the column, the one associated with the attached particles to the bubbles, x_8, is the slowest state. Therefore, the dynamics of this state will define the finite time after which the controller stabilizes the system and brings the states to the steady state from any initial condition.

Two (proportional - integral) PI controllers have been designed to work simultaneously to serve as a point of comparison for the LQR:

- PI_1: The controlled variable CV is the concentration of attached minerals at the top of the column, $x_8(L_2)$. The concentration of minerals in the feed, $X_{1,0}$, is selected as the measured variable MV. The selected controller gains are $K_c = 1$; $K_I = 0.01$ with the reference signal set to zero.

- PI_2: The CV is the concentration of free minerals in the downflow at the bottom of the column, $x_3(0)$. The gas flow rate, Q_a, is selected as the MV, and controller gains are $K_c = 0.5$; $K_I = 0.01$ with the reference signal set to zero.

To compare the rate of stabilization between different control design strategies, the squared norm of the state values has been integrated over the column height, which is an appropriate performance metric for this regulatory control problem. Figures 3.7, 3.8, 3.9 show the evolution of this norm for three representative states. For the case

of free valuable particles in the pulp zone, the squared norm of the state perturbation has been integrated through the pulp height $\int_0^{L_1} x_4^2(z,t)dz$ and plotted over time in Figure 3.7. In the open-loop case, the system exhibits an inverse response, which is a characteristic of a linear system with a positive zero. It can be observed from Figure 3.7 that x_4, which represents the perturbation of the concentration of free valuable particles in the pulp zone, increases initially before it reaches the steady state. It is expected that there is a dynamical interplay between the transport of x_4 in the up-flow along the column and the transfer of free particles between the downflow, upflow and the gas flows. The closed loop system with the PI controller has complex dynamics, as can be seen from Figure 3.7, with the perturbed state increasing and decreasing multiple times before reaching the steady state. A numerical comparison of the performance metric over the entire period of the simulation for Figure 3.7 shows that the metric is 2.25×10^{-3} for the LQR, 0.17 for PI control, and 2.06×10^{-2} for the open loop case. This means that the LQR stabilizes this state an order of magnitude faster than the open loop, and PI control performs worse on this count than even the open loop case. A similar comparison for Figure 3.8 shows the performance metric to be 7.20×10^{-4} for the LQR, 1.68×10^{-3} for the PI controller, and 8.05×10^{-4} for the open loop case.

As Figures 3.7, 3.8 and 3.9, illustrate, the model-based controlled system has the ability to stabilize the initial condition faster than the non-model-based PI controlled system and the open-loop system. The state evolution goes to zero in finite time under the designed optimal control gain, but as was mentioned above, there is a minimum specific finite time (governed by the inherent time scale of the process), which is the fastest that the states can converge to the steady state. Although the

LQR displays better performance than the open loop and the PI controller overall (see Figure 3.9), the difference in the case of x_8 (the slowest state) is not very significant. The performance metric in this case is 5.19×10^{-3} for the LQR, $9.80x10^{-3}$ for the PI controller, and 1.08×10^{-2} for the open loop case. Figures 3.7, 3.8 and 3.9 also illustrate LQR controller rejection of disturbances in addition to robust stabilization of the system. A step disturbance has been applied to these states at 4 minutes. It can be seen that the delay rate in response to the initial perturbation is similar before and after the applied disturbance is rejected.

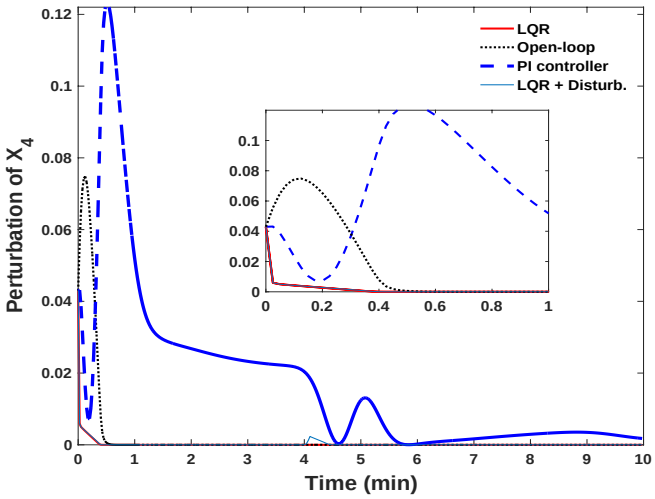

Figure 3.7: Integral of the squared concentration perturbation of free minerals in the up-flow in the pulp, $\int_{L_1}^{L_2} x_4^2(z,t)dz$. Thick line: LQR, dotted: open-loop, dashed: PI, thin line: LQR with disturbance applied at 4 min.

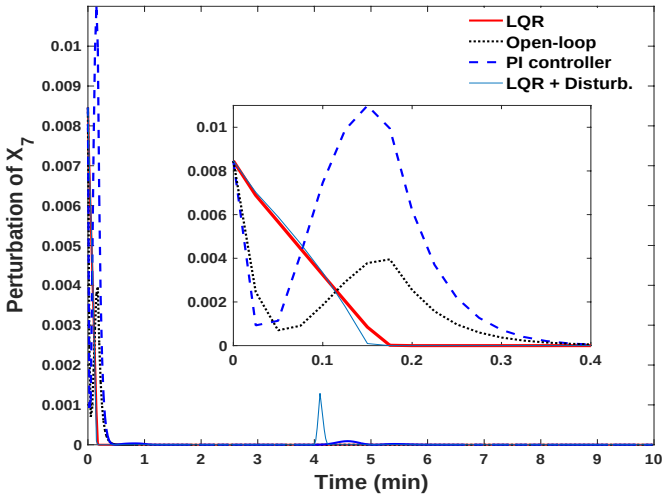

Figure 3.8: Integral of the squared concentration perturbation of free minerals in the up-flow in the froth, $\int_{L_1}^{L_2} x_7^2(z,t)dz$. Thick line: LQR, dotted: open-loop, dashed: PI, thin line: LQR with disturbance applied at 4 min.

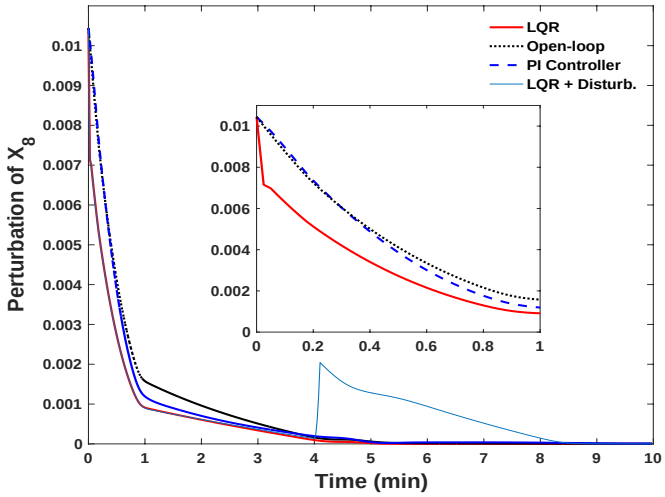

Figure 3.9: Integral of the squared concentration perturbation of attached minerals in the froth, $\int_{L_1}^{L_2} x_8^2(z,t)dz$. Thick line: LQR, dotted: open-loop, dashed: PI, thin line: LQR with disturbance applied at 4 min.

3.5 Conclusions

A fundamental model based on physical principles has been proposed for a hybrid flotation column that includes an agitated section. The model considers bubble-particle attachment and detachment, includes relevant gas and liquid transport phenomena, consists of a set of coupled ODEs and transport hyperbolic PDEs, and goes beyond models proposed in the literature, where it was assumed that the column consists of a series of well-mixed CSTRs. One of the important contribution is that the proposed model of the system is formulated as a state space model prior to be applied for the optimal controller design. Boundary linear quadratic regulation is developed for this system of coupled ODEs and PDEs, and this, too, extends the control formulation available in the literature, due to the complex structure of interconnection between transport flows and boundaries in the hybrid column. Through simulations, we demonstrate the efficacy of the optimal controller in stabilizing the column flotation system and show that it outperforms a non-model-based PI controller by more than an order of magnitude in terms of regulatory control response.

Chapter 4

Monitoring and State Estimation of Column Flotation with Fundamental Dynamic Models

Abstract A two-phase semi-batch flotation column is modelled as the interconnection of two plug-flow reactors (PFR) representing pulp and froth zones. The plant model accounts for the appearance and breakage of three bubble size classes. This distributed parameter system (DPS) is described by sets of nonlinear coupled conservation hyperbolic partial differential equations (PDEs). Two on-line model-based state estimators for a semi-batch flotation column based on a two-phase fundamental dynamic model. The fundamental dynamic model featuring the upward air-liquid mixture belongs to the class of conservative hyperbolic nonlinear transport partial differential equation (PDE) systems. In the two-phase case, the unknown states representing the gas holdup through the column, have been estimated under the assumption that the gas holdup of the bubble size classes at the exit on top of the column can be measured. It is confirmed that the proposed estimator for a two-phase case well predicts the gas holdup propagation through a lab-scaled two-phase semi-

batch column flotation based on experimental data. Later in this chapter, a dynamic estimator for a continuous flotation column based on the three-phase fundamental dynamic model in chapter 2 is proposed and implemented. In the three-phase case, the unknown states, the gas holdup through the column as well as the concentration of attached and free minerals in the upward and downward flows, have been estimated under the assumption that the gas holdup and concentration of attached and free minerals on top of the column can be measured by using machine vision (such as with a camera and the Visiofroth software). For the two-phase case, the performance of model-based EnKF is compared to that of the Luenberger observer with the same operating conditions (air flow rate, reagent and frother concentrations). Gas holdup propagation was captured better by the Luenberger observer for state estimation in the simplified version of the system (two-phase). However, the EnKF has an acceptable performance with the capacity to be used in more complex nonlinear systems (three-phase). Implementation of EnKF for the state estimation of more complex cases such as continuous nonlinear three-phase model of a flotation column with parameter uncertainty is a better option compared to the linear Luenberger observer. The linear Luenberger observer has intrinsic limitations as it would be too complex to be implemented compered to the realization of EnKF.

4.1 Introduction

Column flotation is an efficient separation process to separate valuable mineral(s) from ore based on the differences in the surface minerals hydrophobicity. The complex column flotation separation process offers challenges in process modelling, monitoring, and control. In general, the main objective of column flotation operations is

to maximize the product quality specification (grade and/or recovery) and maintain the operational levels using on-line monitoring and control despite disturbances in the operations. Along this line, it is required to have an accurate process model and real-time estimation of the states of the system.

4.1.1 Column flotation process measurement

In practice, some essential properties for the monitoring and control purposes of column flotation cannot be measured explicitly (for example, the gas holdup through the column which is directly related to the grade and recovery); instead they must be estimated from limited number of available measurements. Basically, on-line instruments may not exist or online measurement would be expensive to maintain and in addition have low sample frequencies. Also, samples need a number of hours to be analyzed. Among all variables that affect the flotation performance, gas holdup propagation and bubbles size distribution have been proven to be the key variables affecting the flotation separation process performance which can be defined as grade and/or recovery [7]. Therefore, this finding implies that we require to measure the gas holdup in the flotation column and possibly to infer bubble size distribution. However, measuring the time evolution of gas holdup throughout the column in real industrial application is really difficult, expensive and sometime impossible. Therefore, the estimation of these process variables is of interest bearing in mind that only few true measurements as outputs are available in the system. Moreover, when it comes to methods for the estimation, the model for column flotation processes are often complex and nonlinear with unknown state variables and/or uncertain parameters. This counts as a challenge for the estimation using the Kalman-based sates

estimators.

An important note to consider is that using hardware sensors in the complex and harsh environment of froth flotation is very challenging. Therefore, a cheap, reliable, and fast alternative is an attractive option to be explored [24]. A remedy for this deficiency is the use of soft sensors, which is also a more cost-efficient alternative. Furthermore, the data from offline measurements can be used as initial guesses for the online estimator and to minimize the error between the model predicted and measured recovery over the time. Among all variables that affect the flotation performance, gas holdup propagation and bubbles size distribution have been proven to be key variables for the flotation separation process. Bubble surface flux, which is a function of these key variables, is reported to have a linear correlation with the flotation rate constant [17].

The bubbles are dynamically interacting and the bubble surface area for attachment of particles changes often. In this chapter, we explore the application of an ensemble Kalman filter (EnKF) and a Luenberger observer as two tools for the state estimation.

4.1.2 State estimation techniques for nonlinear systems

Several known methods for monitoring and state estimation of linear and nonlinear spatiotemporal systems have been explored in the literature, including extensions of the Luenberger observer and Kalman filter concepts to distributed parameter systems [14, 95–101]. Among the first contributions the works of Luenberger [102, 103] and Kalman [104] introduced basic concepts of Luenberger observer and Kalman filter designs. Ray [14] and Yu [101] step further and extended the design to the

PDE systems. Some of the published works concentrated on the optimal location of measurement in axial dispersion or tubular reactor systems [101]. To make estimations of a nonlinear system behaviour, the popular estimators such as Luenberger observer, which involves linearization of the original model, can become very complex for linearization as well as for finding the observer gain for the highly complex infinite dimensional systems. Since 1960, when the Kalman filter (KF) [104] was proposed [105] as the most notable innovation for solving state estimation problem [98], several extensions and application of this method have been reported [106, 107]. The KF is an optimal sequential predictor-corrector based estimator, which means that whenever dynamic data are available, they are sequentially integrated in the model to minimize the estimated error covariance. The most widely used variant of the exponential observers is the extended Kalman filter (EKF). For highly nonlinear systems with non-Gaussian probability distribution functions (pdfs) of the state, the EKF may result in significant estimation errors. To alleviate the deficiencies of linearization in the EKF, derivative-free stochastic observers, namely the unscented Kalman filter (UKF) and Monte Carlo filters, have been developed [108]. These filters are capable of dealing with nonlinear state estimation problems with multimodal and non-Gaussian pdfs [109]. The UKF is capable of estimating the state pdfs with a high accuracy without the need for computing the Jacobian matrices. On the other hand, the Monte Carlo filters have found widespread use owing to the ever increasing computing power. As reported in [110], there is a large variety of Monte Carlo filters used to implement the recursive Bayesian estimation framework. The merit of the Monte Carlo filters lies in their ability to handle nonlinear process dynamics without making any assumptions either on the nature of dynamics nor on the shape or any

other characteristics of pdfs [110–112]. The most common estimators based on the use of an ensemble of particles are the ensemble Kalman filter (EnKF), unscented Kalman filter (UKF), and the particle filter(PF). Note that the UKF does not use Monte Carlo sampling. The EnKF and UKF provide the mean and covariance of the posterior distribution of the states assuming the Gaussian distribution. The PF, which works on Bayesian principles, can provide estimates for the full distribution of the states even in situations where the distribution is not Gaussian by using a set of particles associated with different weights [113]. However, for high dimensional systems, the ensemble Kalman filter has an advantage over the particle filter in that it is scalable to high-dimensional systems without an increase in the size of the required ensemble, under the assumption of Guassian distribution. Another class of nonlinear state estimation techniques known as the high gain observers has also received substantial attention in the literature. The high gain observers are based on the notion of linearization through coordinate transformation. These observers tend to possess similar characteristics as the extended Luenberger observer and the extended Kalman filter [110–112]. Despite the importance and intrinsic complexities in the structure of composite distributed parameter systems utilized in the modelling framework of the column dynamics, there is a lack of published research in the area of ensemble Kalman Filter estimation for these complex systems. This chapter provides a systematic general procedure for the design of an ensemble Kalman filter for a system of two hyperbolic PDEs representing column flotation. By considering 1) a model of boundary coupled hyperbolic PDE system that allows for various transport modelling features and bubble interactions, 2) the online measurement from the more detailed version of the complex model to resemble the plant measurement, 3) design

of an EnKF for coupled ODE-PDEs system such that the calculated Kalman gain from the prediction step of the estimation process was used in the correction step to do a one step ahead prediction of the states (which are the gas fraction propagation through the column), 4) design of a Luenberger observer to do a one step ahead prediction of the states, 5) comparison of the two estimators.

4.2 Monitoring the gas holdup distribution in a two-phase semi-batch column flotation

4.2.1 Two-phase column flotation model development

Gas holdup models (given by equations 4.23 - 2.30 in Chapter 2 of this thesis) account for the bubbles coalescence in the pulp and froth zones. In the present work, bubbles are categorized into three discrete size classes. To compute the velocity of the swarm of bubbles in each bubble size classes, the set of equations 2.31 from Chapter 2 is used. The total rise and decline in bubbles holdup in the size class n due to bubble collisions are calculated using equations 2.32 and 2.33 from Chapter 2. Therefore, this developed interconnected model is used to describe the spatiotemporal propagation of gas fraction through the column flotation. This model, which is used for state estimation, accounts for the spatial distribution of gas fraction through the column (froth and pulp), which has a direct effect on the grade and recovery in the column flotation system. The design relies on a sensor/probe at the top of the system to obtain online bubble size and gas holdup measurements in a transparent semi-batch lab-scale flotation column. The estimation of gas holdup through the measurement of

electrical conductivity/probe is a method that has been widely utilized in the study of two-phase systems. Therefore, the estimated gas holdup can be compared with the experimental data in a simplified case and provide the insight in the accuracy of the estimator.

4.2.2 Ensemble Kalman filtering (EnKF) for a state space model

Consider a dynamic nonlinear state space model represented by:

$$x_t = f(x_{t-1}, u_{t-1}) + w_{t-1} \tag{4.1}$$

$$y_t = Hx_t + v_t \tag{4.2}$$

Here the system is a state space model consists of unobservable/hidden states x_t, inputs u_n, output measurement y_t with an observations given by noisy instantaneous functions of the state process where the observations are Gaussian-linear, $w \sim \mathcal{N}(0, Q_t)$ and $v \sim \mathcal{N}(0, R_t)$ are process and measurement noise respectively.
The EnKF employs a sequential Monte Carlo method. The observed time series (y_t), $t \in \mathbb{N}$ derived from an unobservable state process (x_t), $t \in \mathbb{N} \cup \{0\}$, which is also referred signal. The state process is assumed to be first order Markov, and the observations y_t are assumed to be conditionally independent given the state process (x_t), with y_t depending only on the (x_t). The joint distribution of signal and observations is demonstrated in the following graph.

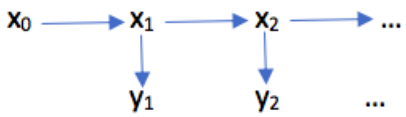

Equivalently, for a highly nonlinear randomized dynamic state space system that is instantaneously observed subject to independent random errors, the model is of the form [114]:

$$x_t = f(x_{t-1}, u_{t-1}, w_{t-1}) \tag{4.3}$$

$$y_t = h(x_t, v_t) \tag{4.4}$$

where f and h are measurable functions, and (w_t), $t \in \mathbb{N}$ and (v_t), $t \in \mathbb{N}$ are independent random sequences, independent of each other and independent of x_0 with Gaussian distributions. Extracting the signal (x_t) from the noisy and incomplete measurement (y_t) is the main task in state estimation. This recursive computation makes the on-line applications possible where observations are collected in real-time. We assume that $x = \mathbb{R}^q$ and $y = \mathbb{R}^d$, where $f \in \mathbb{R}^{q \times q}$ and $h \in \mathbb{R}^{d \times q}$ EnKF is a recursive Monte Carlo filter used to integrate dynamic data to the model as soon as they are acquired. Its ease of implementation and efficiency has resulted in various applications in different fields such as atmospheric physics, oceanography [115], meteorology [116], hydrology [117], and petroleum engineering [118]. These filters represent, with error covariance matrices, the uncertainties in the process model.
The EnKF operates by propagating the model and its uncertainties through time based on a dynamic model describing the process. During each time step, the filter has two stages. The first stage is prediction: its purpose is to propagate the model by running the simulation through the time step of interest. The second stage is updating (or analysis): the model is updated by adjusting the numerical responses with the measurements. The EnKF is based on a Bayesian approach, where the model uncertainties are represented by an ensemble, that is, a group of realizations

for model parameters and for model states. Model parameters are properties that do not change with time, whereas model states change with time (see figure 4.1).

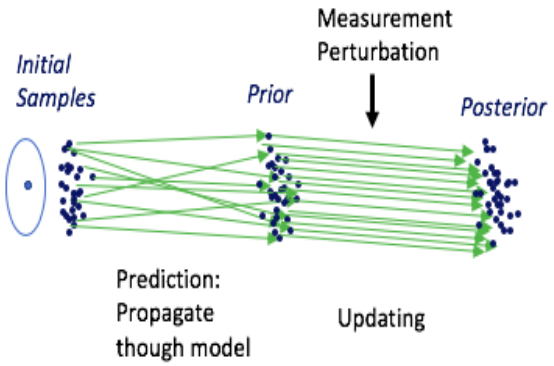

Figure 4.1: Schematic of the EnKF estimation process [119].

In any application of the ensemble Kalman filter, there are some potential error sources as they may affect the reliability of the ensemble as the replacement for the true filter estimation. Those errors can be categorized as the following [120]:

- Sampling error. This can be of a small size of ensemble. This has an effect on the estimation of the prediction covariance matrix.

- Systematic errors. These can also be seen in filter bias such as selecting the linear updating rules while the prediction distribution is non-Gaussian, etc. These can be seen in model bias including misspecification of the observation error statistics, errors of the observer and state dynamics.

1. Prediction Step: In this stage, one generates N realizations from the prior probability distribution to create an initial ensemble of the model. A vector of

states estimation is: [119]

$$x^i_{k|k-1} = \left[f(x^i_{k-1|k-1}) \right] \tag{4.5}$$

The mathematical formulation of the EnKF (Evensen, 2007) requires the computation of the first and second statistical moments, that is, mean and variance for the model states at time instant k given their values up to $k-1$, that are derived from an empirical average over a finite size ensemble of realizations. The procedure uses an ensemble of particles from which the statistical information of the distribution of the states can be calculated. In order to have an explicit analytical expression for the Kalman gain, both prior and posterior distribution are assumed to have Guassian distribution. The procedure for this algorithm is as follows:

At time step n, N particles are selected randomly from the prior distribution to form the prior ensemble $x^i_{k-1|k-1}$, $i = 1, ..., N$. In the prediction step, each member of the ensemble $x^i_{k-1|k-1}$ is evolved through the model of the system $x^i_{k|k-1} = f(x^i_{k-1|k-1}, u_{k-1}, w^i_{k-1})$. $x^i_{k|k-1}$ is the predicted ensemble. Corresponding to each member of the ensemble, a value for the predicted observation is obtained. This is achieved by perturbing the predicted measurement by random measurement noise. $y^i_{k|k-1}$ represents the predicted measurement data.

In the prediction step, two error matrices are defined. The uncertainty matrix in the predicted states with respect to the overall ensemble is defined as:

$$e^i_{k|k-1} = x^i_{k|k-1} - \mu^x_{k|k-1} \tag{4.6}$$

with the mean of the prediction at time instant k given their values up to $k-1$

for any realization i being:

$$\mu^x_{k|k-1} = \frac{1}{N}\sum_{i=1}^{N} x^i_{k|k-1} \tag{4.7}$$

Similarly, the error/uncertainty matrix in the measurement with respect to the overall ensemble is defined as:

$$\epsilon^i_{k|k-1} = y^i_{k|k-1} - \mu^y_{k|k-1} \tag{4.8}$$

where

$$\mu^y_{k|k-1} = \frac{1}{N}\sum_{i=1}^{N} y^i_{k|k-1} \tag{4.9}$$

The covariance matrix of the ensemble is:

$$\hat{P}^{\epsilon,\epsilon}_{k|k-1} = \frac{\sum_{i=1}^{N}(\epsilon^i_{k|k-1})(\epsilon^i_{k|k-1})^T}{N-1} \tag{4.10}$$

and the cross-covariance matrix between the predicted state ensemble and the predicted measurement ensemble is.

$$\hat{P}^{e,\epsilon}_{k|k-1} = \frac{\sum_{i=1}^{N}(e^i_{k|k-1})(\epsilon^i_{k|k-1})^T}{N-1} \tag{4.11}$$

2. Analysis or Correction / Update: In this stage, the state covariance matrix and R (the measurement noise covariance matrix), are used to calculate the Kalman gain as follows:

$$K_{gain} = \hat{P}^{\epsilon,\epsilon}_{k|k-1}(\hat{P}^{e,\epsilon}_{k|k-1} + R)^{-1} \tag{4.12}$$

It is important to note that the measurement noise should be selected according to the accuracy of the measuring device and lack of accuracy in selecting

the measurement noise affects its performance (through the calculated gain) significantly. Later using the measurement, one updates the model states:

$$X^i_{k|k} = X^i_{k-1|k-1} + K_{gain}(y^{i,abs}_k - y^i_{k|k-1}) \tag{4.13}$$

In this stage, we perturb the measurement based on the measurement noise covariance to obtain an ensemble of N measurements. Also we consider that the actual measurement in the real process is noisy with the process noise of ν_k which has a normal distribution with zero mean and R as the covariance:

$$y^{i,obs}_k = y^{obs}_k + \nu^i_k \tag{4.14}$$

$y^{i,obs}$ is the true measurement value at time step k.

The EnKF provides an approximation of the error covariance matrix from an ensemble of finite size. As the size of the ensemble, N_e, increases, the approximation of the error covariance matrix improves. However, increasing the ensemble size induces a computational overburden. Thus, a trade-off exists between the accuracy of the covariance matrix approximation and the computational cost, and the choice of the ensemble size is case dependent [121].

The ensemble Kalman filter requires a repetitive sampling of random variables. Conceptually, the filter is initialized with some ensemble, x^1, ..., x^N of size N drawn from the initial prior, a normal distribution with mean vector the population mean and covariance matrix P, and measurement perturbation is generated for the updating state[120].

The pseudo-code for the EnKF algorithm is given below:

Initial Ensemble

for i=1:N

$x^i_{k-1|k-1}$

end for

for $k = 1 : t_{final}$

y^{obs}_k

Prediction Step

for i=1:N

$x^i_{k|k-1}$=$f(x^i_{k-1|k-1}, u_{k-1}, w^i_{k-1})$

$y^i_{k|k-1} = cx^i_{k|k-1}$

end for

$\mu x_{k|k-1} = \frac{1}{N}\sum_{i=1}^{N} x^i_{k|k-1}$

$\mu y_{k|k-1} = \frac{1}{N}\sum_{i=1}^{N} y^i_{k|k-1}$

for i=1:N

$e^i_{k|k-1} = x^i_{k|k-1} - \mu x_{k|k-1}$

$\epsilon^i_{k|k-1} = y^i_{k|k-1} - \mu y_{k|k-1}$

end for

$\hat{P}^{\epsilon,\epsilon}_{k|k-1} = \frac{\sum_{i=1}^{N}(\epsilon^i_{k|k-1})(\epsilon^i_{k|k-1})^T}{N-1}$

$\hat{P}^{e,\epsilon}_{k|k-1} = \frac{\sum_{i=1}^{N}(e^i_{k|k-1})(\epsilon^i_{k|k-1})^T}{N-1}$

Analysis or Update

$K_{gain} = \hat{P}^{\epsilon,\epsilon}_{k|k-1}(\hat{P}^{e,\epsilon}_{k|k-1} + R)^{-1}$

for j=1:N

$X^i_{k|k} = X^i_{k-1|k-1} + K_{gain}(y^{abs}_k - y^i_{k|k-1})$

$y^{i,obs}_k = y^{obs}_k + \nu^i_k$

end for

end for

Description of simulation parameters in the two-phase system using the EnKF: The two-phase unit simulated in this section is a flotation column with 0.563 m of height and 0.073 m of diameter.

The simulation parameters for the state estimation of the two-phase system are as follows:

Q_a	0.0016	$m^3.min^{-1}$
ϵ_c	$(0.02, 0.04, 0.3)$	-
ϵ_{pp}	$(0.08, 0.24, 0.08)$	-
$d_{b,p}$	(0.0015,0.001,0.0005)	m
ϵ_f	$(0.18, 0.46, 0.06)$	-
$d_{b,f}$	$(0.003, 0.002, 0.001)$	m
ρ_g	1.225	$kg.m^{-3}$
ρ_{sl}	1250	$kg.m^{-3}$

Initially the model for a two-phase semi-batch flotation column was ran for 70000 iterations with $\Delta t = 0.00005$ which is around 3.5 minutes from starting the separation process. 0.99% of the final simulation results have been chosen as the mean point to generate the 80 initial ensemble around 414 states. The noise considered for the system is assumed to have a normal Guassian distribution with zero mean and variance (or standard deviation) related to the order of magnitude of the state value. For example, for the gas hold up of bubble in size class 1 which has the order of magnitude of 10^{-2} the standard deviation of 10^{-2} has been used.

Results of state estimation in the two-phase system using the EnKF

Plant states are the gas holdup / fraction of three size classes of bubbles in the froth and pulp zones of the flotation column. In this section, the column height has

been presented in a dimensionless form ($\frac{Distance\ from\ the\ bottom\ of\ the\ column}{FrothHeight + Pulp\ Height}$) to depict the boundary between pulp and froth phases. Figure 4.2 demonstrates the spatiotemporal propagation of the true state and the estimated gas holdup of bubbles in size classes 1, 2, and 3, in both the pulp and the froth. Along the same lines, the predicted propagation of the total gas holdup (see Figure 4.3) had the same trend as the true states and predicts of summation of all these states.

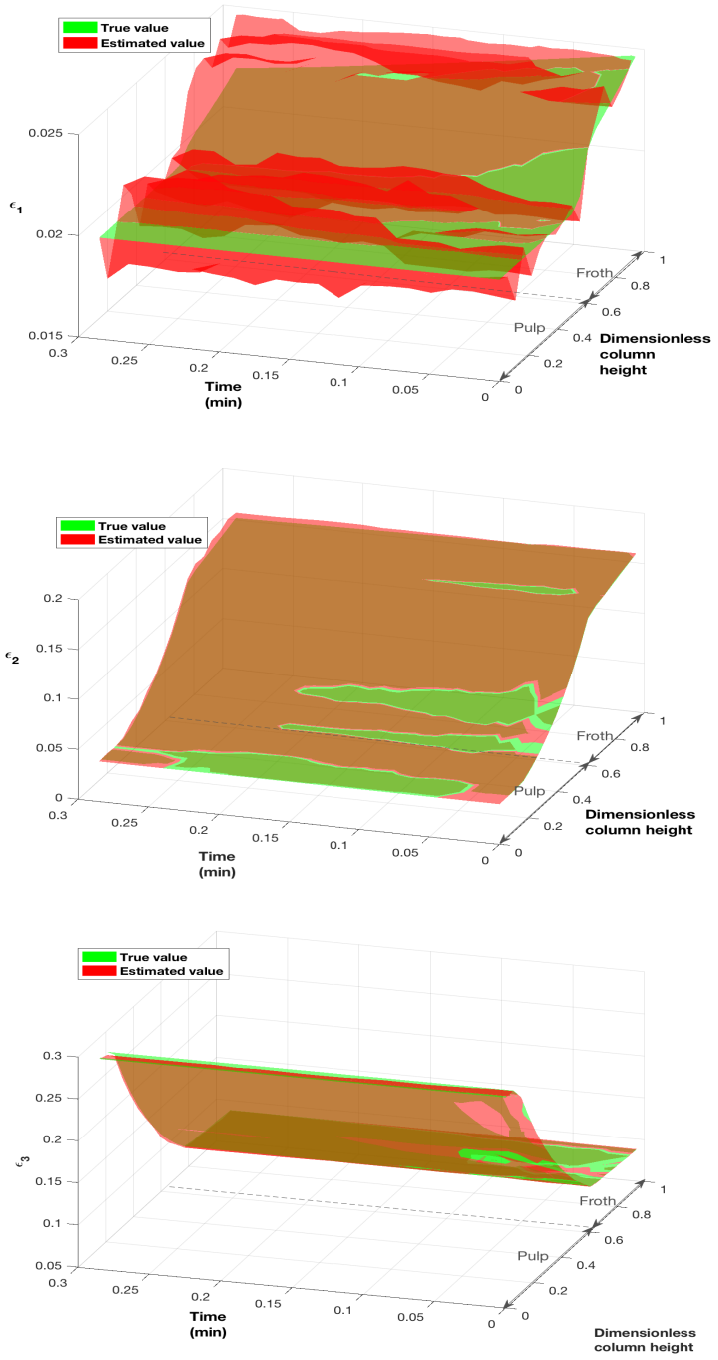

Figure 4.2: True and predicted values, using EnKF, for the gas holdup of three bubble size classes through a two-phase flotation column.

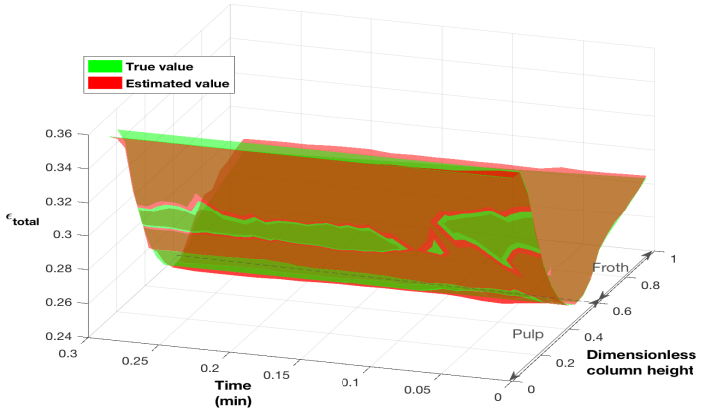

Figure 4.3: True and predicted values, using EnKF, for the total gas holdup through a two-phase flotation column.

The predicted profile reaches the plant states very fast (see Figures 4.4 - 4.5).

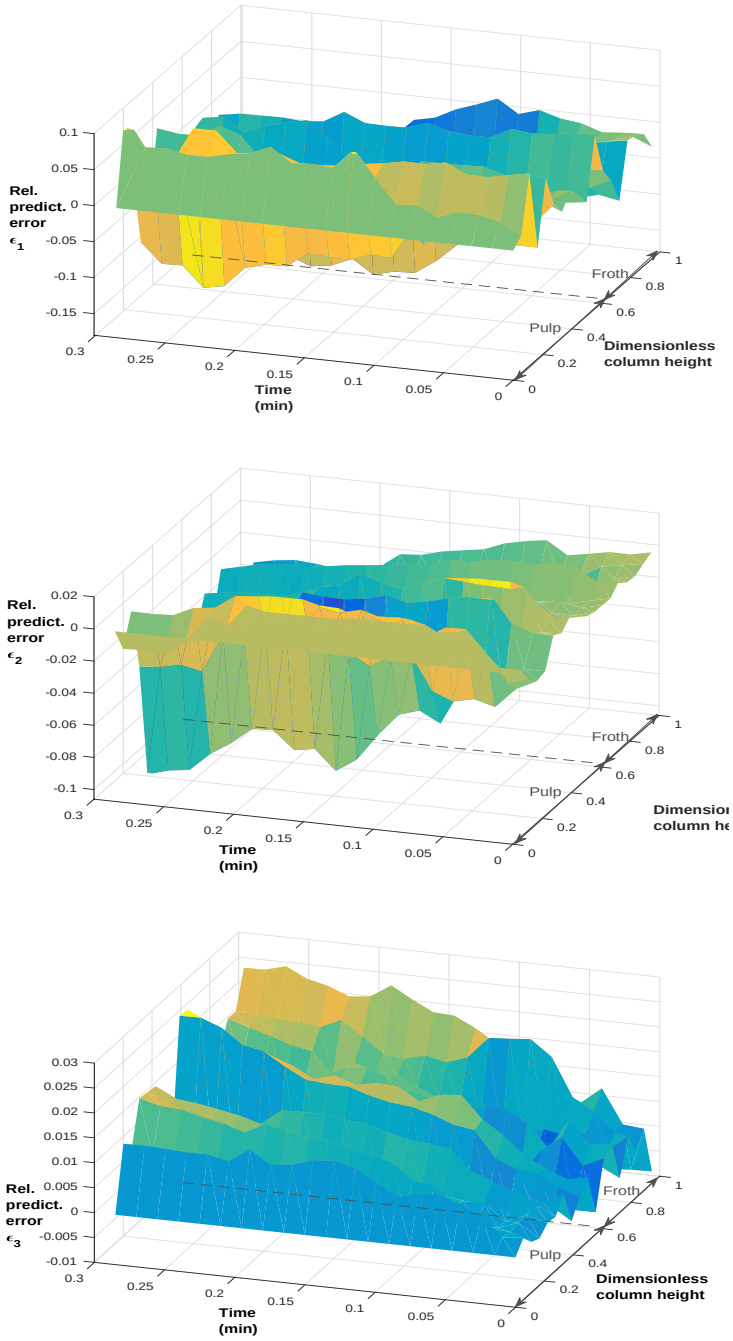

Figure 4.4: Relative prediction error, using EnKF, for the gas holdup of three bubble size classes through a two-phase flotation column.

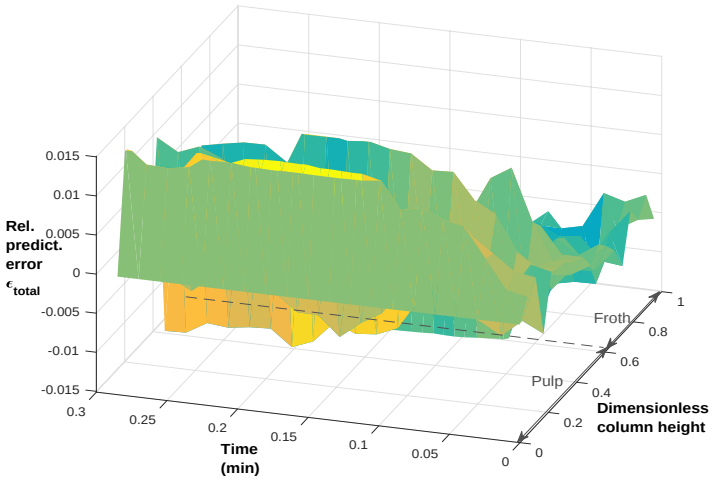

Figure 4.5: Relative prediction error, using EnKF, for the total gas holdup through a two-phase flotation column.

Here, we consider a prior distribution for each states in the state vector, and solve the filtering/estimation problem for the state vector by using this recursive Monte Carlo algorithm, ensemble Kalman filter. Observation y_t with the likelihood $p(y_t|x_t) = \varphi(y_t; H_t(x_t), R_t)$ can be handled with a covariance matrix, R_t. The state vector is updated through states correlations in the prediction distribution.

It is appropriate to use all N state particles as an update based on the same fixed observation error covariance matrix, R. In this case, this algorithm produces correct marginal posteriors asymptotically as $N \longrightarrow \infty$. Therefore, states estimates oscillate and become smooth after 20 assimilation cycles. The choice of the ensemble size and other details are determined by the requirement that the ensemble Kalman filter must be reasonably calibrated and stable. The selected size of the ensemble in this work is $N = 90$. Due to the strong nonlinearity, the ensemble Kalman filter in itself

with the addition of three unknown parameters tends to frequently produce poor state for smaller values of N. The true and predicted values of these three states depending on the process conditions have been demonstrated in Figures 4.2 - 4.3.

4.2.3 Luenberger observers

In this section, we consider a Luenberger observer design for a class of nonlinear hyperbolic PDE system (i.e. the two-phase flotation column used before to design EnKF estimator) (see equations 3.15 and 3.17), which represents the propagation of gas holdup through the column. The assumption is that one can measure gas holdup, $\epsilon_{f,n}$, at $z = L_2$ height (i.e., $y_{f,z=L_2}(t)$), which is the gas holdup/fraction of three classes of bubble sizes on top of the flotation column, and based on that an observer can be designed to estimate both $\epsilon_{f,n}$ and $\epsilon_{p,n}$ through the column.

The Luenberger observer design consists of a copy of the plant plus output injection term in the PDEs which drives observer dynamics. The observer gains (L_p and L_f) are chosen as a linear function through the column height.

The nonlinear model for gas holdup in the pulp zone for the two-phase plant is defined as equation 3.15 and model for gas holdup in the froth and interface zones is defined as equation 3.17.

In the column flotation process, it is desired to have a good estimate of the gas holdup through the column. This goal can be reached by tuning the gains in the observer design such that the estimation error decays. To this aim, the observer gains, L_p and L_f, are found explicitly as linear functions through the column height such that $(A - \mathbf{L}C)$ is stable. In particular, the observer gains L_p and L_f represent linear functions over the space and this simple choice is motivated by the natural stability

of the transport-reaction hyperbolic PDEs which implies that the error dynamics of the observer and plant mismatch exponentially decreases over time. One can also assume some other spatial expressions of the Luenberger gain, providing that $(\mathcal{A} - \mathbf{L}C)$ is stable (see [14]) where the state-space form of the system is:

$$\dot{x}(t) = \mathcal{A}x(t) + \mathcal{B}u(t) + \mathcal{F}(x,t)$$
$$y(t) = \mathfrak{C}x(t)$$

with $x(t) = x_0,\ t > 0$. The measurements are specified with the operator $\mathfrak{C} :\ \boldsymbol{H} \rightarrow \mathbb{R}^2$ is a bounded linear operator. The pair $(\mathfrak{C}, \mathcal{A})$ is said to be observable if and only if $NO(\mathfrak{C}, \mathcal{A}) = 0$ which is known as approximate observability or weak observability [99]. The observer design has the form of:

$$\frac{d}{dt}\hat{x} = \mathcal{A}\hat{x} + Bu + L(y - \mathfrak{C}\hat{x}) + F(x) - F(\hat{x}) \tag{4.15}$$

Such that the error can be defined as:

$$\dot{e}(t) = (\mathcal{A} - \mathbf{L}\mathfrak{C})e(t) + F(x) - F(\hat{x}) \tag{4.16}$$

This is not trivial task since system operator $\mathcal{A}$ contains the PDE spatial operator. where $\mathcal{A} = (-v_{\epsilon,f}\frac{\partial}{\partial z}, -v_{\epsilon,f}\frac{\partial}{\partial z})$, $x(t) = (\epsilon_{f,n}, \epsilon_{p,n})$ (see equations 4.17 and 4.18) with velocities of $(v_{\epsilon,f},\ v_{\epsilon,p})$.

Here we consider measurements at the column outlet ($z = L_2$). Furthermore, we prefer to tune our observer with a continuous linear function, so we let $L_p = L_f$ at the froth/pulp interface ($z = L_1$). Hence, since the observability of hyperbolic transport-reaction system with the measurement realized at the exit of the reactor is always a well-posed problem, the feasibility of the observer is always granted. For

example, the information is transferred from the inlet of reactor and contains all information as it is transferred through the reactor control volume to the exit where measurement is placed. Then, for any initial conditions for $\epsilon_{p,n}$ and $\epsilon_{f,n}$ one can considered the observation error to be exponentially stable with the assumption of accurate modelling description of vector field contribution $F_p(\epsilon_{p,n})$ and $F_f(\epsilon_{f,n})$. Considering terms $F_p(\epsilon_{p,n}) = A_{n,p} - D_{n,p}$ (see equation 4.17) and $F_f(\epsilon_{f,n}) = A_{n,f} - D_{n,f}$ (see equation 4.17). This nonlinear vector field contribution of the error dynamics asymptotically decays over time.

For (control) engineering applications, it may be more interesting to find out the applied functions of L_p, L_f for this system. $L_p = z$ and $L_f = (froth\ depth) * z + (froth\ depth) * L_p|_{L_1}$.

The Luenberger observer model (see Figure 4.6) can be written in the following form:

$$\frac{\partial \hat{\epsilon}_{p,n}}{\partial t} = -v_{\epsilon,p}\frac{\partial \hat{\epsilon}_{p,n}}{\partial z} + F_p(\hat{\epsilon}_{p,n}) + L_p(y - C_p\hat{\epsilon}_{p,n}) \tag{4.17}$$

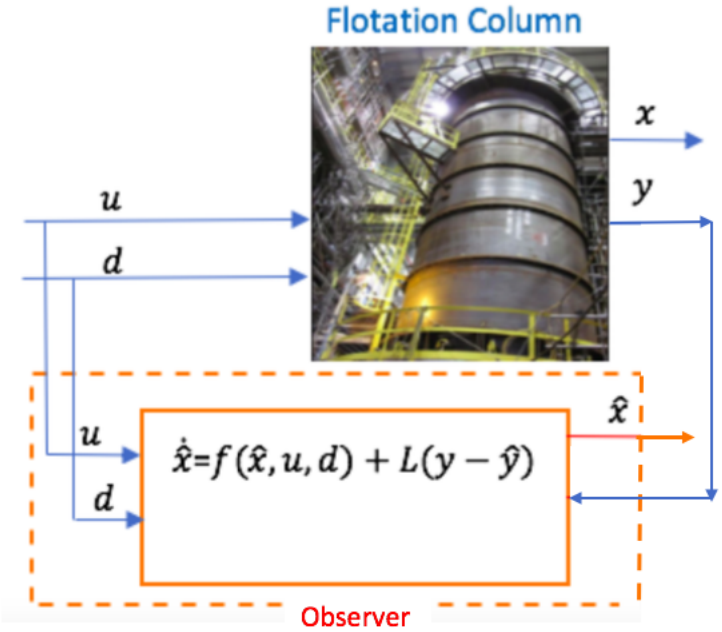

Figure 4.6: Schematic of Luenberger Observer design.

$$\frac{\partial \hat{\epsilon}_{f,n}}{\partial t} = -v_{\epsilon,f}\frac{\partial \hat{\epsilon}_{f,n}}{\partial z} + F_f(\hat{\epsilon}_{f,n}) + L_f(y - C_f\hat{\epsilon}_{f,n}) \tag{4.18}$$

$$\hat{\epsilon}_{f,n}|_{z=L_1} = \hat{\epsilon}_{p,n}|_{z=L_1} \tag{4.19}$$

$$\hat{\epsilon}_p|_{z=0} = \epsilon_c$$

As the equations for the prediction errors $e_{p,n} = \epsilon_{p,n} - \hat{\epsilon}_{p,n}$, $e_{f,n} = \epsilon_{f,n} - \hat{\epsilon}_{f,n}$ are:

$$\frac{\partial e_{p,n}}{\partial t} = -v_{\epsilon,p}\frac{\partial e_{p,n}}{\partial z} + F_p(\epsilon_{p,n}) - F_p(\hat{\epsilon}_{p,n}) + L_p(y_p(t) - C_p e_{p,n}) \tag{4.20}$$

$$\frac{\partial e_{f,n}}{\partial t} = -v_{\epsilon,f}\frac{\partial e_{f,n}}{\partial z} + F_f(\epsilon_{f,n}) - F_f(\hat{\epsilon}_{f,n}) + L_f(y_f(t) - C_f e_{f,n}) \tag{4.21}$$

for $k = 1 : t_{final}$

$\frac{d}{dt}\hat{X} = A\hat{X} + BU + L(y - C\hat{X})$

end for

$$e_{f,n}|_{z=L_1} = e_{p,n}|_{z=L_1} e_{p,n}|_{z=0} = 0 \tag{4.22}$$

In equations 4.20, 4.21, it is assumed that the difference between the nonlinear terms associated with the estimated and true vector fields are going to zero such that the error equations become stable linear hyperbolic PDEs (i.e. $\lim_{t\to\infty} e_{f,n} \to 0$ and $\lim_{t\to\infty} e_{p,n} \to 0$). This assumption is due to the fact that the expressions in $A_{i,n}$ and $D_{i,n}$ (see equations 2.32 and 2.33) behave approximately as a linear function of ϵ. The pseudo-code for the Luenberger observer design algorithm is given below: The observer design has also been modified for another case with the assumption that measurements are taken at two points in the column. The observer measurements are taken at the top of the column (i.e., $y_{f,z=L_2}(t)$) as well as at the pulp/froth interface (i.e., $y_{p,z=L_1}(t)$). Figures 4.9-4.15 illustrate the estimation results for this system.

Description of simulation parameters: For the simulation study, the unit simulated in this section is a flotation column with 0.563 m of height and 0.073 m of diameter. The simulation parameters for the quantitative study of the hybrid model are as follows:

Pulp height	0.35	m
Q_a	0.0016	$m^3.min^{-1}$
ϵ_c	$(0.02, 0.04, 0.3)$	-
$d_{b,p}$	(0.0015,0.001,0.0005)	m
ϵ_{pp}	$(0.08, 0.24, 0.08)$	-
$d_{b,f}$	$(0.003, 0.002, 0.001)$	m
ϵ_f	$(0.18, 0.46, 0.06)$	-
ρ_g	1.225	$kg.m^{-3}$
ρ_{sl}	1250	$kg.m^{-3}$

Results of state estimation for a two-phase semi-batch flotation column by Luenberger observer

The gas holdups of three size classes of bubbles in the froth and pulp zones are the states. In this section, column height has been demonstrated in a dimensionless form.

Measurements at one point: Figure 4.7 demonstrates the spatiotemporal propagation of the true state and the gas holdup for bubbles in size class 1, in the pulp and froth. It is illustrated how the arbitrary initial profile is transported across the column and it washes out over time in approximately 3.5 minutes. Along the same lines, the predicted propagation of this state had the same trend as the true states and predicts this state accurately approximately less than 1.5 minutes and reaches the true profile.

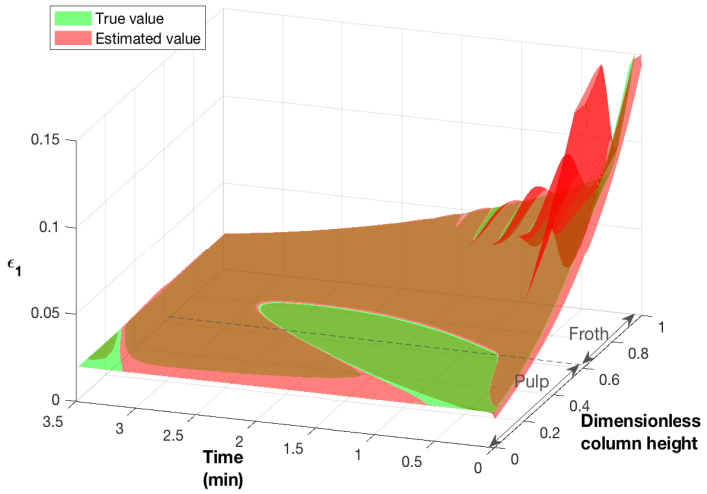

Figure 4.7: The true and estimated state propagation for ϵ_1 through a two-phase flotation column obtained by the Luenberger observer (measurements at the column exit).

Figure 4.8 demonstrates the spatiotemporal propagation of the true state and the gas holdup for bubbles in size class 2, in the pulp and froth. It is illustrated how the arbitrary initial profile is transported across the column and it washes out over time in approximately 3.5 minutes. Along the same lines, the predicted propagation of this state had the same trend as the true states and predicts this state accurately after approximately less than 3 mins and reaches the true profile.

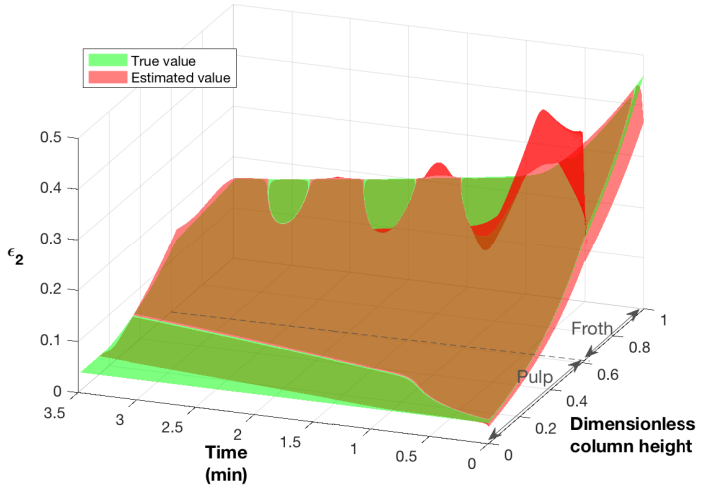

Figure 4.8: The true and estimated state propagation for ϵ_2 through a two-phase flotation column obtained by the Luenberger observer (measurements at the column exit).

Measurements at two points: Figure 4.9 demonstrates the spatiotemporal propagation of the true state and the gas holdup for bubbles in size class 1, in the pulp and froth. It is illustrated how the arbitrary initial profile is transported across the column and it washes out over time in approximately 4 minutes. Along the same lines, the predicted propagation of this state had the same trend as the true states and predicts this state accurately after approximately less than 4 mins and reaches the steady-state profile.

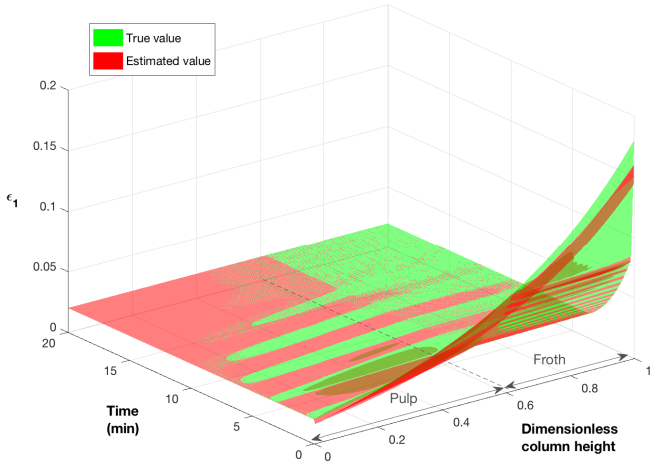

Figure 4.9: The true and estimated state propagation for ϵ_1 through a two-phase flotation column obtained by the Luenberger observer (measurements at the column exit and interface).

Figure 4.10 shows the relative prediction error for ϵ_1. This figure is describing the accuracy of estimation for holdup of bubbles in size class 1, which means that the estimation error starts from a non-zero value and after approximately 4 minutes reaches the zero value through the column height.

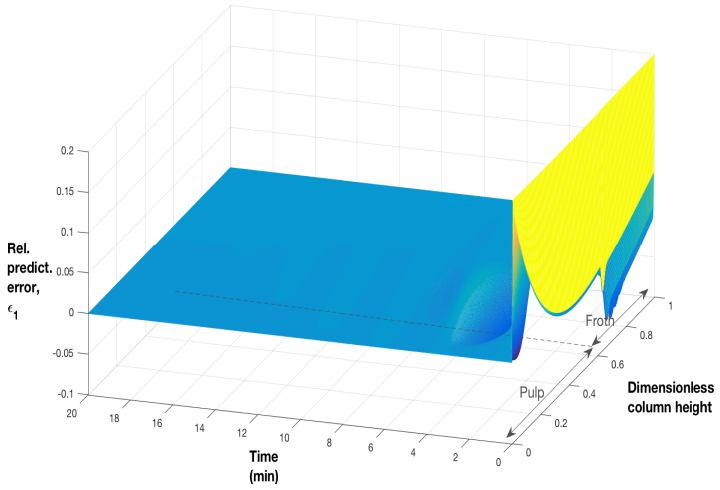

Figure 4.10: Relative estimation error for ϵ_1 through a two-phase flotation column obtained by the Luenberger observer (measurements at the column exit and interface).

Figure 4.11 demonstrates the spatiotemporal propagation of the true state, gas holdup for bubbles in size class 2, in the pulp and froth. It is illustrated how an arbitrary initial profile is transported across the column and it washes out over time in approximately 8 minutes. Along the same lines, the predicted propagation of this state (Figure 4.11(b)) had the same trend as the true states and predicts this state accurately after approximately 10 mins and reaches the steady-state profile.

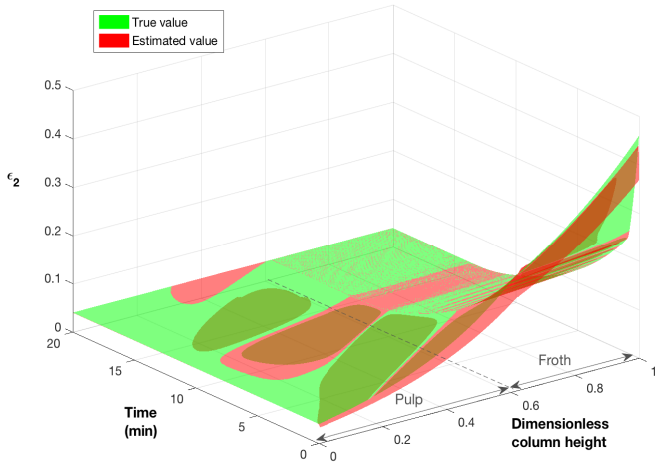

Figure 4.11: The true and estimated propagation for ϵ_2 through a two-phase flotation column by the Luenberger observer (measurements at the column exit and interface).

Figure 4.12 is describing the accuracy of estimation for holdup of bubbles in size class 2, which means that the estimation error starts from a non-zero value and after approximately 12 min reaches the zero value through the column height.

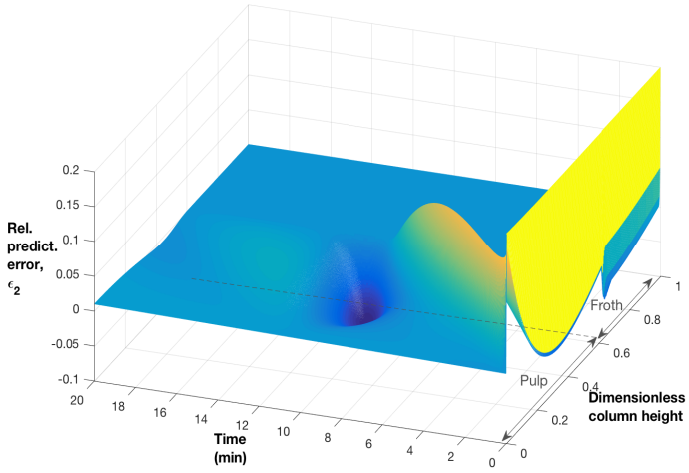

Figure 4.12: Relative estimation error for ϵ_2 through a two-phase flotation column by the Luenberger observer (measurements at the column exit and interface).

Figure 4.13 demonstrates the spatiotemporal propagation of the true state, gas holdup for bubbles in size class 3, in the pulp and froth. It is illustrated how an arbitrary initial profile is transported across the column and it washes out over time in approximately 25 minutes. Along the same lines, the predicted propagation of this state had the same trend as the true states and predicted state converge accurately after approximately 20 mins and reaches the steady-state profile.

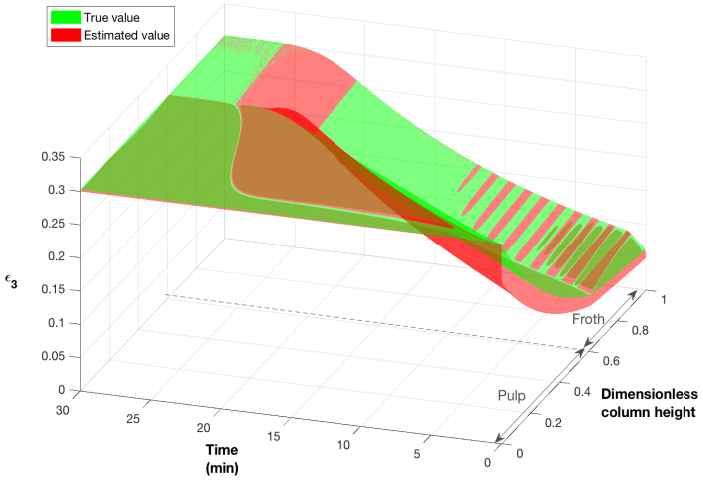

Figure 4.13: The true and estimated propagation for ϵ_3 through a two-phase flotation column by the Luenberger observer (measurements at the column exit and interface).

Figure 4.14 shows the relative prediction error to the real state values. This figure is describing the accuracy of estimation for holdup of bubbles in size class 3, which means that the estimation error starts from a non-zero value and after approximately 20 min reaches the zero value through out the column height.

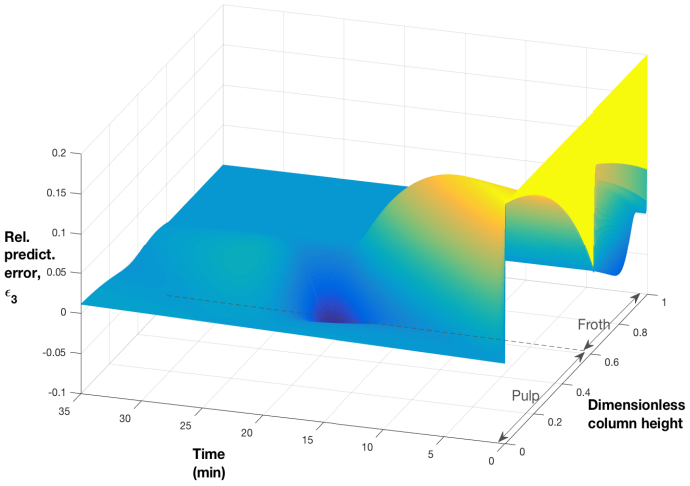

Figure 4.14: Relative estimation error for ϵ_3 through a two-phase flotation column obtained by the Luenberger observer (measurements at the column exit and interface).

Figure 4.15 demonstrates the spatiotemporal propagation of the total gas holdup in the pulp and froth. It is illustrated how the arbitrary initial profile is transported across the column and it washes out over time in approximately 25 minutes (which is the approximate column residence time). Along the same lines, the predicted propagation of the total gas holdup (Figure 4.15(b)) had the same trend as the true states and predicts this state accurately after approximately 20 mins and reaches the true profile.

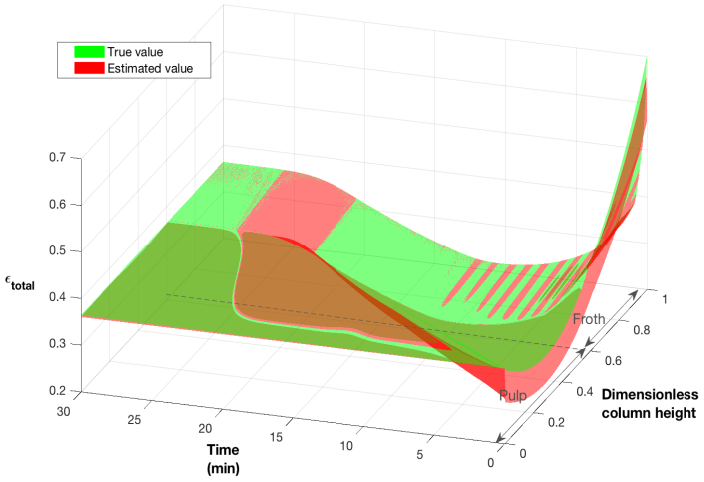

Figure 4.15: The true and estimated state propagation for ϵ_{total} through a two-phase flotation column obtained by the Luenberger observer (measurements at the column exit and interface).

As is illustrated in these figures, infinite dimensional systems have a finite time observability or state reconstruction. This means that for the transport type of systems we have a finite time observability which is associated with the time takes for the bubbles/particles to travel from one end to the other end of the column. In the other word, we cannot reconstruct states faster than the speed of propagation of bubbles, or the residence time, which is related to the column height and the velocity of bubbles. In this case, among the three bubbles, one has a velocity of ten times slower than the others, hence the residence time of this bubble represents the rate of observation. We define the speed of the slowest bubble that leaves the column as the rate of observation which is the velocity that can be measured in the lab for the lab scale flotation column. At steady state, the gas holdup through the column reaches a constant value, which makes sense for a two-phase system. However, the profile

can vary through the column due to the fact that holdup distributions may have larger effect of the bubble appearance $D_{n,i} + A_{n,i}$ and coalescence. Along this line, one needs to approximately provide an initial condition for the observer representing a meaningful holdup distribution across the column.

4.2.4 Experimental Validation

To link the experimental realizations, conducted by our group at the University of Alberta, (see Figure 4.16) with the findings related to the column flotation state reconstruction, the measurement obtained by a probe placed at the interface of the semi-batch lab scaled flotation column is considered. Given the availability of measurements and considering the simulation studies, possible experimental validation is proposed by considering the basic transport and bubble dynamics (bubble coalescence and bubble collapse). The model to obtain the gas holdup distribution across the column is considered and it is given as equations 3.15-3.17.

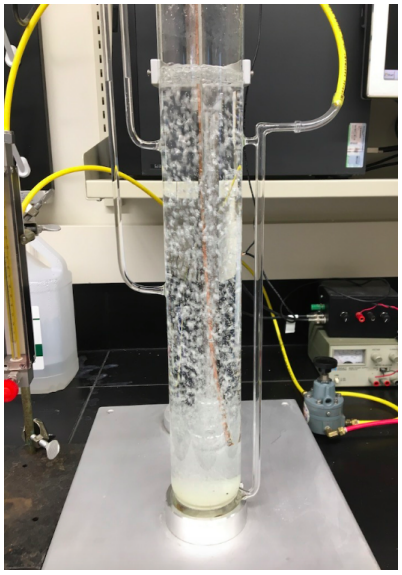

Figure 4.16: Experimental setup for a two-phase semi-batch flotation column.

In particular, the experimental setup provides the insight in linking the probable hold-up calculations with the realistic realization of the air propagation through the column. As it can be seen in the Fig.4.17 the realistic hold up values are reported at steady state conditions. **Description of simulation parameters**:

Pulp height	0.429	m
Q_a	$4.54 * 10^{-5} * 60$	$m^3.min^{-1}$
ϵ_p	(0.0131,0.0011;0.011)	-
$d_{b,p}$	$(0.965 * 10^{-3}, 0.625 * 10^{-3}, 0.285 * 10^{-3})$	m
ρ_g	1.225	$kg.m^{-3}$
ρ_{sl}	997	$kg.m^{-3}$

According to equations 3.15 - 3.17, at steady state the following two terms $\frac{\partial \epsilon_{p,n}(z,t)}{\partial t}$

and $\frac{\partial \epsilon_{f,n}(z,t)}{\partial t}$ are zero. Therefore, these equations can be written as:

$$0 = -v_{\epsilon,n,p}\frac{\partial \epsilon_{p,n}(z,t)}{\partial z} - \mathcal{D}_{p,n}(z,t) + \mathcal{A}_{p,n}(z,t) \tag{4.23}$$

$$\tag{4.24}$$

which is simply integrated from the top of the column:

$$\epsilon_p(n+1) = \epsilon_{p,n} + \frac{\Delta z}{v_{\epsilon,n,p}}(\mathcal{A}_{p,n} - \mathcal{D}_{p,n}) \tag{4.25}$$

with the boundary condition at the interface, where the probe is placed. The probable gas steady state holdup distribution is given in Figure 4.17.

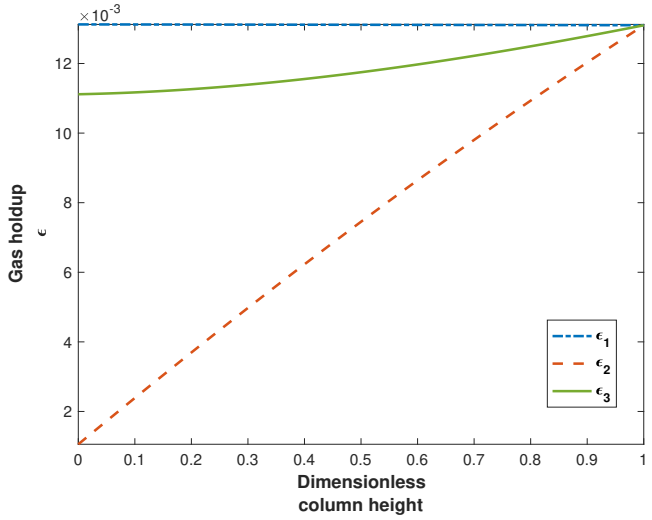

Figure 4.17: Probable steady state propagation of gas holdup for three different bubble size classes in a semi-batch flotation column based on measurement on top of the pulp zone.

Using the obtained probable steady state profiles the reconstruction of the column flotation states by applying the Luenberger observer design are shown in Figures 4.18-4.21. In particular, in figure 4.18 it can be demonstrated that using the Luenberger observer for ϵ_3 estimated and the estimated converges to the true steady state.

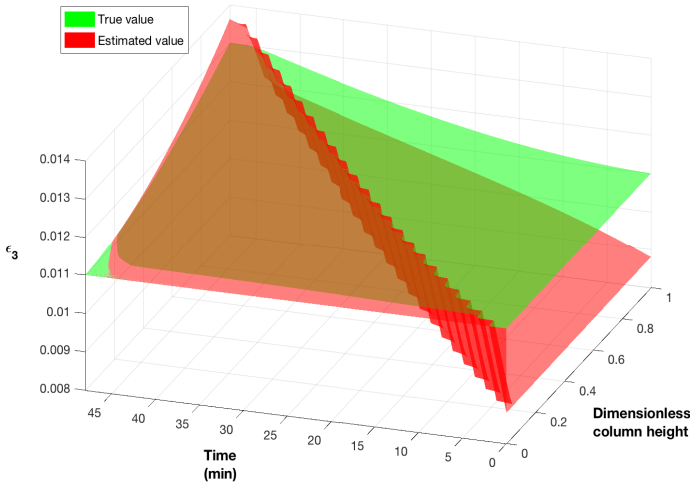

Figure 4.18: Propagation of gas holdup in size class 3 through a semi-batch flotation column by the Luenberger observer based on empirical data.

As it can be seen from Figure 4.18, at initial instance initialize observer does not share the same initial condition as the true profile and converges to the true profile in in almost 45 *minutes*. In order to demonstrate the observer performance, in the following Figure 4.19, observation error evolution is demonstrated. It can be seen that the observer error converges approximately to zero in a finite time which is equal to the residence time of the column $\approx 45min$.

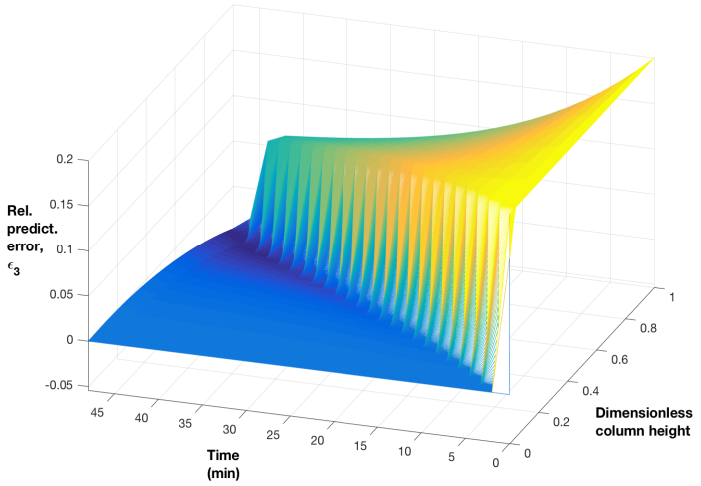

Figure 4.19: Relative prediction error for ϵ_3 through a semi-batch flotation column by the Luenberger observer based on empirical data.

In the following Figure 4.20, it can be demonstrated that the Luenberger observer for the ϵ_{total} is estimated and the estimated converges to the true gas holdup profile. In the same vein, the total gas holdup as expected is accordingly well reconstructed by the Luenberger observer.

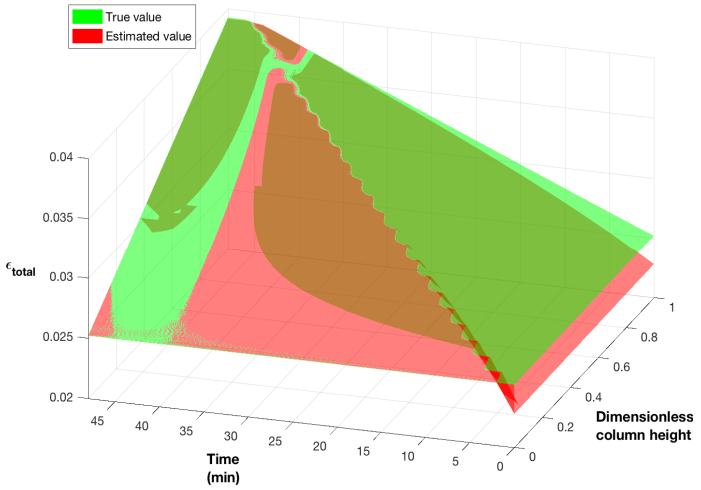

Figure 4.20: Propagation of total gas holdup through a semi-batch flotation column by the Luenberger observer based on empirical data.

In order to demonstrate the observer performance, as it is illustrated in Figure 4.21, observation error evolution is demonstrated. It can be seen that the observer error converges approximately to zero in a finite time which is equal to the residence time of the column $\approx 45min$. This is due to the fact that, among all the bubbles the bubbles in the size class 3 have slower velocity than the others, hence the residence time of bubble in the size class 3 represent the rate of observation.

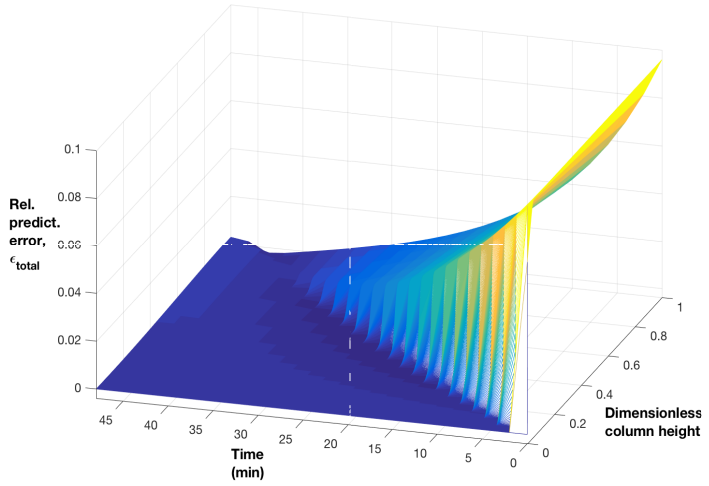

Figure 4.21: Relative prediction error for ϵ_{total} through a semi-batch flotation column by the Luenberger observer based on empirical data.

In order to make improvement of parameters associate with the Luenberger observer one should propose the measurement of at least two independent points, preferably at the bottom and top of the column. In this way, one would estimate the parameters of the model which are velocity and attachment and detachment parameters along the column between these two points. The achieved goal of reconstructing the evolution of gas holdup (throughout the two-phase column) was realized by applying two observers. The algorithms to estimate the flotation column dynamics are realized and implemented. Finally, the comparison between these two approaches and the real experimental values for the gas holdup on top of the column ascertains the confidence in the quality of prediction. Along the line of the state reconstruction, the control algorithm can be utilized to improve column flotation regulation. The natural question in this setting is to ask how do we know that state estimation is

good enough? For the measurements of the pilot plant column in the lab coincide with the findings obtained by modelling efforts.

The Luenberger observer design is a more challenging in terms of applying linearization to the model and/or finding the accurate spatially distributed observer gains. Contrary to the deterministic Luenberger observer, the ensemble Kalman filter as a stochastic optimal estimator which might be computationally more expensive yet easier to implement might be better choice for practitioners.

4.3 Monitoring the recovery, gas holdup, and concentrations in a three-phase continuous column flotation

Complex mineral from ore column flotation separations are difficult processes and process outputs such as grade and/or recovery are characterized by various sub-processes in the pulp and the froth zone. A small disturbance in any of the sub-process could propagate to other sub-processes and affect the type and quantity/quality of solids entering the concentrate. Therefore, it is crucial to monitor the performance in order to maximize the production in the realistic three-phase continuous column flotation.

In this section, we build an estimator that is based on the model developed work in Chapter 2. In particular, a set of fundamental dynamical processes that connects micro-scale sub-processes (particle-bubble attachment/detachment, bubble-bubble appearance/breakage) to macro-scale sub-processes (mass transfer, interphase transfer) is considered in the observer design. In this section, we have proposed and implemented a dynamic monitoring application using the proposed three-phase fun-

damental modelling for real-time measurement of recovery. Also, to account for the model-plant mismatch some noise has been added to the model.

The EnKF estimator designed in this section, for the three-phase system, applied the same algorithm as the EnKF estimator designed and used for the two-phase system. In the three-phase system solids (hydrophobic) have been added to the system, while the two-phase system consists of only water and bubbles of gas . Other differences of these two systems are regarding the scale and operational mode of those two systems. The two-phase system is a semi-batch lab-scaled column however the three-phase system is a continuous pilot-scaled column. For the modelling and simulation purpose, in the two-phase system gas holdup equations for three different classes of bubble sizes in the pulp and froth zones have been applied (see equations 3.15, 3.17) yet for the three-phase system the particle concentration equations (see equations 2.3,2.4,2.6,2.7,2.8,2.16,2.18,2.18) as well as the gas holdup equations (see equations 3.15, 3.17) are used.

Description of simulation parameters: The three-phase unit simulated in this paper is a pilot plant flotation column (0.72 m of height, 0.16 m in diameter). The simulation parameters for the quantitative study of the hybrid model are as follows:

Pulp height	0.35	m	μ_{sl}	$1.24 * 10^{-3}$	$kg.m^{-1}s^{-1}$
Q_a	0.0008	$m^3.min^{-1}$	h	0.002	min^{-1}
Q_w	0.001	$m^3.min^{-1}$	h_2	0.0001	min^{-1}
Q_f	0.1	$m^3.min^{-1}$	h_f	0.002	min^{-1}
Q_t	0.03	$m^3.min^{-1}$	$h_{f,2}$	0.001	min^{-1}
$Q_{e,c}$	0.06	$m^3.min^{-1}$	k	0.8	min^{-1}
$Q_{r,pc}$	0.0005	$m^3.min^{-1}$	k_2	0.75	min^{-1}
$Q_{e,p}$	0.01	$m^3.min^{-1}$	k_{ac}	0.5	min^{-1}
$Q_{r,p}$	0.0005	$m^3.min^{-1}$	k_{dc}	0.0003	min^{-1}
$Q_{e,f}$	0.02	$m^3.min^{-1}$	$k_{a,p3}$	0.2	min^{-1}
$Q_{r,f}$	0.001	$m^3.min^{-1}$	$k_{a,p4}$	0.2	min^{-1}
Q_c	$(Q_f + Q_w - Q_t)$	$m^3.min^{-1}$	k_{dp}	0.005	min^{-1}
α_f, α_p	0.1	min^{-1}	$k_{a,f6}$	0.05	min^{-1}
ϵ_c	(0.02, 0.04, 0.3)	-	$k_{a,f7}$	0.05	min^{-1}
$d_{b,p}$	(0.0015,0.001,0.0005)	m	k_{df}	0.01	min^{-1}
ϵ_{pp}	(0.08, 0.24, 0.08)	-	ϵ_f	(0.18, 0.46, 0.06)	-
$d_{b,f}$	(0.003,0.002,0.001)	m	ρ_{sl}	1250	$kg.m^{-3}$
ρ_g	1.225	$kg.m^{-3}$			

Initially the model described in Chapter 2 was ran for 1500000 iterations with $\Delta t = 0.00005$ which is around 75 minutes from starting the column flotation separation process. In this case representative initial condition is: $x_1(0) = 0.2\frac{kg}{m^3}$, $xq_1(0) = 0.5\frac{kg}{m^3}$, $x_2(0) = 0$. 99% of the final simulation results have been chosen as the mean point to generate the 80 initial ensemble around 414 states.

Figure 4.22 demonstrates the spatiotemporal propagation of the true and estimated

values of the concentration of attached minerals through the column. Column height has been represented in a dimensionless form ($\frac{Distance\ from\ the\ bottom\ of\ the\ column}{FrothHeight + Pulp\ Height}$). It is illustrated how the predicted propagation of the state has the same trend as the true values and predicts this state accurately and reaches the steady-state profile of the true state value. Figure 4.23 shows the relative prediction error. Relative prediction error has been represented as ($\frac{predicted\ value - true\ value}{true\ value}$). This figure is describing the accuracy of estimation for the attached minerals.

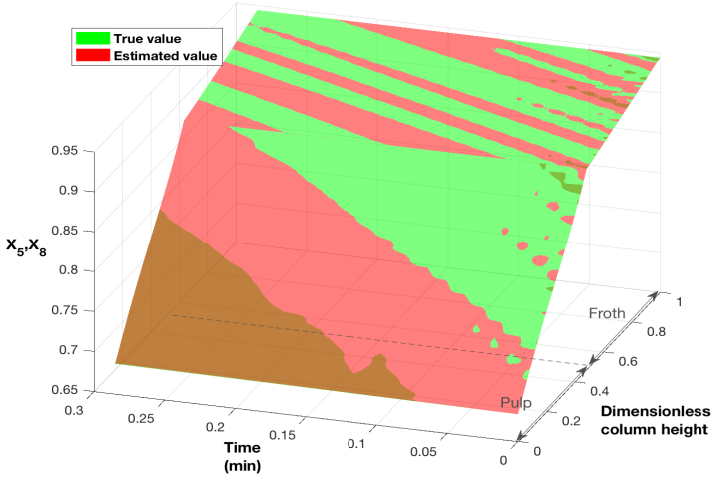

Figure 4.22: True and predicted values, using EnKF, for X_5 (in pulp) and X_8 (in froth) through a three-phase flotation column.

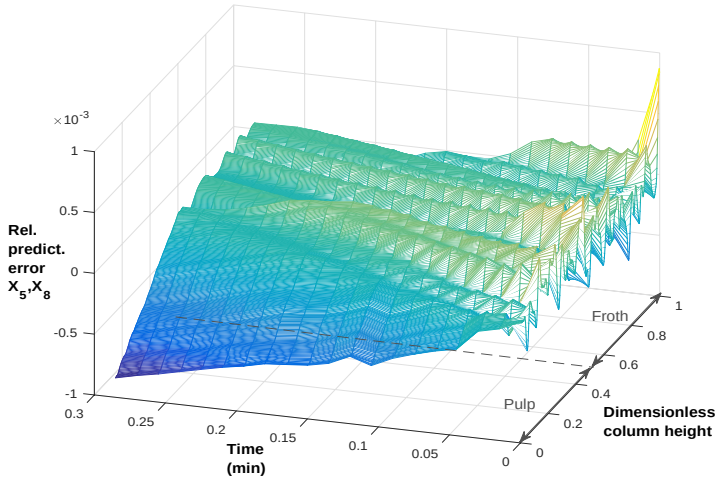

Figure 4.23: Relative prediction error for X_5 and X_8 through a three-phase flotation column.

Figures 4.24 and 4.25 demonstrate the spatiotemporal propagation of the true and estimated values of state, concentration of free upflow and downflow minerals, respectively, through the column. They illustrate how the predicted propagation of the states has the same trend as the true values and predict these states accurately and reach the steady-state profiles of the true state values.

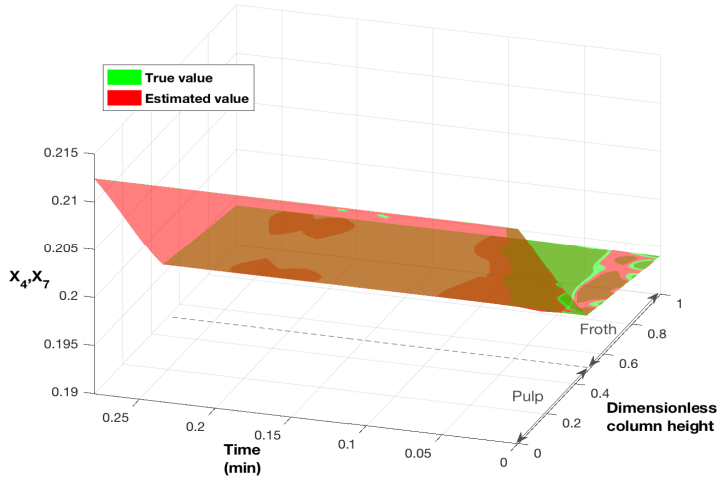

Figure 4.24: True and predicted values, using EnKF, for X_4 (in pulp) and X_7 (in froth) through a three-phase flotation column.

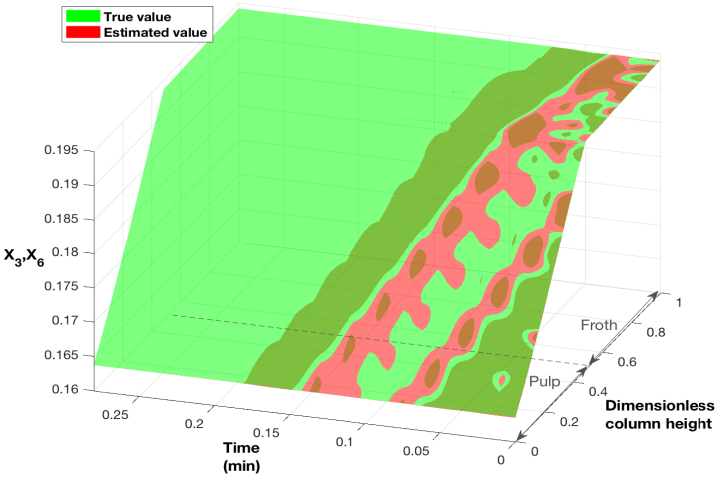

Figure 4.25: True and predicted values, using EnKF, for X_3 (in pulp) and X_6 (in froth) through a three-phase flotation column.

Figures 4.26, 4.27, and 4.28 demonstrate the spatiotemporal propagation of the

true and estimated values of state, gas holdup of bubbles in three size classes, through the column. It illustrates how the predicted propagation of the state has the same trend as the true values and predicts these states accurately.

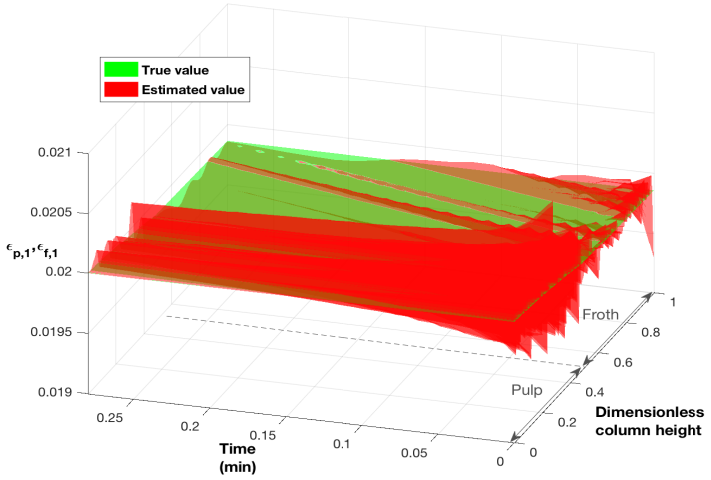

Figure 4.26: True and predicted values, using EnKF, for ϵ_1 through a three-phase flotation column.

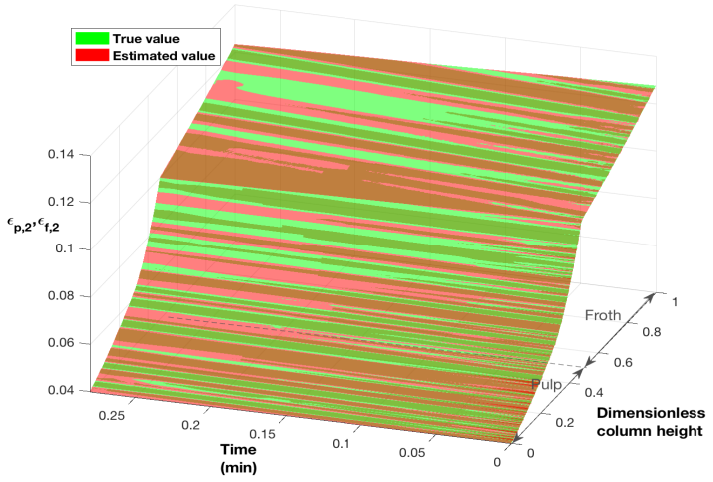

Figure 4.27: True and predicted values, using EnKF, for ϵ_2 through a three-phase flotation column.

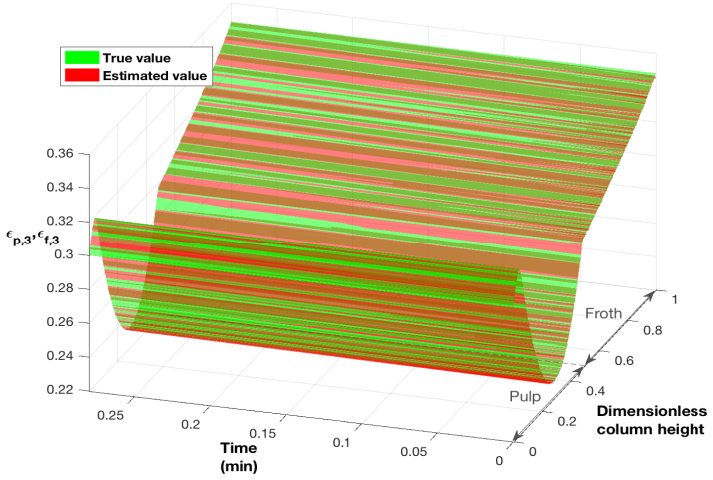

Figure 4.28: True and predicted values, using EnKF, for ϵ_3 through a three-phase flotation column.

Figure 4.29 demonstrates the spatiotemporal propagation of the true and esti-

mated values of the total gas holdup of bubbles through the column. Figure 4.30 shows the relative prediction error to the true state values which illustrates the accuracy of prediction for the total gas holdup.

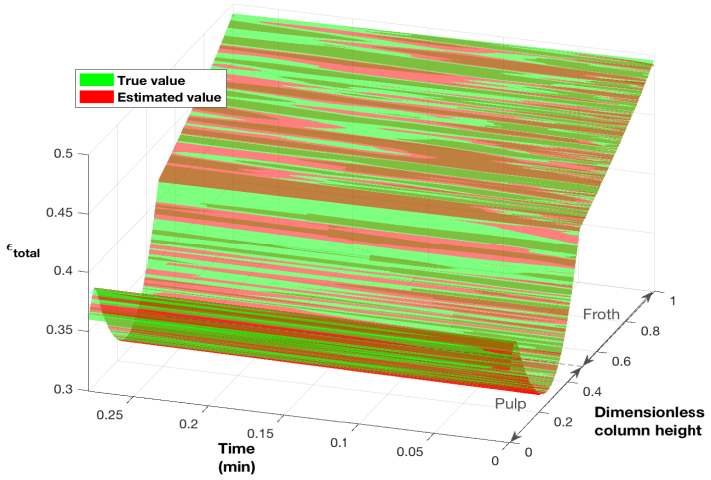

Figure 4.29: True and predicted values, using EnKF, for ϵ_{total} through a three-phase flotation column.

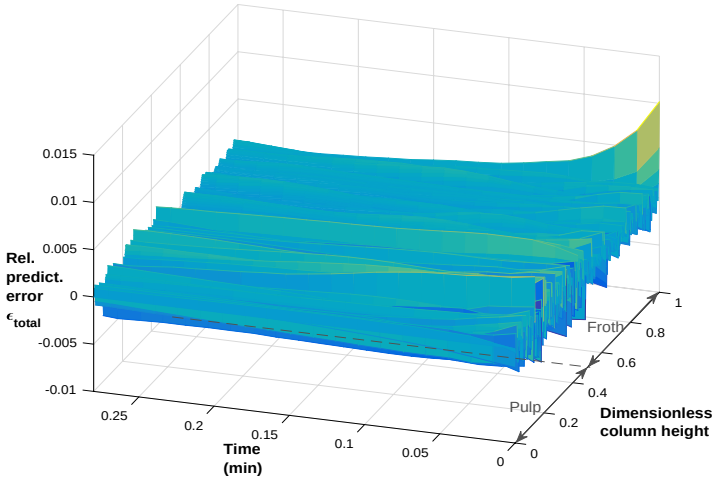

Figure 4.30: Relative prediction error, using EnKF, for ϵ_{total} through a three-phase flotation column.

Figure 4.31 demonstrates the spatiotemporal propagation of the true and estimated values of the recovery of valuable minerals in the column flotation process using equation 2.59. The accuracy of prediction for the recovery is illustrated in this figure. The figure demonstrate that the predicted recovery reaches the steady state value of almost 37% in around 0.3 minutes.

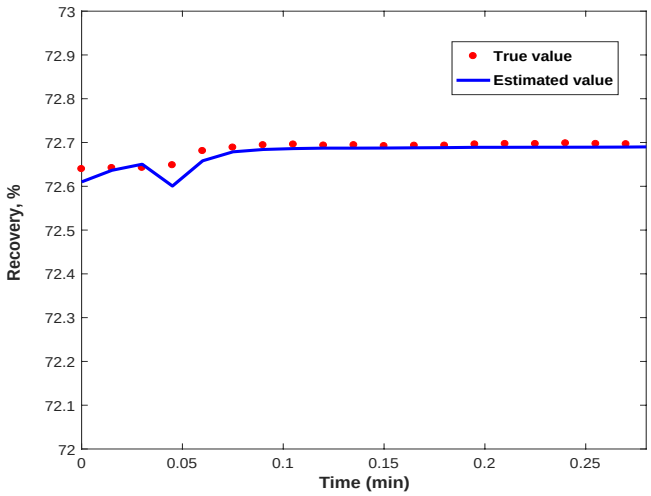

Figure 4.31: True and predicted values, using EnKF, for recovery in a three-phase flotation column.

To predict the process recovery, gas holdup and mineral's concentration on top of the column the EnKF was applied and the algorithm has been realized to estimate the flotation column dynamics.

Chapter 5

Conclusions and Recommendations

5.1 Concluding remarks

The complex nature of column flotation brings about various unidentified disturbances in the system. It is necessary to monitor the process in real-time with diagnosis of the various sub-processes taking part.

This thesis addresses three main aspects of column flotation operations: modelling, control, and estimation of a hybrid column flotation separation process. In this thesis the modelling of a unique continuous flotation column separation process (as a class of distributed parameter system with special emphasis on transport-reaction phenomena) is realized and further utilized for control and monitoring purposes. The pilot plant is unique since a mixer has been added to the column flotation geometry.

5.2 Original contributions

1. A comprehensive hybrid dynamic fundamental model with Danckwerts boundary conditions at the pulp/froth interface has been tailored for the continuous flotation column pilot plant in the mineral processing lab at the University of

Alberta. The considered three-phase continuous hybrid flotation column that seeks to obtain the benefits of both mechanical cells and flotation columns is modelled as the interconnection of a CSTR representing the well-mixed zone and two plug-flow reactors (PFRs) representing pulp (collection) and froth (cleaning) zones; the interconnection is through the boundaries. The model accounts for the micro-scale processes including bubble-particle collision and attachment, the appearance and breakage of bubbles. This complex distributed parameter system is described by set of nonlinear coupled conservation counter-current hyperbolic partial differential equations (PDEs) and one set of ordinary differential equations (ODEs). The movement between phases are given by liquid upflow, liquid downflow, and gas upflow. An important parameter in this simulation is the bubble size, which directly affects the gas holdup, and consequently all states distributions including the concentration of attached minerals through the column.

2. In previous modelling and simulation efforts in the literature, it was assumed that a flotation column consists of a series of well-mixed CSTRs. However, in reality, the froth is not perfectly mixed. Hence, the proposed model is an interconnection of a continuous stirred tank reactor (CSTR) which models the mixing section in the lower compartment, and two transport-reaction tubular reactor models with negligible diffusion terms in the pulp and froth zones.

3. The model accounts for the bubble interactions manifested as appearance and disappearance.

4. The model accounts for the recycle flow on top of the column from upflow to

downflow.

5. The model's insights for gas holdup and solid concentration profiles through the column will offer new possibilities for flotation column control.

6. A model-based optimal controller (OC) design is one of the important contributions of this thesis since it considers a dynamic conservation law based model (proposed in the previous chapter) for the continuous hybrid flotation column including a well-stirred zone, pulp (bubbly), and froth zones in an optimal model-based controller design. The controller design utilizes a linear model obtained by linearization at operation steady states of interest and a full-state optimal feedback control law is designed and controller performance is demonstrated through a numerical simulation of physically meaningful and relevant plant operating conditions. The LQR-based optimal controller outperforms PI-based control and the optimal control problem for a class of distributed parameter systems representing a column flotation with minimum number of simplifying assumptions in the modelling of a three-phase continuous column flotation is realized.

7. The application of OC in a system of coupled ODE and two transport-reaction hyperbolic PDEs is novel and solving this system is not trivial.

8. Also, two on-line model-based state estimators are developed for a semi-batch flotation column based on a two-phase fundamental dynamic model. In the two-phase case, the unknown states, representing the gas holdup through the column, have been estimated under the assumption that the gas holdup of

the bubble size classes at the exit on top of the column can be measured. Later, a dynamic estimator for a continuous flotation column based on the three-phase fundamental dynamic model is proposed and implemented. For the two-phase case, the performance of model-based EnKF with measurement on top of the column is compared to that of the Luenberger observer with the same operating conditions. Gas holdup propagation was captured better by the Luenberger observer for state estimation in the simplified version of the system (two-phase). It is confirmed that the proposed estimator for a two-phase case with measurements at the interface and on top of the column predicts the gas holdup propagation through a lab-scaled two-phase semi-batch column flotation well based on experimental data. However, EnKF has an acceptable performance with the capacity to be used in more complex nonlinear systems (three-phase). The implementation of EnKF for the state estimation of more complex cases such as continuous nonlinear three-phase model of a flotation column with parameter uncertainty is a better option compared to the linear Luenberger observer, which has intrinsic limitations.

9. The application of EnKF in column flotation system is novel.

5.3 Future work

The presented monitoring, control design and dynamic modelling framework provide many research paths toward enhancing the comprehension of the column flotation process and improving the process control scenarios for the industrial application of column flotation. Some ideas and motivation for further studies that could be

conducted based on the work in this thesis are suggested below:

- The fundamental model proposed in this thesis provides a good mechanism to connect various sub-processes to the mineral recovery with the addition of bubble population model which captures the dynamic of bubble breakage and bubble coalescence. The proposed model can be enhanced to include the variation of the pulp/froth interface depth.

- Exploring the application of particle filter (PF) as another estimation method for the online measurements of column flotation variations for the purpose of state and parameter estimation for the case of non-Gaussian distributions.

- Exploring the addition of a facilitated transport membrane to the column flotation geometry.

Bibliography

[1] J. Egan, M. Fairweather, and W. Meekel, "Application of column flotation to lead and zinc beneficiation at cominco," *Separation Science and Technology*, vol. **39**, no. 4, pp. 741–760, 2005.

[2] D. Hodouin, "Methods for automatic control, observation, and optimization in mineral processing plants," *Journal of Process Control*, vol. **21**, pp. 211–225, 2011.

[3] J. Callow, "Pneumatic flotation cell and method," *US Patent 1,366,766*, 1921.

[4] M. Mankosa, "A new paradigm in sulfide processing," *Eriez Flotation Division Technical Bulletin*, 2017.

[5] B. Wills and J. Finch, *An introduction to the practical aspects of ore treatment and mineral recovery In Wills' Mineral Processing Technology*. Boston, US: Butterworth-Heinemann, 2015, pp. 1–27.

[6] J. Bouchard, A. Desbiens, and R. Villar, "Recent advances in bias and froth depth control in flotation columns," *Miner. Eng.*, vol. **18**, pp. 709–720, 2005.

[7] J. Finch and G. Dobby, *Column Flotation*. Oxford, UK: Pergamon Press, 1990, pp. 1–27.

[8] M. Moys, "A study of a plug-flow model for flotation froth behaviour," *International Journal of Mineral Processing*, vol. **5**, pp. 21–38, 1978.

[9] P. Smith and L. Warren, "Entrainment of particles into flotation froths," *Miner. Process. Extr. Metall.*, vol. **5**, no. 1-4, pp. 123–145, 1989.

[10] A. Lynch, N. Johnson, E. Manlapig, and C. Thorne, *Mineral and Coal Flotation Circuits: Their Simulation and Control*. Amsterdam: Elsevier Publishing, 1981.

[11] M. Mankosa, J. Kohmunench, G. Luttrell, J. Herbst, and C. Noble, "Split-feed circuit design for primary sulfide recovery," *International Mineral Processing Congress, Quebec City, Quebec*, 2016.

[12] J. Miller, C. Lin, Y. Wang, M. Mankosa, M. Kohmuench, and G. Luttrell, "Significance of exposed grain surface area in coarse particle flotation of low-grade gold ore with the $hydrofloatTM$ technology," *International Mineral Processing Congress, Quebec City, Quebec*, vol. **78**, no. 7, 2016.

[13] M. Mankosa and G. Luttrell, "Hindered-bed separator device and method," *U.S. Patent 6,264,040*, July 2001.

[14] W. Ray, *Advanced Process Control*. Butterworths publishers, 1989.

[15] M. Fuerstenau, G. J. Jameson, and R. Yoon, *Froth Flotation: A Century of Innovation*. Littleton, CO, USA: Society for Mining, Metallurgy and Exploration, 2007.

[16] D. Moolman, J. Eksteen, C. Aldrich, and J. van Deventer, "The significance of flotation froth appearance for machine vision control," *International Journal of Mineral Processing*, vol. **48**, no. 3-4, pp. 135–158, 1996.

[17] M. Maldonado, A. Desbiens, R. del Villar, and E. Poulin, "Nonlinear control of bubble size in a laboratory flotation column," *IFAC PapersOnLine*, vol. **43**, no. 9, pp. 19–24, 2010.

[18] C. Gomez, A. Uribe-Salas, and J. Finch, "A level detection probe for industrial flotation columns," *In: Dobby, Rao (Eds.) Proceedings of the International Symposium on Processing Complex Ores-28th Annual Conference of Metallurgists of CIM, Pergamon Press, Amesterdam*, pp. 325–334, 1989.

[19] R. DelVillar, M. Gregoire, and A. Pomerleau, "Automatic control of a laboratory flotation column," *Miner. Eng.*, vol. **12**, pp. 291–308, 1999.

[20] M. Moys and J. Finch, "Developments in the control of flotation columns," *Int. J. of Min. Process.*, vol. **23**, no. 3, pp. 265–278, 1988.

[21] C. Aldrich, C. Marais, B. Shean, and J. Cilliers, "Online monitoring and control of froth flotation systems with machine vision: A review," *Int. J. Miner. Process*, vol. **96**, pp. 1–13, 2010.

[22] K. Popli, M. Sekhavat, A. Afacan, S. Dubljevic, Q. Liu, and V. Prasad, "Dynamic modeling and real-time monitoring of froth flotation," *Minerals*, vol. **5**, pp. 570–591, 2015.

[23] A.-E. Sommera, M. Nikpaya, S. Heitkamb, M. Rudolphc, and K. Eckerta, "A novel method for measuring flotation recovery by means of 4d particle tracking velocimetry," *Minerals Engineering*, vol. **124**, pp. 116–122, 2018.

[24] S. Morar, M. Harris, and D. Bradshaw, "The use of machine vision to predict flotation performance," *Minerals Engineering*, vol. **36-38**, pp. 31–36, Oct2012.

[25] C. Gomez and J. Finch, "Gas dispersion measurements in flotation machines," *CIM Bulletin*, vol. **95**, no. 1066, pp. 73–78, 2002.

[26] R. Rodrigues and J. Rubio, "New basis for measuring the size distribution of bubbles," *Minerals Engineering*, vol. **16**, pp. 757–765, 2003.

[27] S. Mohanty, "Artificial neural network based system identification and model predictive control of a flotation column," *Journal of Process Control*, vol. **19**, pp. 991–999, 2009.

[28] B. Shean and J. Cilliers, "A review of froth flotation control," *International Journal of Mineral Processing*, vol. **100**, pp. 57–71, 2011.

[29] J. Bouchard, A. Desbiens, R. Villar, and E. Nunez, "Column flotation simulation and control: An overview," *Minerals Engineering*, vol. **22**, pp. 519–529, 2009.

[30] A. Maffei and I. de Oliveira Luz, "Pulp-froth interface control in the flotation column," *Dev. in Miner. Process*, vol. **13**, pp. C3–1–C3–7, 2000.

[31] I. Jovanovic and I. Milanovic, "Modelling of flotation processes by classical mathematical methods - a review," *Arch. Min. Sci.*, vol. **60**, no. 4, pp. 905–919, 2015.

[32] J. Yianatos, "Fluid flow and kinetic modelling in flotation related processes, columns and mechanically agitated cells-a review," *Trans IChemE, Part A, Chemical Engineering Research and Design*, vol. **85**, no. A12, pp. 1591–1603, 2007.

[33] G. Wang, L. Ge, S. Mitra, Geoffrey, M. Evans, and S. C. J.B. Joshi, "A review of cfd modelling studies on the flotation process," *Minerals Engineering*, vol. **127**, pp. 153–177, 2018.

[34] H. Laurila, J. Karesvuori, and O. Tiili, "Strategies for instrumentation and control of flotation circuits," *Mineral Processing Plant Design, Practice and Control*, vol. **2**, pp. 2174–2195, 2002.

[35] M. Harris, K. Runge, W. Whiten, and R. Morrison, "Jksimfloat as a practical tool for flotation process design and optimization," *Mineral Processing Plant Design, Practice and Control*, vol. **1**, pp. 461–478, 2002.

[36] J. Yianatos, J. Finch, and A. Laplante, "Cleaning action in column flotation froths," *Transactions of the Institution of Mining and Metallurgy, Section C-Mineral Processing and Extractive Metallurgy*, vol. **96**, pp. C199–C205, 1987.

[37] L. Warren, "Determination of the contributions of true flotation and entrainment in batch flotation tests," *International Journal of Mineral Processing*, vol. **14**, pp. 33–34, 1985.

[38] K. Popli, A. Afacan, Q. Liu, and V. Prasad, "Real-time monitoring of entrainment using fundamental models and froth images," *Minerals Engineering*, vol. **124**, pp. 44–62, 2018.

[39] F. Nakhaei, M. Mosavi, A. Sam, and Y. Vaghei, "Recovery and grade accurate prediction of pilot plant flotation column concentrate: Neural network and statistical techniques," *International Journal of Mineral Processing*, vol. **110-111**, pp. 140–154, 2012.

[40] A. Desbiens, D. Hodouin, and E. Plamondon, "Global predictive control: A unified control structure for decoupling setpoint tracking, feedforward compensation and disturbance rejection dynamics," *IEE Proc.-Control Theory Appl.*, vol. **147**, no. 4, pp. 465–475, 2000.

[41] G. Harbort and D. Clarke, "Fluctuations in the popularity and usage of flotation columns: An overview," *Minerals Engineering*, vol. **100**, pp. 17–30, 2017.

[42] K. Sastry and D. Fuerstenau, "Theoretical analysis of a countercurrent flotation column," *Transactions of the SME/AIME*, vol. **247**, no. 1, pp. 46–52, 1970.

[43] E. Cruz, "A comprehensive dynamic model of the column flotation unit operation," Virginia Polytechnic Institute and State University, Tech. Rep., 1997.

[44] J. Bouchard, A. Desbiens, and R. del Villar, "Column flotation simulation: A dynamic framework," *Minerals Engineering*, vol. **55**, pp. 30–41, 2014.

[45] C. Crowe, J. D. Schwarzkopf, M. Sommerfeld, and Y. Tsuji, *Multiphase Flows with Droplets and Particles*. CRC Press; 2 edition, 2012.

[46] R. Yoon and G. Luttrell, "The effect of bubble size on fine particle flotation," *Miner. Process. Extr. Metall. Rev.*, vol. **5**, no. 1-4, pp. 101–122, 1989.

[47] A. Hassanzadeh, M. Firouzi, B. Albijanic, and M. Celik, "A review on determination of particle-bubble encounter using analytical, experimental and numerical methods," *Minerals Engineering*, vol. **122**, pp. 296–311, 2018.

[48] C. Marais and C. Aldrich, "The estimation of platinum flotation grade from froth image features by using artificial neural networks," *The Journal of The Southern African Institute of Mining and Metallurgy*, vol. **2**, pp. 81–85, 2011.

[49] S. Vieira, J. Sousa, and F. Durao, "Fuzzy modeling strategies applied to a column flotation process," *Miner. Eng.*, vol. **18**, pp. 725–729, 2005.

[50] F. Nakhaeie, A. Sam, and M. R. Mosavi, "Concentrate grade prediction in an industrial flotation column using artificial neural network," *Arab J Sci Eng*, vol. **38**, pp. 1011–1023, 2013.

[51] S. Gupta, P. Liu, S. Svoronos, R. Sharma, N. Abdel-Khalek, Y. Cheng, and H. El-Shall, "Hybrid first-principles/neural networks model for column flotation," *AIChE Journal*, vol. **45**, no. 3, pp. 557–566, 1999.

[52] R. King, *Modeling and simulation of mineral processing systems*. Oxford, UK: 1st edition, Butterworth-Heinemann, 2001.

[53] A. Saleh, "A study on the performance of second order models and two phase models in iron ore flotation," *Physicochemical Problems of Mineral Processing*, vol. **44**, pp. 215–230, 2010.

[54] L. Xian-ping, T. Xue-kun, H. Li-ping, and L. Li-ying, "Effects of size distribution on flotation kinetics of chalcopyrite," *International Conference on Environment Science and Engineering IPCBEE, IACSIT Press, Singapore*, vol. **8**, pp. 81–85, 2011.

[55] L. Wang, K. Runge, Y. Peng, and C. Vos, "An empirical model for the degree of entrainment in froth flotation based on particle size and density," *Minerals Engineering*, vol. **98**, pp. 187–193, 2016.

[56] R. Schumann, "Flotation kinetics. part 1. methods for steady-state study of flotation problems," *Journal of physical chemistry*, vol. **46**, pp. 891–902, 1942.

[57] R. Pal and J. Masliyah, "Flow characterization of a flotation column," *Canadian Journal of Chemical Engineering*, vol. **67**, no. 6, pp. 916–923, 1989.

[58] M. Falutsu, "Column flotation froth characteristics stability of the bubble-particle system," *International Journal of Mineral Processing*, vol. **40**, pp. 225–243, 1994.

[59] O. Bascur, "An interactive dynamic flotation model framework," *Developments in Mineral Processing*, vol. **13**, C8a–21–C8a–31, 2000.

[60] J. Yianatos, J. Finch, and A. Laplante, "Apparent hindered settling in a gas-liquid-solid countercurrent column," *International Journal of Mineral Processing*, vol. **18**, no. 6, pp. 155–165, 1986.

[61] A. Vazirizadeh, J. Bouchard, and R. del Villar, "On the relationship between hydrodynamic characteristics and the kinetics of column flotation. part i: Modeling the gas dispersion," *Minerals Engineering*, vol. **74**, pp. 207–215, 2015a.

[62] A. Vazirizadeh, J. Bouchard, R. del Villar, M. G. Barvarz, and C.Duchesne, "On the relationship between hydrodynamic characteristics and the kinetics of flotation. part ii: Model validation," *Minerals Engineering*, vol. **74**, pp. 198–206, 2015b.

[63] J. Masliyah, "Hindered settling in a multi-species particle system," *Chemical Engineering Science*, vol. **34**, pp. 1166–1168, 1979.

[64] K. Sastry and K. D. Lofftus, "Mathematical modeling and computer simulation of column flotation," *Society for Mining, Metallurgy & Exploration*, vol. **65**, no. 721, pp. 369–380, 1988.

[65] G. Dobby and J. Finch, "Flotation column scale-up and modelling," *CIM Bulletin*, vol. **79**, no. 891, 1986.

[66] G. Hanumanth and D. Williams, "A three-phase model of froth flotation," *International Journal of Mineral Processing*, vol. **34**, no. 5, pp. 261–273, 1992.

[67] M. Vera, Z. Mathe, J.-P. Franzidis, M. Harris, and C. O. C. E.V. Manlapig, "The modelling of froth zone recovery in batch and continuously operated laboratory flotation cells," *International Journal of Mineral Processing*, vol. **64**, pp. 135–151, 2002.

[68] D. Ramkrishna, *Population Balances, Theory and Application to Particulate Systems Engineering*. Academic Press; 1 edition, 2000.

[69] M. Bhole, J. Joshi, and D. Ramkrishna, "Population balance modeling for bubble columns operating in the homogeneous regime," *AIChE J.*, vol. **53**, no. 3, pp. 579–588, 2008.

[70] F. Lehr and D. Mewes, "A transport equation for the interfacial area density applied to bubble columns," *Chemical Engineering Science*, vol. **56**, pp. 1159–1166, 2001.

[71] P. Brito-Parada, S. Neethling, and J. Cilliers, "The advantages of using mesh adaptivity when modelling the drainage of liquid in froths," *Minerals Engineering*, vol. **33**, pp. 80–86, 2012.

[72] Y.Tian, M. Azhin, X. Luan, F. Liu, and S. Dubljevic, "Three-phases dynamic modelling of column flotation process," *IFAC PapersOnLine*, vol. **51**, no. 21, pp. 99–104, 2018.

[73] R. Burger, S. Diehl, and M. C. Marti, "A system of conservation laws with discontinuous flux modelling flotation with sedimentation," *Journal of Applied Mathematics*, vol. **84**, pp. 930–973, 2019.

[74] K. Runge, R. Crosbie, T. Rivett, and J. McMaster, "An evaluation of froth recovery measurement techniques," *XXV International Mineral Processing Congress, Brisbane, Australia*, pp. 2313–2324, 2010.

[75] B. Gorain, F. Burgess, J. Franzidis, and E. Manlapig, "Bubble surface area flux: A new criterion for flotation scale-up," *Proceedings of the 6th Annual Mill Operators Conference, (The Australasian Institute of Mining and Metallurgy: Melbourne)*, pp. 141–148, 1997.

[76] Z. Mathe, M. Harris, C. O. Connor, and J. Franzidis, "Review of froth modelling in steady state flotation systems," *Minerals Engineering*, vol. **12**, no. 3, pp. 397–421, 1998.

[77] G. Dobby and J. Finch, "Mixing characteristics of industrial flotation columns," *Chemical Engineering Science*, vol. **40**, no. 7, pp. 1061–1068, 1985.

[78] Z. Zhou, N. Egiebor, and L. Plitt, "Frother effects on bubble motion in a swarm," *Canadian Metallurgical Quarterly*, vol. **32**, no. 2, pp. 89–96, 1992.

[79] K. Sastry, "Mathematical modeling of pellet growth processes and computer simulation of pelletizing circuits *Paper presented at the 2nd International Symposium on Agglomeration.*," Nuremberg, Germany, Tech. Rep., 1981.

[80] M. von Smoluchowski, "Versucheiner mathematischen theorie der koagulations kinetic kolloider lousungen.," *Z. Phys. Chem*, vol. **92**, pp. 129–168, 1917.

[81] B. Pyke, D. Fornasiero, and J. Ralston, "Bubble particle heterocoagulation under turbulent conditions," *Journal of Colloid and Interface Science*, vol. **265**, pp. 141–151, 2003.

[82] K. Popli, "Real-time process monitoring for froth flotation processes using image processing and dynamic fundamental models," University of Alberta, Tech. Rep., 2017.

[83] J. Duan, D. Fornasiero, and J. Ralston, "Calculation of the flotation rate constant of chalcopyrite particles in an ore," *Int. J. Miner. Process.*, vol. **72**, pp. 227–237, 2003.

[84] Z. Dai, S. Dukhin, D. Fornasiero, and J. Ralston, "The inertial hydrodynamic interaction of particles and rising bubbles with mobile surfaces," *J. Colloid and Interface Sci.*, vol. **197**, pp. 275–292, 1998.

[85] Z. Dai, D. Fornasiero, and J. Ralston, "Particle?bubble attachment in mineral flotation," *J. Colloid and Interface Sci.*, vol. **217**, pp. 70–76, 1999.

[86] Z. Dai, D. Fornasiero, and J. Ralston, "Particle-bubble collision models - a review," *Advances in Colloid and Interface Science*, vol. **85**, pp. 231–256, 2000.

[87] D. Tao, "Role of bubble size in flotation of coarse and fine particles-a review," *Separation Science and Technology*, vol. **39**, no. 4, pp. 741–760, 2005.

[88] S. Gautam and G. J. Jameson, "Versucheiner mathematischen theorie der koagulations kinetic kolloider lousungen.," *Minerals Engineering*, vol. **132**, pp. 316–325, 2019.

[89] A. Tagawa, N. Dohi, and Y. Kawase, "Volumetric gas - liquid mass transfer coefficient in aerated stirred tank reactors with dense floating solid particles," *Industrial and Engineering Chemistry Research*, vol. **51**, pp. 1938–1948, 2012.

[90] G. Mathieu, "Comparison of flotation column with conventional flotation for concentration of a molybdenum ore," *CIM Bulletin*, vol. **65**, no. 721, pp. 41–45, 1972.

[91] R. Tuteja, D. Spottiswood, and V. Misra, "Mathematical models of the column flotation process: A review," *Minerals Engineering*, vol. **7**, pp. 1459–1472, 1994.

[92] J. E. Dickinson and K. Galvin, "Fluidized bed desliming in fine particle flotation-part i," *Chem. Eng. Sci.*, 2014.

[93] A. Bensoussan, G. D. Prato, M. C. Delfour, and K. Mitter, *Representation and control of infinite-dimensional systems. Systems and Control: Foundations & Applications*. Boston: Birkhauser, 2007.

[94] A. A. Moghadam, I. Aksikas, S. Dubljevic, and J. F. Forbes, "Boundary optimal (lq) control of coupled hyperbolic *pdes* and *odes*," *Automatica*, vol. **49**, no. 2, pp. 526–533, 2013.

[95] J. Xie and S. D. Q. Xu D. Ni, "Observer and filter design for linear transport-reaction systems," *European Journal of Control*, vol. **49**, pp. 26–43, 2019.

[96] D. Vries, K. Keesman, and H. Zwart, "Luenberger boundary observer synthesis for sturm-liouville systems," *Int. J. Control*, vol. **83**, no. 7, pp. 1504–1514, 2010.

[97] A. Wouver and M. Zeitz, "State estimation in distributed parameter systems," *Control Systems, Robotics and Automation*, vol. **XIV**: Nonlinear, Distributed, and Time Delay Systems-III, p. 92, 2009.

[98] D. Simon, *Optimal State Estimation: Kalman, H Infinity, and Nonlinear Approaches*. Wiley-Interscience, 2006.

[99] J. Winkin, D. Dochain, and P. Ligarius, "Dynamical analysis of distributed parameter tubular reactors," *Automatica*, vol. **36**, pp. 349–361, 2000.

[100] Q. Xu and S. Dubljevic, "Linear model predictive control for transport-reaction processes," *AIChE J.*, vol. **63**, no. 7, pp. 2644–2659, 2017.

[101] T. Yu and J. Seinfeld, "Observability and optimal measurement location in linear distributed parameter systems," *Int. J. Control*, vol. **18**, no. 4, pp. 785–799, 1973.

[102] D. Luenberger, "Observing the state of a linear system," *IEEE Trans. Military Electron.*, vol. **2**, no. 8, pp. 74–80, 1964.

[103] D. Luenberger, "An introduction to observers," *IEEE Trans. Autom. Control*, vol. **16**, no. 6, pp. 596–602, 1971.

[104] R. Kalman, "A new approach to linear filtering and prediction problems," *Transactions of the ASME Journal of Basic Engineering*, vol. **82**, no. Series D, pp. 35 –45, 1960.

[105] R. Kalman and J. Bertram, "Control system analysis and design via the second method of lyapunov," *J. Basic Eng. Trans., ASME*, vol. **82**, p. 371, 1960.

[106] M. Geetha, P. Kumar, and J. Jerome, "Comparative assessment of a chemical reactor using extended kalman filter and unscented kalman filter," *Procedia Technol.*, vol. **14**, pp. 75–84, 2014.

[107] V. Prasad, M. Schley, L. Russo, and B. Bequette, "Product property and production rate control of styrene polymerization," *Journal of Process Control*, vol. **12**, pp. 353–372, 2002.

[108] S. Julier and J. Uhlmann, "Unscented filtering and nonlinear estimation," *Proceedings of the IEEE*, vol. **92**, pp. 401–422, 2004.

[109] S. Arulampalam, S. Maskell, N. Gordon, and T. Clapp, "A tutorial on particle filters for online nonlinear/non-gaussian bayesian tracking," *IEEE Transactions on Signal Processing*, vol. **50**, pp. 174–188, 2002.

[110] A. Mesbah, A. Huesmana, H. Kramer, and P. V. den Hof, "A comparison of nonlinear observers for output feedback model-based control of seeded batch crystallization processes," *Journal of Process Control*, vol. **21**, pp. 652–666, 2011.

[111] D. Dochain, "State and parameter estimation in chemical and biochemical processes: A tutorial," *Journal of Process Control*, vol. **13**, p. 80, 2003.

[112] R. Kandepu, B. Foss, and L. Imsland, "Applying the unscented kalman filter for nonlinear state estimation," *Journal of Process Control*, pp. 753–768, 2008.

[113] R. Li, V. Prasad, and B. Huang, "Gaussian mixture model-based ensemble kalman filtering for state and parameter estimation for a pmma process," *Processes*, vol. **4**, no. 2, p. 9, 2016.

[114] G. Evensen, *Data assimilation: The ensemble Kalman filter*. Berlin, Germany: Springer, 2007.

[115] V. Haugen and G. Evensen, "Assimilation of sla and sst data into ogcm for the indian ocean," *Ocean Dynamics*, vol. **52**, pp. 133–151, 2002.

[116] G. Evensen, "Sequential data assimilation with a nonlinear quasi-geotrophic model using monte carlo methods to forecast error statistics," *Journal of Geophysical Research Ocean*, vol. **99**, no. C5, pp. 10,143–10,162, 2011.

[117] S. Margulis, D. McLaughlin, D. Entekhabi, and S. Dunne, "Land data assimilation and estimation of soil moisture using measurements from the southern great plains 1997 field experiment," *Water Resources Research*, vol. **38**, no. 12, pp. 35.1–35.18, 2002.

[118] G. Naevdal, T. Mannseth, and E. Vefring, "Reservoir monitoring through ensemble kalman filter," *Near-well SPE/DOE Improved Oil Recovery Symposium, April 13-17, Tulsa, Oklahoma*, vol. **124**, p. 9, 2002.

[119] A. Raghu, "Reservoir history matching using constrained ensemble kalman filter and particle filter methods," *A thesis or the degree of Master of Science in Process Control, Department of Chemical and Materials Engineering, University of Alberta*, 2014.

[120] M. Frei and H. R. Kunsch, "Bridging the ensemble kalman and particle filters," *Biometrika*, vol. **100**, no. 4, pp. 781–800, 2013.

[121] L. Heidari, V. Gervais, M. Ravalec, and H. Wackernagel, "History matching of reservoir models by ensemble kalman filtering :the state of the art and a sensitivity study," *Uncertainty analysis and reservoir modeling: AAPG Memoir 96*, vol. **85**, pp. 249–264, 2011.

Appendix A: Simulation example for Chapter 2

The unit simulated in this paper is a pilot plant flotation column (0.72 m of height, 0.16 m in diameter). The simulation parameters for the quantitative study of the hybrid model are as follows:

- CSTR – $0.56(height) * 0.16(width) * 0.16(depth) m^3$
- Q_f : 0.1 m^3/min
- Q_t : 0.03 m^3/min
- Q_a : 0.0008 m^3/min
- Q_w : 0.001 m^3/min
- Q_{rp} : 0.0005 m^3/min
- Q_{rf} : 0.001 m^3/min
- Q_{ep} : 0.01 m^3/min
- Q_{ef} : 0.02 m^3/min
- k : 0.8 ; k_2 : 0.75
- k_{ac} : 0.5 min^{-1}
- k_{dc} : 0.0003 min^{-1}
- k_{ap3}, k_{ap4} : 0.2 min^{-1}
- k_{dp} :0.005 min^{-1}
- k_{af6}, k_{af7}: 0.05 min^{-1}

- k_{df} :0.01 min^{-1}
- α_f, α_p : 0.1 min^{-1}
- ϵ_c:$[0.02, 0.04, 0.3]$
- $d_{b,p}$:$[0.0015, 0.001, 0.0005]$ m ; ϵ_{pp} :$[0.08, 0.24, 0.08]$
- $d_{b,f}$:$[0.003, 0.002, 0.001]$ m; $\epsilon_f = [0.18, 0.46, 0.06]$
- $\xi_{p,n,j}$:$[2.7, 1.3, 0.25; 1.3, 2.7, 0.1; 0.25, 0.1, 2.7]$
- $\xi_{f,n,j}$:$[5.4, 2.6, 0.5; 2.6, 5.4, 0.2; 0.5, 0.2, 5.4]$

We used the following initial conditions as one representation of the system: $x_{1,0} = 0.2\ kg/m^3$, $x_{q1,0} = 0.35\ kg/m^3$, $x_{2,0} = 0$.

Appendix B: Detailed expressions for the elements of $\mathscr{F}$

Detailed expressions for the elements of $\mathscr{F}$ in equation 3.80 are provided here:

$F_{11} = -V_{6ss}\frac{\partial}{\partial z_f} + A_{311},\ F_{12} = A_{312},\ F_{13} = A_{313},\ F_{15} = A_{312}\delta(L_1 - z)$

$F_{16} = A_{313}\delta(L_1 - z),\ F_{21} = A_{321} - A_{221}\delta(L_1 - z),\ F_{22} = -V_{7ss}\frac{\partial}{\partial z_f} + A_{322}$

$F_{23} = A_{323},\ F_{24} = A_{323},\ F_{25} = -A_{221}\delta(L_1 - z)$

$F_{26} = -A_{222}\delta(L_1 - z) + A_{322}\delta(L_1 - z),\ F_{31} = (A_{323} - A_{223})\delta(L_1 - z)$

$F_{32} = A_{331} - A_{231}\delta(L_1 - z),\ F_{33} = A_{332},\ F_{34} = -V_{8ss}\frac{\partial}{\partial z_f} + A_{333}$

$F_{35} = -A_{231}\delta(L_1 - z),\ F_{36} = (A_{332} - A_{232})\delta(L_1 - z)$

$F_{41} = -A_{311}\delta(L_1 - z) + A_{211}\delta(L_1 - z),\ F_{42} = -A_{312}\delta(L_1 - z)$

$F_{43} = -A_{313}\delta(L_1 - z),\ F_{44} = -V_3\frac{\partial}{\partial z_p} + A_{211}$

$F_{45} = A_{212} - A_{312}\delta(L_1 - z),\ F_{46} = A_{213} - A_{313}$

$F_{51} = A_{221}\delta(L_1 - z),\ F_{54} = A_{221},\ F_{55} = -V_4\frac{\partial}{\partial z_p} + A_{222},\ F_{56} = A_{223}$

$F_{61} = A_{231}\delta(L_1 - z),\ F_{64} = A_{231},\ F_{65} = A_{232},\ F_{66} = -V_{5ss}\frac{\partial}{\partial z_p} + A_{233}$

Appendix C: Simulation Parameters for Chapter 3

The unit simulated in this paper is a pilot plant flotation column with the following geometry: 0.72 m of height, 0.16 m in diameter. The simulation parameters for the quantitative study of the hybrid column are as follows:

- CSTR : $0.56(height) * 0.16(width) * 0.16(depth)m^3$
- Q_f : $0.1m^3/min$
- Q_t : $0.03m^3/min$
- Q_a : $0.0008m^3/min$
- Q_w : $0.001m^3/min$
- Q_{rp} : $0.0005m^3/min$
- Q_{rf} : $0.001m^3/min$
- Q_{ep} : $0.01m^3/min$
- Q_{ef} : $0.02m^3/min$
- k : 0.8 ; k_2 : 0.75
- $G = 8.08$; $m = 0.45$
- K_{dc} : 0.0003 $1/min$
- K_{ap3}, K_{ap4} : 0.2 $1/min$
- K_{dp} : 0.005 $1/min$
- K_{af6}, K_{af7}: 0.05 $1/min$

- K_{df} : 0.01 $1/min$
- α_f : 0.1 $1/min$
- ϵ_c:$(0.02, 0.04, 0.3)$
- $D_{b,p}$:$(0.0015, 0.001, 0.0005)$; ϵ_p :$(0.08, 0.24, 0.08)$
- $D_{b,f}$:$(0.003, 0.002, 0.001)$; $\epsilon_f = (0.18, 0.46, 0.06)$

A representative initial condition is: $x_1(0) = 0.2\frac{kg}{m^3}$, $xq_1(0) = 0.5\frac{kg}{m^3}$, $x_2(0) = 0$.